This is to certify that the
dissertation entitled

FORWARD ERROR CORRECTION BIOSENSORS: PRINCIPLES, MODELING, AND FABRICATION

presented by

Yang Liu

has been accepted towards fulfillment
of the requirements for the

Ph.D. degree in Electrical Engineering

Major Professor's Signature

02/22/2010

Date

MSU is an Affirmative Action/Equal Opportunity Employer

FORWARD ERROR CORRECTION BIOSENSORS: PRINCIPLES, MODELING, AND FABRICATION

By

Yang Liu

A DISSERTATION

Submitted to
Michigan State University
in partial fulfillment of the requirements
for the degree of

DOCTOR OF PHILOSOPHY

Electrical Engineering

2010

ABSTRACT

FORWARD ERROR CORRECTION BIOSENSORS: PRINCIPLES, MODELING, AND FABRICATION

By

Yang Liu

Reliability is a field of research that has been largely overlooked in the area of biosensing. As a result, rapid-response biosensors which have been shown to work remarkably well under controlled laboratory conditions, fail to reproduce similar results when deployed in the field. This degradation in reliability can be attributed to several factors which include device level artifacts, variations in experimental protocols, transducer and measurement noise, stochastic interaction between biomolecules and background interference. With advances in micro-nano-fabrication, the emerging biosensors can integrate an increasing number of detection elements on the same device. This has opened the possibility that exploiting spatial redundancies across multiple detection experiments could be used to alleviate the effects of biosensor noises and artifacts. This system level approach, also known as "forward error correction" (FEC) has been extensively used for designing ultra-reliable communication and storage systems. However, its application in the area of biosensing has remained largely unexplored. This thesis represents a first-of-its-kind research that investigates novel FEC interfaces to biosensors which potentially could lead to detection systems that deliver near-perfect reliability in detecting pathogens.

This thesis demonstrates that the application of encoding-decoding principles in biosensors can improve the reliability and the accuracy of biosensors. Based on the nature of biomolecular interactions, we first develop a stochastic model for affinity-based biosensors that mathematically captures the nature and sources of "biological" noise. We then present a framework for designing and evaluating biosensor encoder and decoding algorithms based on FEC principles that can improve the reliability

of pathogen detection. To demonstrate these concepts, two biosensor platforms (lateral flow immunosensor and silver-enhanced gold nanoparticle based biochip) have been adopted as model biosensor encoders. In each of these platforms different encoder structures have been generated by synthetically patterning redundant biological probes. One of the contributions of this thesis is to demonstrate that a biosensor asymmetric code delivers a more reliable performance than a repetition code which is commonly used in many of the existing biosensor platforms. The thesis also describes a corresponding factor-graph based decoding algorithm which is used to detect the presence or absence of target biomolecules in a given sample.

The equivalent biosensor circuit models and the encoding-decoding algorithms have been integrated into a computational framework which facilitates rapid evaluation of FEC strategies for biosensors without resorting to painstaking and time-consuming experimental procedures. In behavioral simulation study, we demonstrate the efficacy of employing biosensor encoding/decoding scheme. One of the salient outcome of this study is a novel "co-detection" principle that uses nonlinear coupling property of the asymmetric code to detect trace quantities of pathogen in a given sample. "Co-detection" is similar in spirit to many noise exploitation techniques like stochastic resonance which has been reported in physics and biology, where it has been shown that addition of random noise into a non-linear system in fact improves the system sensitivity. We report experimental results where the "co-detection" principle has been successfully used to detect of trace quantity of mouse IgG in the presence of large background biomolecules. One of the key applications where "co-detection" could be used in the future is in the early diagnosis of Human immunodeficiency virus (HIV).

DEDICATION

Dedicated to my family

ACKNOWLEDGMENT

The work presented in this thesis would not have been possible without the support, contribution, and encouragement of many individuals that I have had the privilege of interacting with during my stay at MSU. Indeed this is now a unique opportunity to acknowledge them, even though in a very small way. First, and foremost, I would like to express my deep gratitude to my advisor, mentor, and friend, professor Shantanu Chakrabartty, for his generous support and guidance throughout my time at MSU. It has been a great privilege of having him as my great mentor these years and it's always been a pleasure learning from him in many ways. His broad vision and encouragement has always been a source of inspiration for me. His enthusiasm and wise criticism have had a tremendous influence on my professional development.

I would also like to thank professor Evangelyn C. Alocilja for serving as my associate advisor. Her insightful and seasoned guidance has greatly influenced the makeup of the research outcomes presented in this thesis. I am also grateful for the opportunities she has provided for me to interact with many talent graduate students.

I am also grateful to professor Tim Hogan and professor Andrew Mason for serving on my committees. They have always been an exceptional source of support for me at MSU. Their technical feedback and original ideas greatly expanded the scope of my research and its contributions.

I also thank Dr. Paul Satoh at Neogen for his coaching and numerous support for my research. I also wish to thank Dr. Michael A. Mansfield at Millipore for giving me so many valuable advices in developing lateral flow immmunoassays. I thank for Brian Iglehart at Johns Hopkins Hospital for sharing me with the knowledge of immunology, and of course, a nice tour of Johns Hopkins Hospital. Special thanks are also due to Dr. Weidong Liu at Synopsys who always give me encouragement and spiritual momentum during my Ph.D. study.

I am greatly indebted to all my colleagues and friends at Adaptive Integrated

Microsystems Lab and Nano-Biosensors Lab. Special thanks to Dr. Sudeshna Pal, Dr. Amit Gore, Deng Zhang, Emma Setterington, Mike Anderson, Ming Gu, Yilun Luo, Chenling Huang, Amin Fazel, and Ravi Shaga, Yun Wang, Edith Torres-Chavolla.

My utmost gratitude, love and affection belong to my family. My parents always unconditionally love and support me and I thank them for everything they have given me. I would like to thank my wife, Xiaowen Liu, who accompanied me through the past years at Michigan State University and always there when I was down. She is the person who truly believe my dream. I dedicate this thesis to them.

TABLE OF CONTENTS

LIST OF TABLES

LIST OF FIGURES

Chapter 1

Introduction

1.1 Motivation

Every year approximately 5000 deaths in the United States are attributed to disease outbreaks due to food-borne pathogens. The United States Department of Agriculture (USDA) estimate indicates a loss of $2.9-6.7 billion due to medical costs and lost productivity because of these outbreaks [1]. In this regard, biosensors have emerged as important analytical tools for the rapid detection of pathogens in the field, and thus they play a key role in controlling disease outbreaks. A typical architecture of a biosensor consists of a biological recognition layer as a reactive surface in proximity to a transducer. The transducer converts the binding between the analyte and the recognition layer into a measurable electrical or optical signal. However, the stochastic interaction between the biomolecules, transducer device artifacts and environmental variability (eg. pH of the analyte) directly affect the reliability and the accuracy of biosensors. As a result, rapid-response biosensors which have been shown to work remarkably well under controlled laboratory conditions, fail to reproduce similar results when deployed in the field [2, 3, 4, 5]. Most of the reported methods in biosensing aim to reduce the effect of these artifacts by either improving the physical properties of

the biosensor device [6] or by using pre-filtering techniques [7], pre-concentration [8] or target-amplification (e.g. polymerase chain reaction or PCR) [9, 10] to boost the signal-to-noise ratio. With advances in micro-nano-fabrication, the emerging biosensors can integrate an ever increasing number of detection elements on the same device [11]. This has opened the possibility that exploiting spatial redundancies across multiple detection experiments could be used to alleviate the effects of biosensor artifacts. This system level approach, also known as "forward error-correction (FEC)" has been extensively used for designing ultra-reliable communication and storage systems [12].

However, even though miniaturizing the biosensing elements can facilitate detection of analytes down to pico-molar (pM) to femto-molar (fM) concentration levels [13], the reliability of detection detoriates significantly due to reduction in the signal-to-noise ratio [14]. In Fig. 1.1, we illustrate the sensitivity and integration trend in micro and nano-scale DNA arrays as example biosensors. Also shown in figure is the degradation in reliability in micro and nano arrays, which has been largely overlooked in biosensor research.

This thesis address some of these key issues by proposing a systematic way of analyzing, modeling and fabricating FEC biosensors which can potentially achieve near-perfect reliability in detecting target biomolecules in a given sample.

1.2 Contributions

The vision underlying this doctoral research is illustrated in Fig. 1.2, where FEC principles will be used to exploit the high specificity and sensitivity offered by biomolecular interfaces (for e.g. antibodies or aptamers) in conjunction with high computational reliability offered by silicon integrated circuits. The uniqueness of FEC biosensors compared to conventional architecture lies in the integration of the biomolecular en-

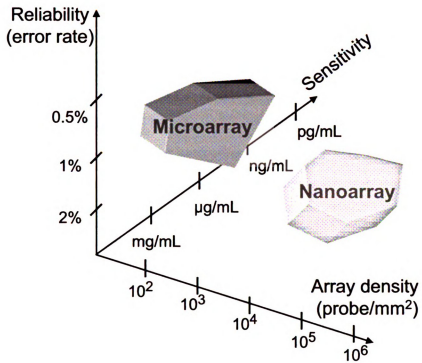

Figure 1.1: Reliability degradation in the micro and nano-scale DNA arrays. [13, 15, 16, 17, 18].

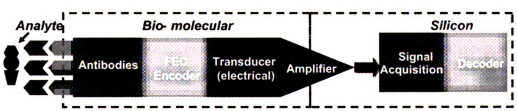

Figure 1.2: The schematic illustration of FEC biosensors.

coding layer as shown in Fig. 1.2. The biomolecular interface will be synthesized to embed spatial redundancies which will later be exploited by silicon circuits to correct for any errors. Based on this integration, the key contributions are the following:

1. We first describe the fabrication, characterization and modeling of fundamental logic gates that can be used for designing biosensors with embedded forward error-correction (FEC). The proposed biomolecular logic gates (AND and OR) are constructed by patterning antibodies at different spatial locations along the substrate of a lateral flow immunosensor. The logic gates operate by converting binding events between antigens and antibodies into a measurable electrical signal using polyaniline nanowires as the transducer. In this study, *B. cereus* and *E. coli* have been chosen as model pathogens. The functionality of the AND and OR logic gates has been validated using conductance measurements with different pathogen concentrations. Experimental results show that the change in conductance across the gates can be modeled as a log-linear response with respect to varying pathogen concentrations. Equivalent circuit models for AND and OR logic gates have been derived based on measured results. **To our best knowledge this is the first reported study that describes the construction for biomolecular logic circuits for an FEC biosensor.**

2. We present a framework of designing a biosensor encoder and decoder. We also describe a simulation framework for analyzing the reliability of biosensor circuits constructed by using these biomolecular transistors. At the core of the proposed framework is a library of electrical circuit models that capture the stochastic interaction between biomolecules and their variability to environmental conditions and experimental protocols. Reliability analysis is then performed by exploiting probabilistic dependencies between multiple circuit elements by using a factor graph-based decoding technique. The proposed computational approach

facilitates rapid evaluation of FEC strategies for biosensors without resorting to painstaking and time-consuming experimental procedures. The analysis presented in this paper shows that an asymmetric FEC biosensor code outperforms a repetition FEC biosensor code which has been proposed for microarray technology. **We believe that the proposed simulation framework is the first-of-its-kind that can evaluate the reliability of biomolecular circuits.**

3. In this study, we extend the FEC principle to a silver-enhanced gold nanoparticle based biochip. We apply the silver enhancement technique for biomolecular signal amplification in a gold nanoparticle based conductometric biochip. We show that the response of the silver enhanced biochip comprises of two distinct regions namely: (a) a sub-threshold region where conduction occurs due to electron hopping between silver islands and the electrolyte and (b) an above-threshold region where the conduction is due to a direct flow of electrons. These two regions are characterized by different conduction slopes and we show that combining the information from both these regions can improve the sensitivity of the biochip. Results from fabricated prototypes show a dynamic range of more than 40 dB and with a detection limit less than 240 pg/mL. The fabrication of the biochip is compatible with standard complementary metal-oxide-semiconductor (CMOS) processes making it ideal for integration in next-generation CMOS biosensors. We implemented AND and OR logic function on this gold nanoparticle based biochip and demonstrated the performance improvement over the logic gates using lateral flow immunosensors as platforms. **Even though silver-enhancement based techniques have been proposed for many biosensing platforms (DNA and antibodies), we believe that this study is the first-of-its-kind to extend this principle**

for designing biosensor logic gates.

4. Based on our study, an ultra-reliable approach for detecting trace quantities of biomolecules is reported. The technique called "co-detection" exploits the non-linear redundancy amongst synthetically patterned biomolecular logic circuits for deciphering the presence or absence of target biomolecules in a sample. The "co-detection" phenomena is similar in spirit to many noise exploitation techniques like stochastic resonance which has been reported in physics [19] and biology [20, 21], where it has been shown that addition of random noise into a non-linear system in fact improves the system sensitivity. One of the key applications where "co-detection" could be used in the future is in the early diagnosis of HIV. Early diagnosis of HIV requires detecting trace quantity of HIV biomolecules that are usually accompanied by other non-specific biomolecules that directly interfere in the detection process and hence requires a large amount of time for confirmation tests. The improvement in reliability offered by "co-detection" could reduce the window period for positive or negative diagnosis and hence can facilitate rapid screening. In our research, we experimentally verify the "co-detection" principle on a reported gold-nanoparticle based biochip that uses a silver-enhancement technique for signal amplification. **The co-detection principle is one of the key contributions of this thesis and it demonstrates for the first time that background interference in immunosensors can indeed be exploited to improve the detection reliability of pathogens.**

5. Another contribution of this thesis is the stochastic modeling of the biomolecular interaction using Markov random-walk which can be used to theoretically understand the proposed FEC technique. Using this model, we have hypothesized the "co-detection" principle which has later been verified experimentally.

In this regard, the proposed modeling approach is unique and novel.

Chapter 2

Fundamentals of Biosensors

2.1 Biosensor Technology

The history of biosensors started in 1962 with the development of enzyme electrodes by scientist Leland C. Clark [22]. Since then, research communities from various fields such as very large scale integration (VLSI), physics, chemistry, and material science have come together to develop more sophisticated, reliable, and mature biosensing devices. Applications for these devices are in the fields of medicine, agriculture, biotechnology as well as the military and bioterrorism detection and prevention. In literature, various definitions and terminologies of biosensors are used depending on the field of application. One commonly cited definition by International Union of Pure and Applied Chemistry (IUPAC) is "A biosensor is a self-contained integrated device, which is capable of providing specific quantitative or semi-quantitative analytical information using a biological recognition element (biochemical receptor) which is retained in direct spatial contact with a transduction element" [23].

2.2 Applications of Biosensors

Biosensors can be applied in many domains, e.g. disease diagnostics, food protection and safety, environmental monitoring, international commerce, and homeland security. Clinical and medical applications are foreseen as the most lucrative and important avenues for biosensors and many research and development has been devoted to this area. A popular example of a biosensor that is commercially available are the portable glucose sensors/meters that are used in the treatment of diabetes. Biosensors based on similar principles as the glucose sensors are now readily available for detecting hormones (e.g. pregnancy strips), drugs and proteins. Another area where rapid-response biosensors are having a significant impact is in the area of genomics. World-wide biomedical research has significantly increased our knowledge base of how biomolecules and cells function in the human body. Numerous studies, especially in the area of genomics have led to the identification of novel markers, i.e. biomolecules which provide unique information about a specific disease or a physiological condition. New markers will generate new applications, thus highlighting the importance of biosensor research in the area of diagnostics.

Food safety is another important application for biosensors where it has been used for the detection of contaminants, verification of product content, product freshness, and monitoring raw materials conversion [24, 25]. The ourbreaks of poisoning from Escherichia coli (E. coli) and Salmonella have awaked public awareness of those diseases. There is also a huge demand for biosensors which can detect product freshness, especially with fish, meat, and fruit. In the application of environmental monitoring, biosensors can detect any heavy metals, pesticide run-off, and volatile organic compounds affecting ground-water purity and the health of lakes and rivers.

As the potential threat of bioterrorism, there is a great need for a tool that can quickly, reliably, and accurately detect contaminating bioagents. Biosensors can es-

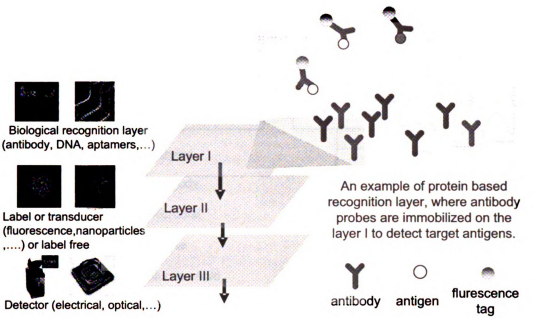

Figure 2.1: Structure of biosensors, which is composed of biological layer, a transducer element, and the detector.

sentially serve as low-cost and highly efficient devices for this purpose. Reliable and accurate detection of pathogens is very important for home-land security applications where trace quantities of highly infectious pathogens are required to be screened. Ideally, biosensors used in field should be compact, reliable, high-sensitive, and multiplexed and some of key challenges still remain. The context of the biosensor measurement is an important part of any solution and it may be different in diagnostics, food industry, environmental and defense application.

2.3 Architecture of Biosensors

Biosensors are typically composed of three parts: a biological recognition layer, a transducer element, and the detector. The basic concept of a biosensor's operation can be illustrated in Fig. 2.1, which shows an example of protein based recognition layer. A specific biological recognition element such as an enzyme, recognizes a specific

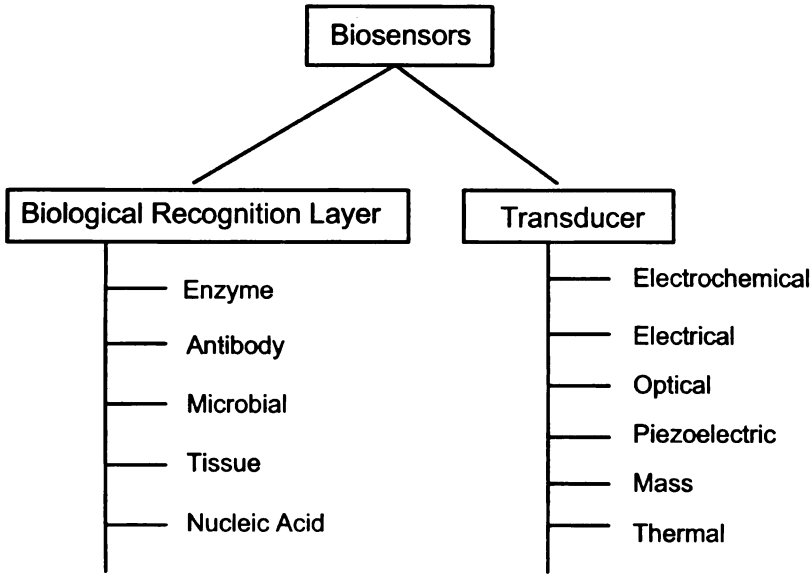

Figure 2.2: Elements of biosensors.

analyte and the transducer converts the biomolecular binding events into a measurable signal. As shown in Fig. 2.2, the biological recognition elements could be enzyme, antibody, nucleic acid, or tissue. Depending on the transducing mechanism used, the biosensors can be categorized into: electrochemical biosensors, optical biosensors, electrical biosensors, piezoelectric biosensors, mass and thermal biosensors.

2.3.1 Recognition Layer

Biological recognition layer is one of key elements in biosensors which determines the selective recognition capability for a target analyte. Recognition layers can be categorized into three types: catalytic, as typified by enzymes; affinitive, of which antibodies are the best-known example; hybrid types of the catalytic and affinitive types.

Catalytic Based Recognition Element

Enzymes are protein molecules, long chains of 20 different amino acids which are so structured as to confer a remarkable ability for catalysing specific reactions [26]. In enzymatic reactions, the molecules at the beginning of the process are called substrates, and the enzyme converts them into different molecules, called the products. Some of 3000 natural enzymes have been identified, of which about 200 are now commercially available and perhaps 80 have been used in sensing applications [27]. Compared with non-biological catalysts, enzymes are 10^8-10^{13} more active and are capable of producing hundreds or thousands of molecules per second [27]. From an analytical point of view, one of most important enzymes is the oxidoreductase, which uses oxygen or nicotinamide adenine dinucleotide (NAD) to catalyse the oxidation of compounds, or hydrolases, which catalyse the hydrolysis of compounds [28, 29].

Affinity Based Recognition Element

Compared with catalytic based biological receptor, the affinity based recognition elements are more specific in the nature of the binding with binding constants of 10^9-10^{12} [30]. For affinity based biosensors, the binding between the target and the probe is regarded as irreversible. However, changing the pH in the solution can reduce the affinity and could break the binding complex.

Antibody/antigen are the dominant type of affinity recognition elements. Antibodies (also known as immunoglobulins, abbreviated Ig) are gamma globulin proteins that are found in blood or other bodily fluids of vertebrates, and are used by the immune system to identify and neutralize foreign objects, such as bacteria and viruses [30]. They are made of basic structural units-each with two heavy chains and two small light chains. There are several different types of antibody heavy chains, and several different kinds of antibodies, which are grouped into different isotypes based on which heavy chain they possess. Five different antibody isotypes are known

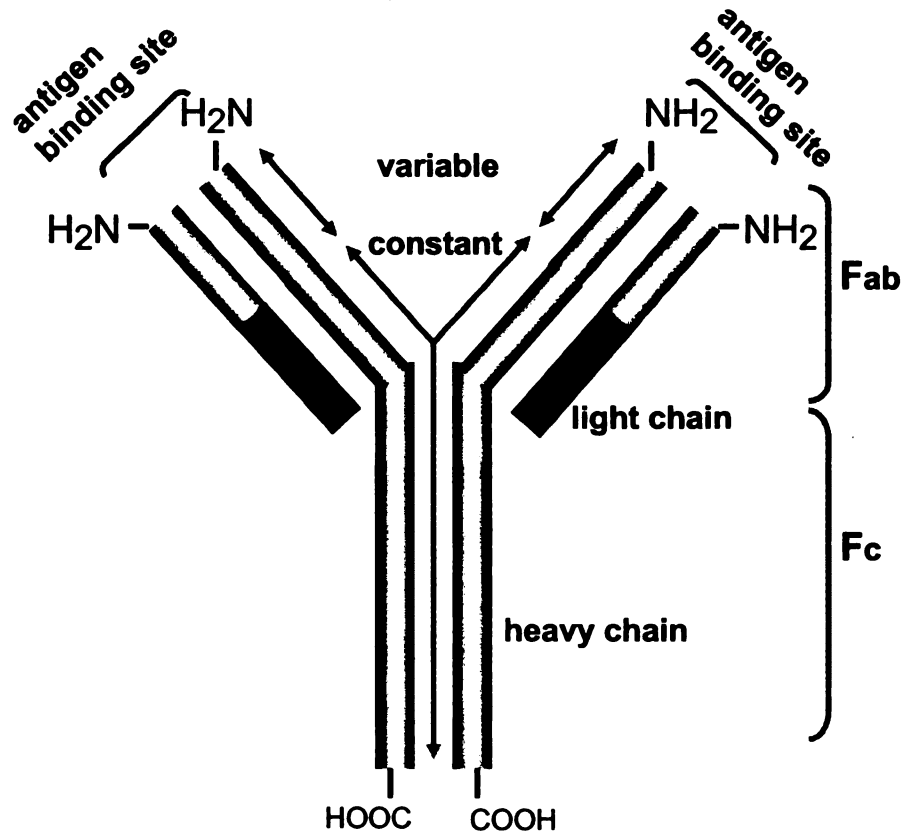

Figure 2.3: The structure of antibody.

in mammals, which perform different roles, and help direct the appropriate immune response for each different type of foreign object they encounter [31].

Antibodies are typically represented schematically as Y-shaped structures (see Fig. 2.3). The antibody consists of two identical Fab (fragment antibody) portions hinged to an Fc (fragment crystallizable) part. Though the general structure of all antibodies is similar, a small region at the tip of the protein is extremely variable, allowing millions of antibodies with slightly different tip structures, or antigen binding sites, to exist. The variable region of the Fab fragments are where the amino acids are organized to generate a binding site for the specific antigen and each antibody has two binding sites. The Fc fragment of the antibody does not combine with

the antigen but contains carboxy terminal amino acids which allow linkage to solid substrates through some biochemical treatment [30]. Each antibody consists of four polypeptides: two heavy chains and two light chains joined to form a "Y" shaped molecule. The variable region in the tips of the "Y" varies greatly among different antibodies and it is composed of 110-130 amino acids, give the antibody its specificity for binding antigen. The variable region includes the ends of the light and heavy chains. Treating the antibody with a protease can cleave this region, producing Fab or fragment antigen binding that include the variable ends of an antibody. The constant region determines the mechanism used to destroy antigen. Antibodies are further classified as five major types, IgA, IgD, IgE, IgG, and IgM, based on their constant region structure and immune functions.

The variable region is further subdivided into hyper-variable (HV) and framework (FR) regions. Hyper-variable regions have a high ratio of different amino acids in a given position, relative to the most common amino acid in that position. Within light and heavy chains, three hypervariable regions exist-HV 1, 2 and 3. Four FR regions which have more stable amino acids sequences separate the HV regions. The HV regions directly contact a portion of the antigen's surface. For this reason, HV regions are also sometimes referred to as complementarity determining regions, or CDRs. The FR regions form a beta-sheet structure which serves as a scaffold to hold the HV regions in position to contact antigen [32]. Since the antibody-antigen reaction is very specific, each can be used as a specific chemical detector for another.

Hybrid Receptors

Another type of biological receptors have characteristics of both the catalytic and irreversible receptors involving a high-affinity recognition step followed by an amplification, cycling or cascade step [33]. Studies have been shown that the attachment of single-stranded DNA to a transducer with its ability to recognize and bind to its

complement offers such a possibility [34, 35].

DNA based Receptors

Deoxyribonucleic acid (DNA) is a nucleic acid that contains the genetic instructions used in the development and functioning of all known living organisms and some viruses. DNA is regarded as a storage of information, which is similar as a set of blueprints or a code contains the instructions needed to construct other biological components. The DNA segments that carry those genetic information are called genes. DNA consists of two long polymer chains of simple units called nucleotides, with backbones made of sugars and phosphate groups joined by ester bonds [36]. These two strands run into opposite directions to each other and are therefore anti-parallel. Attached to each sugar is one of four types of molecules called bases. It is the sequence of these four bases along the backbone that encodes information. This information is read using the genetic code, which specifies the sequence of the amino acids within proteins. The code is read by copying stretches of DNA into the related nucleic acid RNA, in a process called transcription [37].

DNA is well suited for biosensing application due to the base-pairing interactions between complementary sequences. In a typical configuration, a single-stranded probe sequence is immobilized into the recognition layer, where base-pairing interactions bind the target DNA to the surface. In a typical DNA microarray detection, the RNAs are initially reverse transcribed into cDNA by a simple polymerization reaction, and fluorescently labeled with fluorophore molecules (for example Cy3 and Cy5 dyes [38]). These targets are then purified, mixed together and simultaneously hybridized to the same microarray. In optical DNA microarray, the optical intensity of fluorescence in each spot is scanned followed by the hybridization reaction. The fluorescence intensity reflects the expression level of that certain gene.

Aptamer based Recognition

Aptamers are nucleic acid ligands (RNA, ssDNA, modified ssDNA, or modified RNA) that are isolated from libraries of oligonucleotides by an in vitro selection process called SELEX (Systematic Evolution of Ligands by EXponential enrichment) [39]. They are capable of folding into three-dimensional structures due to their self-annealing properties and these DNA/RNA ligands are believed to recognize the target by shape instead of sequence [40].

Aptamers can bind with high affinity and specificity to a broad range of target molecules, and have proven suitable for biosensing application [41]. Recently, an aptamer based surface acoustic wave biosensor for monitoring blood-coagulation cascade complex formation has been reported [42]. In another study, cantilever surfaces have been functionalized with aptamers to detect proteins [43]. Liss also reported label free detection of IgE using a aptamer based quartz crystal microbalance system [44].

Regarding the binding affinities, aptamers are comparable with monoclonal antibodies. Aptamers offer many unique benefits compared to proteins. They are more resistant to denaturation and degradation, their binding affinities and specificities can easily be manipulated and improved by rational design. Aptamers have higher temperature stability (stable at room temperature) and because of their small size, denser receptor layers could be generated [40].

2.3.2 Biosensor Transducers

The transducer converts the biochemical interactions into a measurable electrical or optical signal. Electrochemical, electrooptical, acoustical, and mechanical transducers are among the many types found in biosensors. Of these types, electrochemical biosensors are the most popular ones and they are mainly used for the detection of hybridized DNA, protein binding event, and glucose concentration. The underlying

Type	Amperometric	Conductimetric	Potentiometric
Measured parameters	Current	Conductance/ resistance	Potential/ voltage
Fabrication	FET+Enzyme 2electrodes	FET+Enzyme	FET+Enzyme Oxide electrode
Applied voltage	DC potential	AC potential	Ramp voltage
Sensitivity	High	Low	High

Figure 2.4: The comparision of electrochemical biosensors.

principle for electrochemical biosensor transducers is that many chemical reactions produce or consume ions or electrons, causing some change in the electrical properties of the solution, which can be sensed as a measuring parameter. Electrochemical biosensors can be further classified based on the measured parameters as conductimetric, amperometric, and potentiometric. A comparative discussion of these three types of electrochemical biosensors is given in Fig. 2.4.

Amperometric is a highly sensitive biosensor that can detect electroactive species in samples. Enzymes are needed to catalyze the production of radioactive species since the biological samples may not be intrinsically electroactive. In conductimetric biosensors, electrical conductance or resistance is the sensor parameter because conductivity of the solution changes when electrochemical reactions produce ions or electrons. The electrical field is generated using a sinusoidal voltage and conductance measurements have relatively low sensitivity. In the potentiometric biosensor, the measured parameter is the oxidation or reduction potential of an electrochemical reaction. The operating principle relies on the fact that when a ramp voltage is applied to an electrode in solution, a current flow occurs because of electrochemical reactions. The voltage at which these reactions occur indicates a particular reaction and particular species [6].

The biosensor transducer can work either directly or indirectly. There are two detection methods involved: direct detection and indirect detection method. In the direct detection sensors, biological interaction is directly measured in real-time. The most common direct detection biosensor systems use evanescent wave, or surface plasmon resonance (SPR) technology which measures resonant oscillation of electrons on the surface of a metal [45]. Other types of direct recognition sensors, such as quartz resonator transducers that measure changes in acoustic resonance [46] and optomechanical biosensors (microcantilevers) [47].

Indirect detection biosensors rely on secondary elements that are often catalytic elements such as enzymes. Enzyme alkaline phosphatase and fluorescently tagged antibodies are some examples of secondary elements. Optical fluorescence is another common indirect detection methods, where fluorescence of the secondary ligand is measured. The work [48] described the use of optical fluorescence to develop a multi-analyte indirect detection biosensor. Fluorescence resonance energy transfer (FRET), a process where energy from an excited fluorophore is transferred to a neighboring acceptor molecule, is also used for indirect detection. Finally, light-addressable potentiometric sensors (LAPS) combine electrooptics and electrochemistry for indirect detection.

2.4 Biomolecule Immobilization

A biosensor is an analytical device containing an immobilized biological sensitive material (enzyme, antibody, antigen, organelles, DNA, cells, or tissues) in contact with or integrated within a transducer. One of key factors in biosensor design is the development of immobilization methods for stabilizing biomolecules and tethering them to surfaces. Immobilization techniques are crucial because they will affect biosensor performance such as reproducibility, selectivity, and sensitivity. Many immobiliza-

tion methods involve lots of biochemistry treatment on the surface and many of the procedures still in use have evolved from trial and error experiments. During the immobilization process, the active biological components must retain their activity and the immobilized film must have long-term stability. Specificity and sensitivity are other important immobilization criteria and the desired orientation of biological probes is a key factor for those criteria.

One common problem in the immobilization phase is a "non-specific" binding between biological probes and solid surface. Fortunately we have many mature biochemistry protocols to minimize the effect of "non-specific" binding. Another practical method is to introduce non-specific proteins or blocking agents such as bovine serum albumin (BSA).

The biomaterials and the sensor transducer elements can be coupled together in one of the four possible ways: physical adsorption, covalent binding to a surface, membrane entrapment, and cross-linking between molecules [49]. In addition to these conventional methods, more recently the methods of sol-gel entrapment, Langmuir-Blodgett (LB) deposition and electropolymerization have all been extensively used to immobilize biological components [50].

2.4.1 Physical Adsorption

The physical adsorption scheme is dependent on a combination of van der Waals forces, hydrophobic forces, hydrogen bonds, and ionic forces to attach the biomaterial to the substrate of biosensors. Physical adsorption can be used to immobilize biomolecules onto various solid substrates including plastics, glass, and metals. The physical adsorption is relatively simple under mild conditions. However, binding force is not very strong and the immobilization tend to be a certain degree of reversibility under certain condition change. Another problem with the physical adsorption is a high degree of non-specific adsorption of biomolecules on solid surfaces due to the

physical nature of adsorption method, as observed in [51]. Also aggregation and multilayering of proteins has the potential for obscuring the active sites required for the binding of subsequent specific species [51]. Despite those problems, the physical adsorption remains a major immobilization approach in many clinical biosensors such as enzymelinked immunosorbent assays (ELISA), where proteins are directly deposited on polystyrene microtiter wells.

2.4.2 Covalent Binding

An alternative approach to the attachment of biomolecules to sensor surfaces is through covalent binding, where biomolecules have been immobilized on solid surfaces through the formation of defined linkages [49]. Covalent binding of biomolecules to the surface is a favored method and procedures resulting in minimal loss of biomolecule activity [52]. Compared to the physical adsorption, this method has been employed to improve uniformity, density and distribution of the binded proteins, as well as reproducibility of the surfaces. Gluteraldehyde, succinimide esters, periodate, maleinimides, and carbodiimide are extensively used for covalent immobilization. Covalent binding requires biomolecules to have functional groups that can be attached with. Amino-acid side chains, sulfhydryl groups (cysteine), carboxyl groups (aspartate and glutamate), phenolic, thiol and imidazole groups are popular functional groups, which are not required for their biological activity. The binding force is strong compared to the physical adsorption. Many surfaces can be modified to have functionality coupling with biomolecules. For example, gold or silver surfaces can be modified by biofunctional reagent (hydroxyalkanethiol) to generate hydroxyl, carboxyl or amino groups which may be reacted with enzymes or proteins [53]. Silica surfaces have been reacted with amino silanes such as trichloro- and trialkylsilanes to have a surface-bearing amino functionality. Proteins or enzymes can then be coupled to these surfaces using gluteraldehyde or carbodiimide chemistry. Porous membrane such as nitrocellulose

has been commercially available to modify its surface to covalently bind protein, enzymes, and DNA. Compared with physical adsorption, covalent binding can generally yield a more uniform oriented surface that has more bio-activity.

2.4.3 Membrane Entrapment

In the membrane entrapment scheme, a semipermeable membrane separates the analyte and the biomaterials. The immobilization of an enzyme in a polymeric gel or behind a membrane is a straightforward process. Many polymers can be used for the inclusion of enzymes and cells and some of examples include polyvinyl alcohol, polyacrylamide, polycarbonate, and polyvinyl chloride. The drawback of membrane entrapment is the leakage of biological species during the immobilization process, resulting in bio-activity loss. Cross-linking entrapped enzymes or proteins can often alleviate the problem of biomolecule leakage [49].

2.4.4 Cross-linking

Cross-linking method is to use some multifunctional chemical reagents to offer covalent binding with biomolecules onto support. One of widely used reagents is Gluteraldehyde, which couples with the lysine amino groups of enzymes. Typically, the modification of functional groups such as carboxyl, sulfhydryl, phenol and imidazole is needed before using cross-linking method. However, the biggest problem with this approach is that cross-linking can result in the formation of multilayers of protein/enzyme and it will lead to low bio-activity of the immobilized layer.

Recently sol-gel method becomes more popular with the advance of materials and biochemistry. Biological molecules are entrapped in an aqueous micro-environment in a porous matrix such as a polymeric oxo-bridged SiO_2 network [49]. The porous matrix are wet gels formed by dydrolysis and condensation-polymerization of metal and

semimetal alkoxides, mostly SiO_2 materials [54]. Optically transparent property of matrices allows the interactions of entrapped biomolecules to be optically monitored. In the methods of sol-gel entrapment, LB deposition and electropolymerization have all been extensively used to immobilize biological components. LB technique make it possible to form oriented monolayers of biomolecules whose activity exceeds that of biomolecules immobilized by traditional methods [55]. Studies have been shown that enzymes and proteins immobilized directly onto 3-glycidoxypropyltrimethoxysilane (GOPTS) activated supports by LB deposition exhibited only a slight loss of activity with respect to solution values [50]. The 40 % bio-activity improvement has been reported to immobilize immunoglobulin G (IgG) onto a sublayer of protein A using the LB method compared with IgG LB deposited onto chemically immobilized protein A [56]. The advantages of sol-gel methods include chemically, thermally stable and the ability of retain bio-activity. However, efficient diffusion within porous matrix remains one of main problems.

The overall requirements for immobilization methods are long-term stability and durability and a high degree of specificity to a particular biological component. These conditions must be satisfied for an efficient biosensor.

2.5 Electronic Detection and Multiplexed Biosensing

Traditional optical methods based on fluorescence spectroscopy [57] have dominated the detection technique in biosensors. Actually, the most popular detection mechanism relies on microarray technology and the use of optical readout for detecting hybridization events [58, 59]. The main reason for the dominance of such a method is its robustness and fidelity in terms of chemistry and detection apparatus. However, the current trend toward creating cost-efficient arrays and point-of-care molecular di-

agnostic systems [60] requires miniaturized and low cost detection devices instead of the conventional and bulky fluorescence spectroscopy systems. Integrated electronic biosensor systems that utilize a combination of biochemical reactions and electronic sensing are promising candidates for the next generation of biosensor systems. Electronic sensing of biomolecules eliminates the need for the bulky and expensive optical instrumentation required in traditional fluorescence-based sensing assays.

CMOS technology is emerging as a powerful new tool for rapid analysis of biological objects, including cells, proteins, DNA, and viruses. For example, bioanalytical instruments are being miniaturized on integrated circuits (ICs) to study neural activities [61]– [66] and detect biological objects such as proteins, DNAs, viruses, and cells [67]– [79]. Advances in CMOS technology provide a suitable tool for electronic biosensor integration since CMOS circuitry can be post-fabricated directly beneath biological recognition layer. Thus, integrated electronic biosensors enable to miniaturize the sensing platform, enhance their portability in the point-of-care applications while maintaining high-throughput and highly parallel analysis. Pioneering work of integrated CMOS based electronic biosensors have been reported in [80, 81].

In addition to the development of electronic detection, detecting multiple pathogens in biological samples is also an active area of research in academia as well as industry. In literature, different architectures of multiplexed biosensors have been proposed. In [82], a multi-array pathogen detection is based on a lateral flow immunoassay where multiple target-capture molecules are immobilized along the flow of the analyte. Different antibodies are immobilized on these capture pads to capture corresponding pathogens. The technique, however, suffers from the interference of preceding target capture zones and the difference in signal intensity that decays along the direction of the flow. An electrokinetically-controlled heterogeneous immunoassay was developed for detecting multiple pathogens in [83]. Specificity experiments have been reported for three different pathogens where an optical device was used

in the detection method. Recently, nanotechnology provides an alternative solution that greatly increases the sensitivity. Multiplexed nanowire-based biosensor has been fabricated by Lieber group from Harvard University [84]. These devices are based on nanoscale field-effect transistors (FETs) made of semiconductor nanowires. Such a device can be used as a biosensor to detect viruses at the single-virus level in real time with high sensitivity. Multiplexed detection of several viruses simultaneously can be accomplished by modifying individual nanowire devices with antibodies specific for different viruses [85].

Chapter 3

Reliability of Biosensors

The Websters dictionary defines "reliability" as the extent to which a device, experiment or test yields the same results on repeated trials. For biosensors, an effective measure of reliability is the total detection error rate (DER) which is the sum of two types of errors: (a) false positive error-rate or the probability that the biosensor incorrectly detects the presence of pathogens when they are actually absent in the sample; and (b) false negative error-rate or the probability that the biosensor fails to detect the presence of pathogens when they are actually present in the sample. In this chapter, we discuss different factors that affect the reliability of biosensors. Even though the main focus of this chapter will be on affinity based biosensors, many of the sources of noise are also applicable to other biosensing platform.

3.1 Effect of Noise on Biosensor Performance

In the study [86], microarrays from three main microarray manufactures: Affymetrix, Agilent, and Amersham arrays are compared in the study of gene activities. Unfortunately, most data from three microarrays can not be cross-validated. Fig. 3.2 summarizes the finding and shows little overlap between three microarray systems

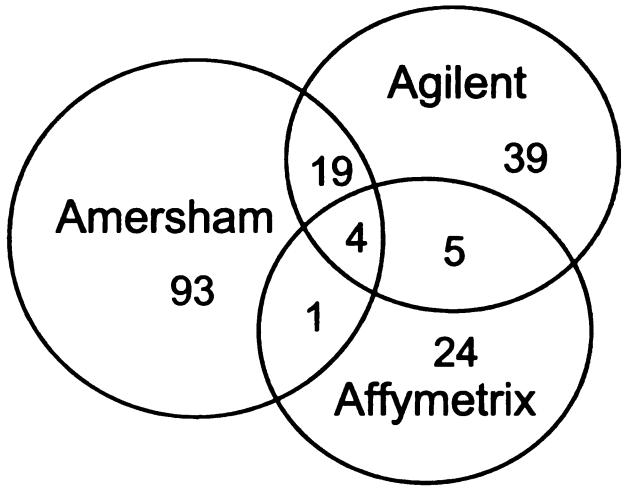

Figure 3.1: The inconsistence problem in microarray. Adapt from [86].

rated the activity of 185 genes differently in one test. One of the reasons is that probes often respond not only to gene products that exactly fit the sequence but also to those that "cross-hybridize" with near matches. Even every manufacturer claims to have avoided this problem, the fact is that microarray probes targeting almost the same region of a given gene give wildly different intensity signals [86]. The study also tell us the reliability issue has been largely overlooked by researchers and biosensor manufactures even superior sensitivity has been claimed.

It is an example how biological noise will affect biosensor's reliability. However, the reliability may affect other performance criteria such as sensitivity, reproducibility, stability, dynamic range, and selectivity as well. It is important to understand those performance criteria and the relations between them. Those performance criteria of biosensors are briefly discussed below. Assume the target analyte concentration is c; the steady-state response of target bimolecules is R_s; the control (background) response is R_c. The sensitivity of biosensors is defined as the ratio $(R_s - R_c)/c$ and the sensitivity is the slope of the calibration curve. The limit of detection (LOD) takes into account the blank and the signal fluctuation (noise) and biosensor selectiv-

ity depends upon the choice of biological receptor and transducer. The operational stability of a biosensor response may vary considerably depending on the biosensor geometry, method of preparation, as well as on the applied receptor and transducer. Furthermore, it is strongly dependent upon biological recognition reaction.

The accuracy of biosensors can be defined as the degree of conformity of the measured quantity to its true value. Given a set of measurements, the accuracy of the biosensor is usually measured by comparing mean or median to the actual value. An ideally accurate technique would have the mean exactly equal to the actual value. Reproducibility or repeatability is the degree to which repeated measurements of the same quantity will show the same or similar results. Usually, measurements are affected by errors that makes repeated measurements differ from each other. Given a set of measurements, the precision is usually measured by comparing some variance or standard deviation with zero. The reliability of biosensors depends both on their selectivity and their reproducibility. It has to be determined under actual operating conditions, i.e. in the presence of possible interfering substances. In order to be reliable for an analyst, the biosensor response should be directly related to the analyte concentrations.

In the reported literatures, microarrays typically can provide 93-100% specificity. Regarding reproducibility, most microarray platforms produce highly reproducible measurements. Some oligonucleotide arrays (Affymetrix, Agilent and Codelink) provide correlation coefficients of >0.9 [87, 88]. However, most commercial microarrays can only reach 70-90% true detection rate. The best one which can achieve 85-90% reliable detection rate is Affymetrix GeneChip [89, 90]. Commercial available lateral flow immunoassay even suffer around 30% coefficient of variation (CV) [91]. So the reliability issue become one of biggest issues in biosensors.

Fig. 3.2 describes those performance criteria related to the reliability. We should remember those criteria correlat with each other. For example, the selectivity of

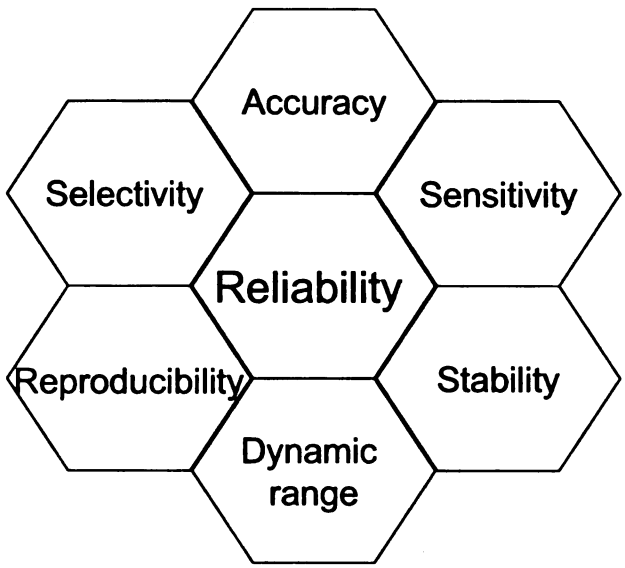

Figure 3.2: Performance criteria of biosensors.

biosensor determines how sensitive the biosensor is and low sensitivity in biosensors might result in large measurement variance, thus affecting reproducibility and reliability. Fig. 3.3 shows an example of how reproducibility can affect the dynamic range of microarrays.

Fig. 3.3 (a) shows the signal intensity from individual spots of typical microarray systems in addition to noise sources. If the background noise is constant everywhere, the noise can be regarded as signal independent noise and can be removed by defining a confidence threshold. If the noise in biosensor systems becomes larger, the signal will be accompanied with a larger level of uncertainty as shown in Fig. 3.3(b). Also observed from the graph, minimum detectable level (MDL) is higher than necessary and the detection limit will be decreased accordingly. It will contribute to low SNR in biosensors and the dynamic range of biosensors will be reduced.

The real challenge of biosensors research is to create a compact biosensor system that integrates all required process steps and that improves the key performance parameters: sensitivity, specificity, speed, accuracy, dynamic range, robustness, and

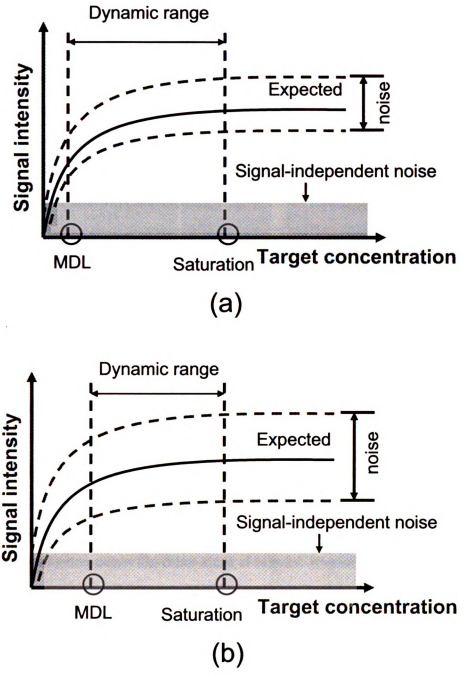

Figure 3.3: The effect of noise on the biosensor performance. (a)signal intensity in addition to noise sources. (b) larger noise level will affect dynamic range and detection limit. Adapt from [14].

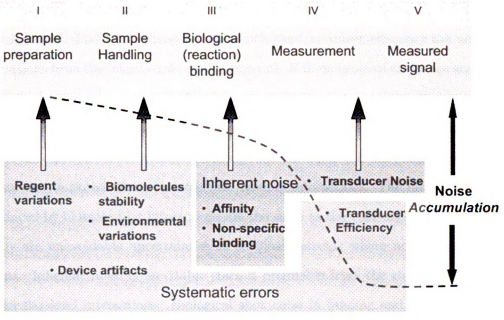

Figure 3.4: Source of errors introduced in affinity-based biosensors.

ease of use.

3.2 Source of Errors

To improve the biosensor performance, it is important to understand where do those biosensor errors come from. Deep understanding of error sources will assist us to find appropriate solutions to reduce errors. Although biosensors suffer similar device artifacts and detection noises like other kinds of sensors. However, the stochastic nature of biomolecular interactions make biosensors unique and the noise behavior becomes even more complex at low expression levels where non-specific binding dominates [92]. We will explain this unique phenomenon in this section, as well as other statistical factors introduced in biosensors, by first distinguishing between systematic errors and inherent noise in biosensors.

Let's first examine possible variances and errors that could be introduced in the development and testing phase of biosensors. First, reagent variations, biomolecular

stability, and environmental variations could be introduced in the phase of biosensor development. Those variations together with the transducer efficiency are unwanted deviations from the intended detection protocol. If these types of errors are accurately evaluated we could compensate for them in theory, by post-experiment data processing. If not, they result in a particular type of measurement uncertainty, typically referred to as systematic noise [92]. While inherent noise will exist in the bio-reaction phase due to probabilistic biomolecular binding interactions. The inherent noise introduced by biomolecular interactions are the same as the transducer noise in nature. They are unavoidable uncertainties in an ideal detector where no systematic error exists. Inherent noise is inevitable since it originates from the stochastic nature of molecular-level interactions. Biological shot noise in binding and photodiode shot-noise are examples of such noise sources [93]. Fig. 3.4 summarizes sources of errors that are introduced due to biosensor fabrication and testing artifacts. These different kinds of errors will ultimately accumulate to contribute to the total error of biosensors (shown in 3.4). That's why typical biosensor experiments suffer a high level of biochemical noise and variations [94], resulting in high uncertainty for each measurement run.

3.3 Current Techniques for Reducing Biosensor Errors

As mentioned in last section, the variations in biosensors can originate from a number of sources. Few systematic approaches have been reported to compensate biosensor errors. However, we will discuss the general approaches of reducing errors by taking microarray as an example. One general approach to reduce liquid handling errors and probe density variations in microarray is to measure a normalized target concentration by calculating the concentration ratio of the unknown target to a known target. In

DNA microarrays for instance, the known targets are housekeeping genes, defined as the genes involved in basic metabolic functions needed for the sustenance of the cell and they are always constitutively expressed. If there are systematic errors during the sample handling, purification or labeling, it will affect the unknown and the known target as well. Hence, the concentration ratio will keep constant, making microarray insensitive to those systematic errors.

Another approach to reduce the array fabrication variations and probe non-uniformities is repetition and averaging techniques [95, 96]. In this methodology, replica protein or DNA spots are positioned at different locations within the array. Generally, there are always variations in the fluorescent intensity due to non-uniformities of the capturing probes within individual spots. To decrease the effects of this kind of variation, the fluorescent intensity at each spot is averaged, subsequent to estimating probe areas [60]. The intensities at spots that have identical probes are also averaged so that any surface variation gradient is suppressed as well. However, spatial averaging might reduce uncorrelated noises and errors, but does not reduce the effects of correlated noise sources (e.g., noise of sample extraction) [14].

Some of systematic errors can be suppressed to some degree by these methods, inherent noises in biosensors (e.g., non-specific binding) are not. The interfering signals originating from non-specific bindings are generally referred to as "background signals". Widely used method is to define a confidence threshold level for the signal intensity with respect to background, which divides the signals into irrelevant (below threshold) and relevant (above threshold) regimes [97]. However, this approach is not always valid since the background and fluctuation level vary between spots. Another drawback of this simple background subtraction is the result of a reduced detection limit (dynamic range) since the minimum detectable level (MDL) is higher than necessary. Actually, very little work has been reported on analyzing and compensating biosensor inherent noises. Hassibi has given a comprehensive analysis of the stochas-

tic behavior of biomolecular interactions and proposed an optimal estimation method based on a derived biosensor stochastic model [93]. In this method, he proposed to incorporate non-specific binding statistics into the estimation algorithms to extract the original target concentration and significantly increase the detection dynamic range as well as the resolution. However, there is a practical shortcoming. The optimal estimation requires all the binding probabilities should be evaluated beforehand, which is challenging or even impractical regarding to high density binding sites in microarrays. In his thesis, he further argues that real-time detection can actually increase the accuracy of detection because more available samples can improve the estimation of expected values [14]. In conventional microarrays, the measurement is made when the aqueous solution is taken away and binding event is stopped. So in this case, only one sample from the process is measured. While in real-time detection, a number of samples are detected, which can improve the estimation of the expected value based on the simple fact of improving the SNR by averaging technique.

The survey presented in this chapter emphasizes the need for a systematic framework for reducing errors induced in biosensors and improving the reliability and detection accuracy of biosensors. In this research we will apply forward error correction techniques in biosensors by fist developing stochastic model of biosensors. Using the stochastic model, we discuss the presence of inherent biological noise in biosensors. In next chapter, we will have some discussions about the possibility of designing error-free biosensors.

Chapter 4

Fundamentals of Forward Error Correction Biosensor

Affinity-based biosensors are one of widely used biosensor platforms since they take advantage of the selectivity and specificity of biomolecular interactions such as DNA hybridization and antibody-antigen interactions. However, affinity-based biosensors suffer variabilities induced by biomolecular stochastic behavior [14]. In this chapter, we first describe the underlying biophysical processes in affinity-based biosensors. We then propose a mathematical model which captures the biomolecular stochastic interaction using Markov chains. Based on the stochastic biosensor model, we explain effects of biological noise and recommend ways in which their effects can be alleviated. We then discuss information theoretic results which can be used to obtain an upper-bound on the reliability of biosensors. In this regard, we compare a typical biosensor system with a communication system and propose forward error-correction (FEC) techniques to improve the reliability of biosensors.

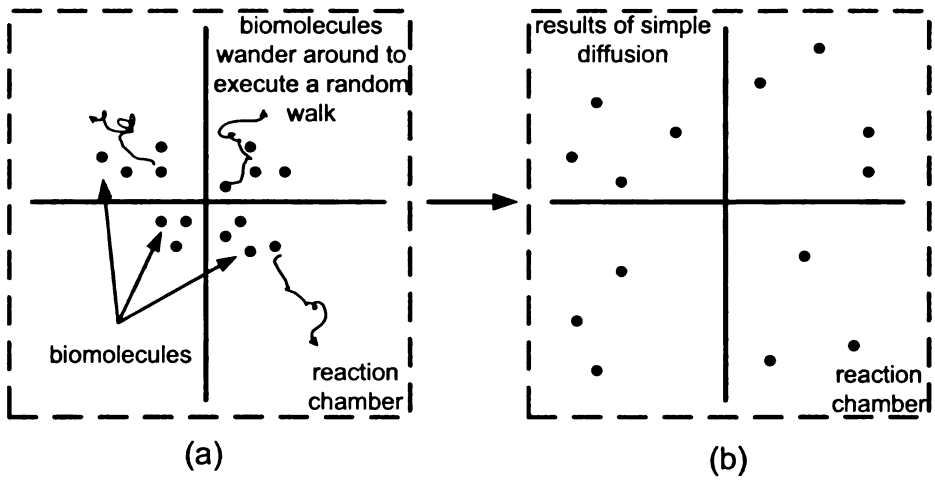

Figure 4.1: Initially particles confined in a small region of space (a) diffuse symmetrically outward (b).

4.1 Stochastic Model of Affinity-Based Biosensors

Understanding the dynamics at the biomolecular level is important in the design of reliable biosensor systems. The aim of the stochastic modeling of biosensors is to provide, as accurately as possible, a prediction of its behavior and the underlying sources of variability. Numerous modeling studies already exist which have been used in the design of biosensors [98, 99, 100, 101]. But most of models are related to specific biosensors such as acoustic wave biosensor [102], an amperometric biosensor [103], a silicon-based thermo-biosensors [104], and a cell-based biosensor [105]. The following treatment assumes that all the biomolecules exist in an acqueous environment and they are subject to thermal fluctuations.

4.1.1 Markov Model of Biomolecular Interaction

The motion of biomolecules is due to diffusion, which is the random migration due to thermal energy. A particle at absolute temperature T has a kinetic energy associated with movement along each axis of $kT/2$, where k is Boltzmann's constant. In other

words, particles, regardless of the size, all follow Brownian movement. A particle of mass m and velocity v on the x axis has a kinetic energy $mv^2/2$. This quantity fluctuates, but on the average $< mv^2/2 >= kT/2$, where $< >$ denotes an average over time. So we can compute the mean square velocity,

$$< v^2 >= kT/m \tag{4.1}$$

and the root-mean-square velocity,

$$< v^2 >^{1/2}= (kT/m)^{1/2} \tag{4.2}$$

We can use this equation 4.2 to calculate the instantaneous velocity of a particle. Unfortunately, this is not true in real scenario because the biosensor reaction chamber is not a vacuum and biomolecules are immersed in an aqueous medium. Biomolecules will collide with molecules of water. As a result, they are forced to wander around to execute a random walk. Fig. 4.1 (b) shows that a number of particles just spread out in all directions from initial position (shown in Fig. 4.1 (a)). It is an example of simple diffusion. However, due to the gravity, biomolecules tend to move outward and downward.

In a more general case where multiple analytes need to be detected within a multiple probe chamber, different kinds of biomolecules all obey random-walk statistics. It is possible for a biomolecule to bind with non-specific probes, a event called non-specific binding (shown in Fig. 4.2). Actually, study has been shown that non-specific binding may dominate the biosensor behavior in the low concentration of the analyte [14]. As a result, the fluctuation in the number of captured targets at each spot (specific and nonspecific) is a function of the concentration of all targets. Also taking into account biomolecular kinetics, there is always a non-zero probabil-

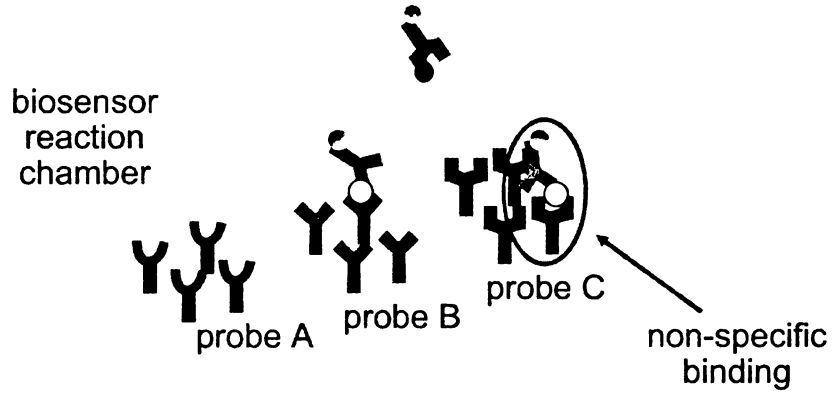

Figure 4.2: In multi-analyte multi-probe affinity-based biosensors, the target biomolecule not only can bind with its specific probe, but also to nonspecific probes.

ity of biomolecules switching from bounded state to free state and resuming random walk. This probability can be found by calculating association and disassociation rate according to:

$$X + Y \overset{k_1, k_{-1}}{\longrightarrow} XY \tag{4.3}$$

$$\frac{d[XY]}{dt} = k_1[X][Y] - k_{-1}[XY] \tag{4.4}$$

Where X and Y represent a target particle and a specific probe with an association rate k_1, and disassociation rate k_{-1}. the symbol [ ] indicates analyte concentration. We can then apply the following approximation to find the transition probabilities between the bounded state of the biomolecule and the unbounded state:

$$\begin{cases} P^b = k_1[X_m]\Delta t \\ P^r = k_{-1}\Delta t \end{cases} \tag{4.5}$$

The parameters P^b and P^r are also defined as the association and disassociation probabilities. The quantity $[X_m]$ is the saturation concentration of probe X. Δt is a

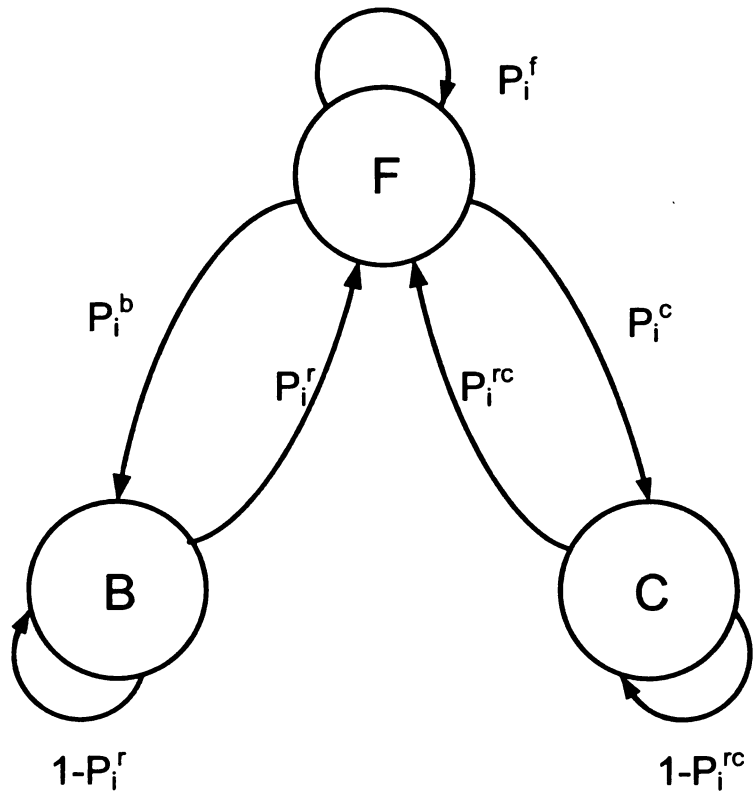

Figure 4.3: Markov chain modeling states of a target biomolecule. In a multiple probes and multiple analyte scenario, a target biomolecule can specifically bind with its probe (state marked with B) or non-specifically bind with other probes (state marked with C) or becomes an unbound biomolecule that exhibits a random walk in the solution (state marked with F).

sufficiently small time interval for each step of biomolecular random walk.

Hence, a target biomolecule may be bounded with specific probes, or cross-reactive to non-specific probes, or in the free status. Based on this simple fact, we can model biomolecular interaction with Markov chain, which reflects the stochastic nature of biomolecular motion. A Markov chain is a discrete random process with the Markov property. The Markov property states that the probability distribution for the system at the next step only depends on the current state of the system, and not additionally on the state of the system at previous steps. A Markov chain process consists of a

finite number of states and some known probabilities P_{ij}, where P_{ij} is the probability of moving from state j to state i.

For a general multiplexed biosensor, where M different types of probes are immobilized on the biosensor substrate and each probe is designed to capture one of the possible targets in the sample that is required to be detected. Also we assume that a total of n molecules of different N types of biomolecular targets, $N \leq M$, each consisting of $c_1, c_2, c_3, ..., c_N$ molecules, are present in the sample. We denote the number of spots with probes that are specific to the target of the type i by M_i. Like we discussed before, each target biomolecule of type i may also bind with non-specific probes. In particular, for each target i, we will denote by k_i the number of nonspecific binding. Fig. 4.3 shows the Markov chain model of states each biomolecule has. Any target biomolecule of type i can be in one of states: one state corresponding to a specific binding to probe, a state corresponding to a non-specific binding to probes, and one unbound (free) state. The transition probabilities between these states are given by the probabilities P_i^b, P_i^r, P_i^c, P_i^{rc}. P_i^b denotes the probability that a target of type i binds to its specific probe. P_i^r denotes the probability that a target releases from a bounded state. Associate state and disassociate state are reversible processes that is governed by equation 4.3, 4.4, and 4.5. Similarly, P_i^c denotes the probability that a target of type i binds to its non-specific probe and P_i^{rc} denotes the probability that a non-specific bounded target releases to free state. The diffusion of the unbound target molecules is modeled as a random walk. Thus, in equilibrium, the distribution of the molecules is assumed to be uniform.

The Markov chain shown in Fig. 4.3 only depicts the behavior of biomolecular interactions. However, it does not include any mass transfer process, which could be useful to examine any spatial dependency among the probes. Fig. 4.4 illustrates a general Markov chain modeling states of a target biomolecule considering a one dimensional mass transfer process, where biomolecules also execute a random walk along

one direction of biosensor reaction chamber. In this case, there are two Markov chain models involved: one for one dimensional mass relocation ((marked with 1,2,3,...,N) in the figure), and another one for the biomolecular interactions. In each mass transfer relocation, there is an associated Markov chain to describe the biomolecular interaction. In reality, the biomolecules may execute random diffusion in 3 dimensions, the general Markov model can be modified by incorporating another dimensional Markov chain. However, the model and computation will become much more complex. If we ignore the locational dependency of probes and only focus on the biomolecular interaction itself, we can use simplified model shown in Fig. 4.3, which is sufficient for many applications. In the following studies, we will utilize a simplified model to study the non-specific binding effect on the biosensor performance.

What we are interested in is the probability that a given biomolecule of type i is in any of the aforementioned states, once equilibrium state is reached. Let's denote $P_i(B)$ is the probability of specific biomolecular binding of type i, $P_i(F)$ is the release probability and $P_i(C)$ represents a probability of type i biomolecule binds with non-specific probes. These probabilities are given by the stationary distribution of the Markov chain and they satisfy

$$P_i = [P_i(B), P_i(C), P_i(F)]' = AP_i \tag{4.6}$$

$$P_i(B) + P_i(C) + P_i(F) = 1 \tag{4.7}$$

where the transition matrix A is given by

$$A = \begin{bmatrix} 1 - P_i^r & 0 & P_i^b \\ 0 & 1 - P_i^{rc} & P_i^c \\ P_i^r & P_i^{rc} & P_i^f \end{bmatrix} \tag{4.8}$$

the constraint satisfies,

$$P_i^f = 1 - P_i^c - P_i^b \tag{4.9}$$

The probability P_i^f denotes the likelihood that an unbounded target biomolecule remains free and it can be calculated by equation 4.9 given probabilities P_i^b and P_i^c. Since the motion of analyte particles is statistically independent, transition matrix A becomes independent resulting in a homogeneous Markov process. It is a reasonable assumption where saturation is not met. If the number of target biomolecules is too large, there is less probes to bind with targets, leading to saturation condition. In this case, P_i^b and P_i^c are not independent anymore. However, our study will assume the condition of saturation is never been reached and we assume P_i^b and P_i^c are constant. It is valid for most scenario. We can expand the model with calibration experimental data to include the saturation phase later on.

As we discussed above, in a general case, a target biomolecule can potentially bind with all different probes with different probabilities. As a result, the fluctuation in the number of captured targets at each probe (specific and nonspecific) is a function of the concentration of all target biomolecules. Consider the lth probe, and let the number of target biomolecules of type i that are bound to it be given by n_{li}. Clearly, the total number of biomolecules bound to probe is given by $n_l = \sum_{i=1}^{N} n_{li}$. Each n_{li} is an independent binomial random variable, one of which corresponds to specific binding and the remaining to possible non-specific binding. Let's denote X_j is the number of captured biomolecules at probe j. Since the total number of biomolecules of type i that are available or the concentration is given by C_i, The distribution of X_j is given by

$$P(X_j = n) = \begin{pmatrix} C_i \\ n \end{pmatrix} P_{ij}^n (1 - P_{ij}^n)^{C_i - n} \tag{4.10}$$

where P_{ij} is the probability that a target of type i binds with probe of type j, and it

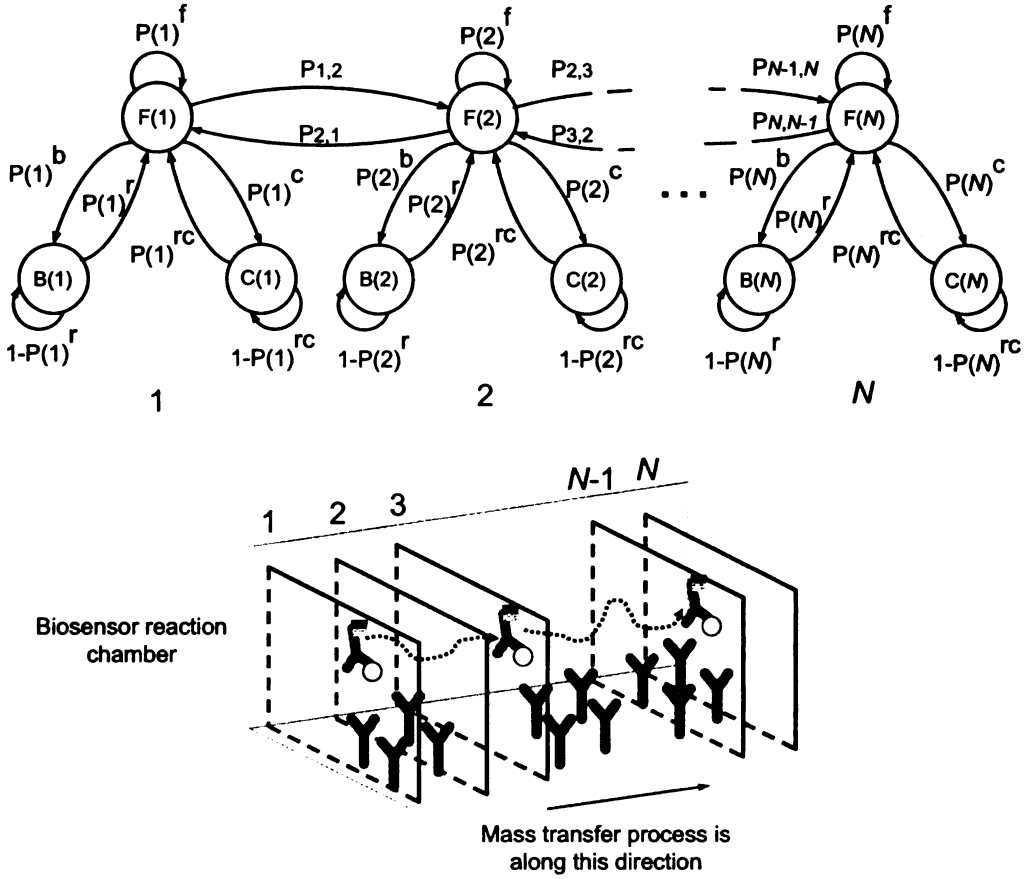

Figure 4.4: A general Markov chain modeling states of a target biomolecule considering a one dimensional mass transfer process, where biomolecules also execute a random walk along one direction of biosensor reaction chamber. There are two Markov chain models involved: mass transfer relocation and biomolecular interactions. In each mass transfer relocation (marked with 1,2,3,...,N), there is an associated Markov chain to describe the biomolecular interaction.

is the result calculated from the Markov chain model:

$$P_{ij} = \begin{cases} P_i(B) & \text{specific binding} \\ P_i(C) & \text{nonspecific binding} \\ 0 & \text{otherwise} \end{cases} \tag{4.11}$$

Since the number of biomolecules involved is large, it is well approximated by a Gaussian random variable with the mean of

$$\overline{X_j} = \sum_{k=1}^{m} P_{ij} C_i \tag{4.12}$$

and the variance of

$$\sigma_i^2 = \sum_{k=1}^{m} P_{ij}(1 - P_{ij}) C_i \tag{4.13}$$

With those parameters, we can easily find the signal-to-noise (SNR) performance of such a system in equilibrium state. We need to first identify the signal as well as the noise sources. Generally, what we are interested in a biosensor is the measure of analyte concentration in a reaction chamber. Assume the transducer can only observe captured particles, we can define the signal of biosensors to be the number of captured biomolecules in equilibrium state. The biological noise only come from the fluctuations of the number of analyte particles in equilibrium state. In this case the SNR is defined as the signal power divided by the noise power, then we have SNR for a general biosensor:

$$SNR = \frac{(\sum_{k=1}^{m} P_{ij} C_i)^2}{\sum_{k=1}^{m} P_{ij}(1 - P_{ij}) C_i} \tag{4.14}$$

Note it is SNR of biosensors with only biological noise that is taken into account. When the transducer is noisy, the overall SNR should also take into account the added noise of the transducer. If this transducer noise is independent of the biological binding events and has a variance σ_T^2 normalized to the number of the captured

biomolecules, we have

$$SNR = \frac{(\sum_{k=1}^{m} P_{ij}C_i)^2}{\sum_{k=1}^{m} P_{ij}(1 - P_{ij})C_i + \sigma_T^2} \tag{4.15}$$

We can use Markov chain model to simulate any kinds of affinity-based biosensors and predict their behavior, which provides a valuable tool for biosensor designers. It can also facilitate the design process by choosing optimal parameters.

4.1.2 Simulated Results using the Biomolecular Markov Model

With the Markov chain, we can construct a virtual biosensor model to predict its behavior. For an ideal biosensor platform in which the sensing area has infinite capacity for particle capture, it is possible to calibrate out the average amount of nonspecific capture by simply subtracting the expected number of nonspecific biomolecules from the signal.

Table 4.1: Specifications of a model protein based biosensor for simulation [14, 106, 107]

Parameter	Simulation value
associate rate (k_1)	$3 \times 10^6 M^{-1}S^{-1}$
disassociation rate (k_{-1})	$0.9S^{-1}$
Probe saturation concentration ($[X_m]$)	1μM
Simulation time increment (Δt)	4.7μS

Here we present a numerical example of how Markov chain model can be used to study the biosensor behavior. Assume we want to detect target biomolecules in a biosensor chamber and only biomolecular interactions are considerated (no mass transport process is involved). We use some reported protein based biosensor specifications for simulation parameters. The associate rate and disassociate rate are

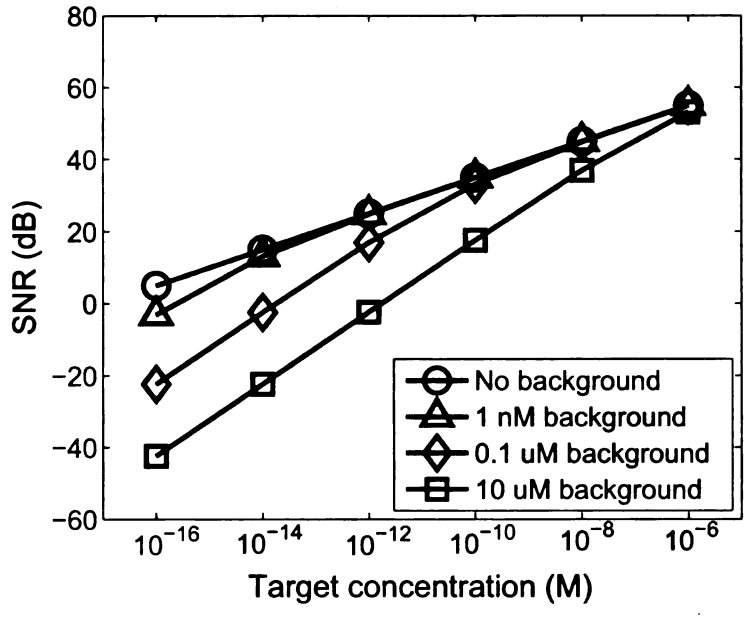

Figure 4.5: SNR of a general biosensor with as a function of target biomolecule numbers. It is compared with the cases where another background biomolecule presents.

$3 \times 10^6 M^{-1}S^{-1}$ and $0.9S^{-1}$ respectively. The probe saturation concentration $[X_m]$ is set to be 1μM and the simulation time interval is set to 4.7 μS. Those specifications are summarized in Table 4.1.

The probability of specific binding of a biomolecule target with its probe P^b and the release probability P^r can be calculate from the equation 4.5. The probability of non-specific binding P^c is assumed to be 0.001. For simplicity, these probabilities are assumed to be the same for all types of the probes. The free target biomolecules perform a random walk within the reaction chamber. At each time step of the random walk, the bounded target biomolecules may be released, upon which they resume the random walk. The release probabilities of from both specific and the non-specific states for all targets are assumed to be the same. In this case, non-specific binding is the only contributor to noise source of the biosensor. The simulations are run sufficiently long so that the equilibrium states of the Markov chains are reached.

We also introduce a background biomolecule other than target biomolecule into the biosensor reaction chamber. Fig. 4.5 shows the SNR of a affinity based biosensor where the SNR is log-linear function with the target biomolecular concentration. However, due to the background noise (non-specific binding), the SNR decreases with the increased degree of the presence of background biomolecules. As is evident from Fig. 4.5, the non-specific binding degrade the biosensor performance in terms of reduced SNR. This is especially obvious in the low concentration of target biomolecules. It verifies an important phenomena that non-specific binding may dominate biosensor behavior in the low concentration of target biomolecules [92]. Also, the results match reported biosensor datasets [14], demonstrating the validity of our modeling approach.

4.2 Limits on Biosensor Reliability

In last section, we presented analytical results which computed signal-to-noise ratio using the Markov model and we used the simulation results to explain the effect of non-specific binding on the SNR of biosensors. We have described current techniques for reducing the biosensor noise. However, these methods either focussed on improving the physical properties of biosensors or suppressing the systematic noise. An alternate approach which is at the core of the proposed research is to exploit synthetic redundancies across multiple "noisy" biosensing elements to significantly improve the reliability of detection and possibly achieve error-free detection.

The advantage of using a system level approach over a traditional biosensor signal enhancement can be understood based on the celebrated *noisy-channel coding theorem* by Claude Shannon [108]. Shannon's theorem tells us that noisy information can be communicated over a noisy channel at a non-zero rate with arbitrarily small error probability. Information theory addresses both the limitations and the possibil-

ities of communication. The noisy-channel coding theorem asserts both that reliable communication at any rate beyond the capacity is impossible, and that reliable communication at all rates up to capacity is possible.

The theorem adapted for a biosensing application states that error-free detection using a "noisy" biosensor is possible as long as the rate of detection R is less than a statistical measure called the biosensor channel capacity $C > 0$. For the biosensor channel, the rate of detection is given by $R = K/B$, where K is the number of different types pathogens (E. coli, Salmonella,etc.) and B is the number of probe elements in a biosensor array. Based on information theoretic arguments [108], the channel capacity C quantifies the theoretical limits of biosensor reliability where lowering C results in larger DER. If the "noise" or sources of errors across different biosensor elements are independent and obey Gaussian statistics (a worst case assumption), biosensor channel capacity C can be expressed as:

$$C = B \log (1 + SNR) \tag{4.16}$$

where SNR is the signal-to-noise ratio of the biosensor array.

Equation 4.16 illustrates the following key points with regards to achieving error-free detection:

1. Increasing the signal-to-noise ratio using amplification techniques like the PCR in DNA biosensors or pre-concentration in affinity based biosensors increases the capacity C or the reliability of the biosensor array only logarithmically.

2. Increasing the number of probe elements B in the array while maintaining a constant SNR increases the capacity and hence the reliability linearly.

Fig. 4.6 explains these two key points, where shows the relation between the biosensor channel capacity and the SNR with the constant probe elements B=600; the linear increase of capacity with the increase of the biosensor bandwidth B (the

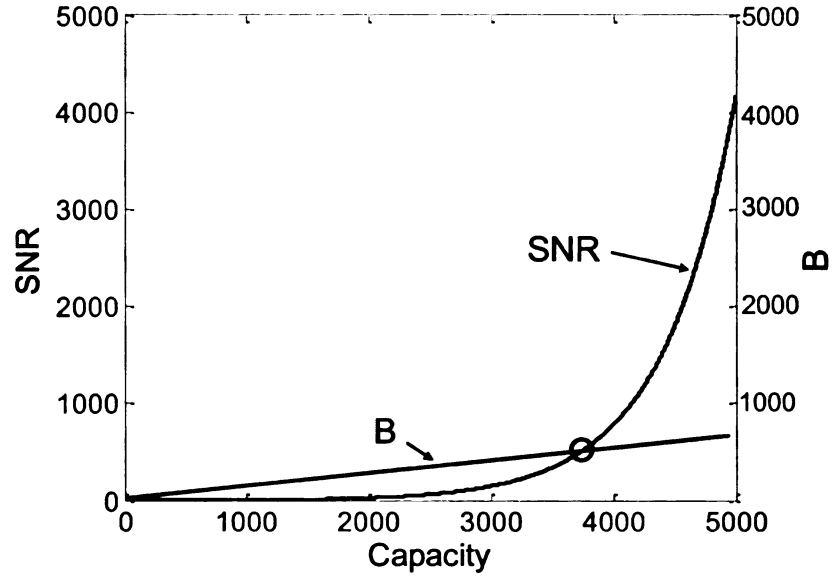

Figure 4.6: Channel capacity vs. SNR and B for a biosensor channel with white Gaussian noise.

number of probe elements) while maintaining a constant SNR=600. There is a cross point shown in the figure, after which approaching a biosensor channel capacity can be achieved by increasing B at a reasonable cost. However, the same capacity could be reached by increasing SNR logarithmically, which is not a good solution in the power constraint application. Thus equation 4.16 shows that significant improvement in reliability of detection is possible when appropriate redundancy is introduced in a biosensor channel as opposed to just enhancing the biomolecular signal. However, the equation 4.16 only provides an upper-bound on the capacity and does not prescribe a specific FEC approach for achieving error-free detection. Therefore a systematic approach is required for designing a FEC biosensor which can achieve the limits of reliability dictated by the upper-bound in equation 4.16 given the constraints on size and fabrication accuracy.

4.3 Forward Error Correction (FEC) Techniques for Improving the Reliability of Biosensors

4.3.1 The Application of FEC to Nano Bio Systems

Forward error correction (FEC) is a technology, which is widely used in telecommunication systems, to provide robustness to systems. This allows the receiver to detect and correct errors (within some bound) without the need to ask the sender for additional data. Also, FEC technique is applied to most mass storage devices to protect against damage to the stored data.

In the literature, FEC principles have been used for improving reliability of nanoscale systems, which suffer from similar computational artifacts as storage systems. Some of the examples include design of fault-tolerant circuits [109] and next generation flash memory [110]. Other work in related areas include application of the FEC principle for understanding biological systems [111, 112]. For example, error-correcting codes were proposed for a DNA microarray, where redundant gene spotting was used to reduce drop-out errors [113]. This work was extended in [114] where the error-control coding scheme and quality control were integrated for fabricating DNA microarrays using multiplexed DNA strands.

4.3.2 Similarity between Communication, Storage Systems and Biosensor Systems

Fig. 4.7 shows the overview of a communication or storage system. An information source transmits a sequence of binary digits (bits), called the uncoded sequence μ. This sequence is transformed into the coded sequence x by an encoder. The coded sequence x is corrupted by a noise vector n during transmission over the noisy communication channel. Then we will observe a noisy sequence y at the input of the

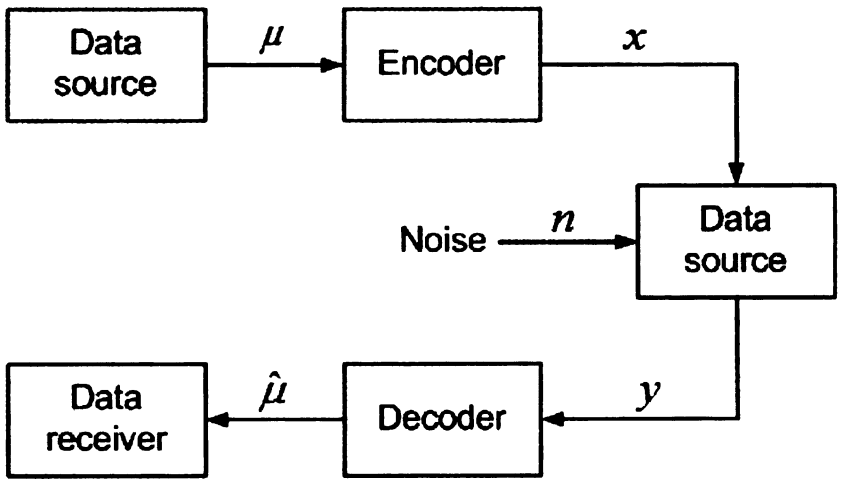

Figure 4.7: Simplified model of a communication or storage system.

decoder. The decoder then estimates the original information message $\hat{\mu}$ using observed measurement y.

In typical communication systems, a discrete set of messages or bits is processed by an encoder that implements popular low-density parity-check code (LDPC) [115] or hamming code [116] to add redundancy to the transmitted messages. These encoded bits are transformed into a signal representation that is specific to a communication channel. The channel adds randomness to the transmitted bits, which are then transformed at the receiver before being decoded. The role of the decoder is to reliably decipher what was being transmitted by the transmitter. In the case of a biosensor, the transmitted message correspond to a biological sample containing possible pathogens in different concentrations. The transformation module is implemented by biomolecular interaction between the target pathogen and detector probe. The noisy biosensor channel can be attributed to the non-specific biomolecular binding as well as environmental variations and device artifacts. At the receiver side, the transform module is implemented by an electrical transducer that translates the biomolecular interaction to a measurable signal. The Fig. 4.8 summarizes the similarities between the communication system and biosensor systems and it motivates us that information

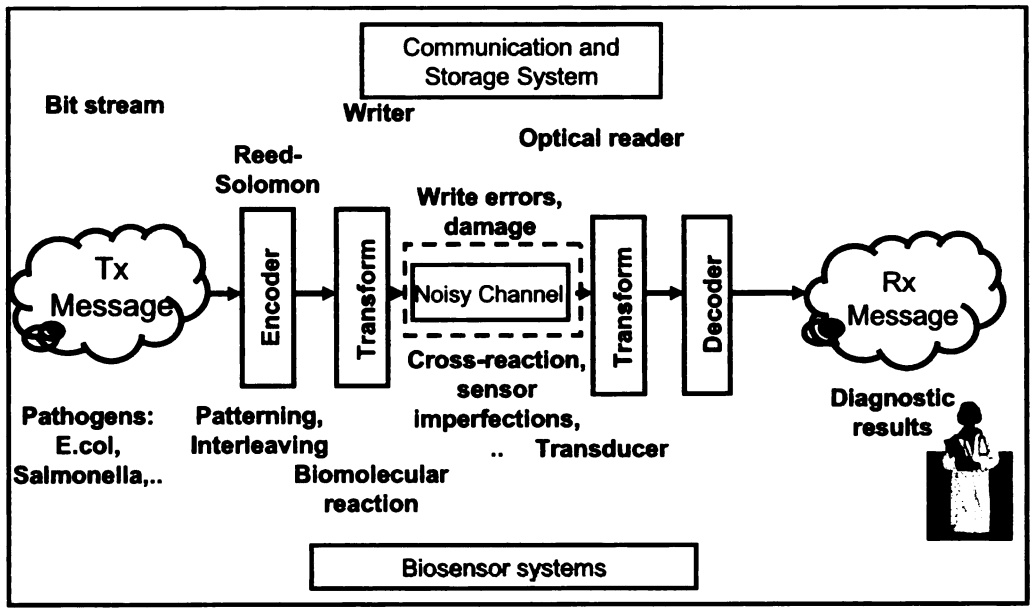

Figure 4.8: Similarity between communication systems and biosensor systems.

theoretic principles could be applied to achieving reliable biosensing.

4.3.3 Design Flow of FEC Biosensors

Regarding the design of FEC biosensors, first, we need to embed the encoder directly into the biosensor structure. The logic functions of the encoder can be achieved by biomolecular circuits, which will be demonstrated in next chapter. The reason of constructing encoder in biosensor structure is to provide redundant encoded biosensor information. A decoding algorithm then exploits this redundancy to compensate for systematic errors due to experimental variations and for random errors due to stochastic biomolecular interactions. If we follow the logic of this design flow, we will have to evaluate and verify the biosensor encoder from the beginning. Typically a biosensor experiment is very time-consuming and labor-intensive. To solve this problem, we present a simulation framework for examining different FEC biosensor topologies and analyzing the reliability of FEC biosensors constructed using these biomolecular en-

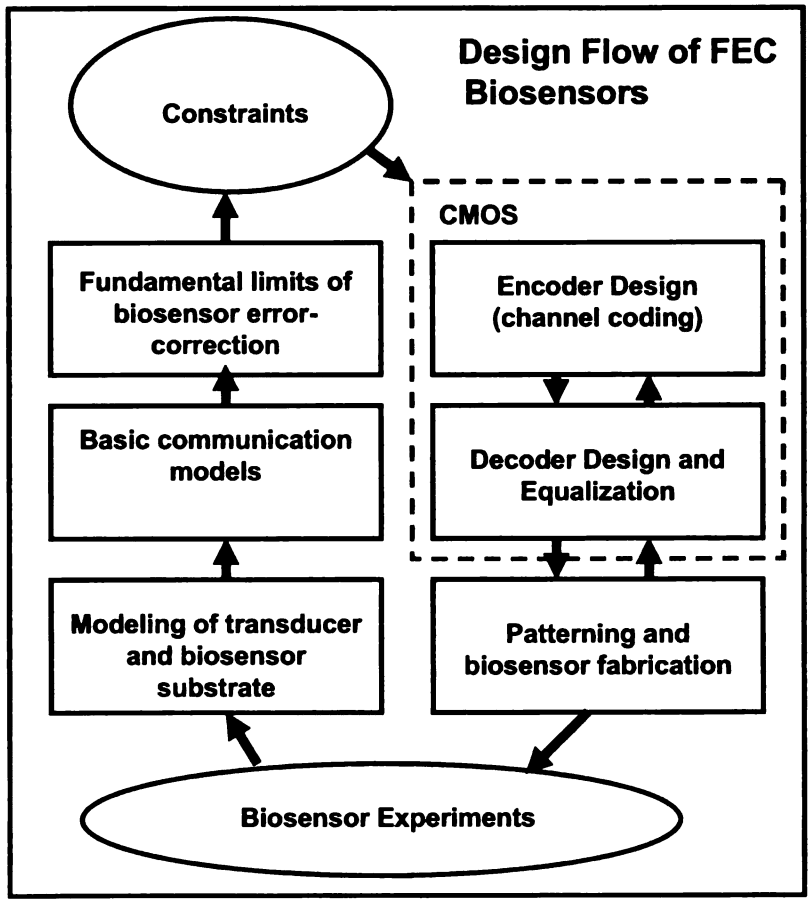

Figure 4.9: The design flow of FEC biosensors.

coder and corresponding decoding algorithm. At the core of the proposed framework is a library of electrical circuit models that capture the stochastic interaction between biomolecules and their variability to environmental conditions and experimental protocols. The proposed computational approach facilitates rapid evaluation of forward error correction (FEC) strategies for biosensors without resorting to painstaking and time-consuming experimental procedures. Taking the biosensor constraints into consideration, an alternative design flow of FEC biosensors can be followed as shown in Figure 4.9. Similar to an integrated circuit design flow, the design of a FEC biosensor entails iterative fabrication, modeling and simulation steps as illustrated in Figure 4.9. The first step in the design flow is the fabrication of fundamental device and logic circuits (for e.g. soft-AND and soft-OR logic gates). The responses of the fabricated devices and logic circuits are first measured and the experimental data are used to generate equivalent circuit models and the nature and magnitude of biosensor noise. These circuit and noise models are then used to simulate the response of different biosensor topolgies without resorting to painstaking fabrication and experimental procedures. The simulation framework can also incorporate practical constraints imposed by the size of the biosensor elements, element cross-talk, analyte propagation and transducer artifacts. The performance of different biosensor FEC topologies obtained using Monte-Carlo studies and the results are compared against the target DER. The last step in the design flow involves fabricating prototypes of the FEC biosensor and validating its performance using a limited number of experiments. Our final objective is to close the design loop, where the reliability of the biosensor encoding and decoding algorithms are validated using in-lab experiments. The following chapters will describe the detailed design of an FEC biosensor by following this design flow.

Chapter 5

Design of Forward Error Correction Biosensors: Biosensor Encoder

The similarity between the reliable communication, storage systems and biosensor systems motivates us to apply similar encoding/decoding schemes in the biosensor systems. The purpose of this thesis is to replicate the same success of telecommunication systems to FEC biosensors. Encoding and decoding concepts and algorithms are fairly straightforward in communication systems. While in FEC biosensor systems, the corresponding concepts such as codewords and channel capacity are not so obvious. We need explore appropriate and equivalent theoretical framework for FEC biosensors. One of main challenges of building biosensor encoder is that constructing a biomolecular encoder is limited by the biosensor structures and principles. For example, XOR logic is the fundamental function for digital or analog circuits and many popular code such as Hamming code based on the XOR logic function. However, XOR logic may be difficult or even impossible to achieve in biosensors due to the structure or principle constraints. If the encoder logic functions are very limited, how

would one design an efficient encoder and decoding algorithm for the reliable biological information transmission? Those problems are uncommon in the communication systems, but are immediate challenges for engineered FEC biosensor systems.

In this chapter, we will first illustrate the framework of FEC biosensors and describe the function of every integral component. Then, we demonstrate constructing biosensor encoder with two biosensor platforms: lateral flow immunoassay and gold nanoparticle based biochips. Two basic logic functions (AND and OR) are built by patterning different biomolecular probes onto different spatial locations of biosensor substrate. Detailed fabrication procedures and methods will be described.

Evaluating the reliability of different FEC biosensor configurations using direct experimental techniques has proven to be impractical due to the time-consuming and labor-intensive nature of sample preparation and handling. This has motivated us to develop an analytical simulation framework for evaluating the performance of different biosensor FEC topologies. We developed equivalent circuit models that capture the stochastic response of respective biomolecular circuit elements. A similar analytical approach for modeling the biomolecular stochastic interaction has been reported in [14]. In this work, two kinds of biosensor noise sources were identified and modeled: 1) systematic noise that was induced by sample handling errors and errors introduced by device artifacts and 2) random noise due to probabilistic biomolecular binding interactions [117, 118]. In comparison, our approach directly uses a system identification approach for approximating the experimental data using a log-linear model [119] and extracts the parameters of the noise sources based on the regression and random errors.

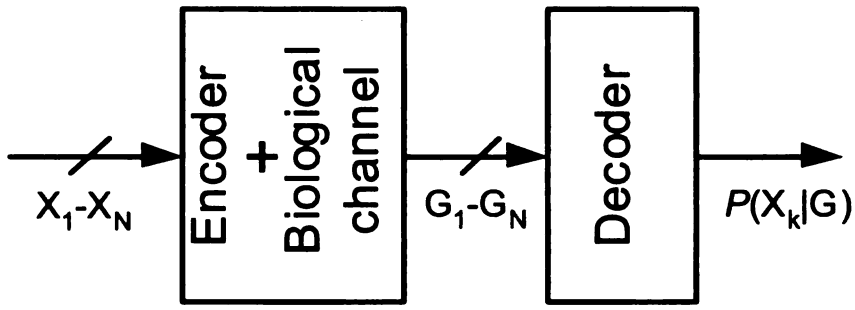

Figure 5.1: The Framework of FEC Biosensor.

5.1 The Framework of FEC Biosensors

A system level architecture of a proposed FEC biosensor is shown in Fig. 5.1, which consists of an encoder that is an ensemble of N biomolecular logic circuits that convert the biological binding into a measurable signal , a biological communication channel that introduces random and systematic errors and a decoder that uses the noisy measurements to produce probability estimates indicating the presence or absence of pathogens in a sample. The decoder processes the noisy measured conductances $G_i, i = 1, .., N$ and produces posteriori probability estimates $P(X_k|G_1, .., G_N), k = 1, .., N$, where $X_k \in \{0, 1\}$ is a boolean variable corresponding to the logical operation of the k^{th} biomolecular circuit. In the mathematical treatment that follows, it will be assumed that the channel is the only source of randomness and the encoding/decoding operation is perfectly reliable. Computations otherwhere are perfectly reliable.

What interest us is the posteriori probability, which tell us the information of biological phenomena based on the measurements. Mathematically, the posteriori

estimate $P(X_k|G_1,..,G_N)$ can be simplified according to

$$\begin{aligned} P(X_k|G_1,..,G_N) &= \propto \sum_{\sim X_k} P(X_1,..,X_N,G_1,..,G_N) \\ &= \sum_{\sim X_k} \prod_{j=1}^{N} P(G_j|X_k) P(X_1,..,X_N) \\ &= \sum_{\sim X_k} f(X_1,..,X_N) \prod_{j=1}^{N} P(G_j|X_k) \end{aligned} \tag{5.1}$$

where $\prod_{j=1}^{N} P(G_j|X_k)$ models the response of the biomolecular circuit elements and $f(X_1,..,X_N)$ represents a boolean function that captures the logical dependency between the variables $X_k, k = 1,..,N$ and hence models the structure of the encoder. The encoder function $f(.)$ can be represented in a tabular form where each table entry represents a state of the variables $X_1,..,X_N$ for which $f(X_1,..,X_N) = 1$ and zero otherwise. We will provide some specific examples of the encoder function in next section. Equation 5.1 also describes the decoding algorithm used for computing the a-posteriori probability estimates.

An example architecture of a FEC biosensor is shown in Fig. 5.2 which comprises of biomolecules as a reactive surface in close proximity to a transducer that converts the binding of the analyte with the biomolecule into a measurable signal. The uniqueness of FEC biosensors compared to conventional architecture lies in the integration of the biomolecular encoding layer as shown in Fig. 1. This encoding could be achieved by spatially patterning biomolecular entities (for e.g. antibodies, aptamers or DNA) to form logic circuits-an antibody based example is illustrated in Fig. 5.2 (b). Also required for an FEC biosensor is a decoder which can then suitably correct for errors. Typically the decoder could be implemented on silicon circuits and could be integrated in proximity with the biomolecular encoder as illustrated by an example in Fig. 5.2.

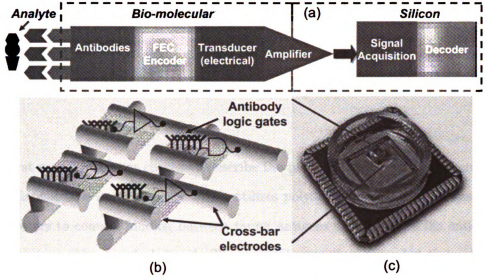

Figure 5.2: Architecture of an FEC biosensor which comprises of a biomolecular encoder that interfaces with a silicon decoder.

5.2 Biosensor Logic Gates

Biosensor encoder is an integral component in FEC biosensor and biomolecular logic circuits are basic units in biosensor encoder. Fig. 5.2 (b) illustrates an example of biosensor encoder, where redundant biological probes are patterned on the biosensor cross-bar substrate. As we mentioned before, biomolecular logic gates can be constructed by patterning different biomolecular probes along different spatial substrate locations. Single biomolecular probe can provide information equivalent to a single bit data while the logic biomolecular circuits could provide information equivalent to a complex data bit. In CMOS technology, basic transistors can form different basic logic functions: OR, AND, XOR,.... However, biomolecular transistors have the limitation of building logic functions due to the constraints of biosensor structure. In the following sections, we introduce the methods of fabricating two basic biosensor logic gates (AND and OR) using two different biosensor platforms.

5.3 Case Study I: Membrane Based Biosensor Logic Gates

The first model biosensor chosen to describe the proposed framework is a membrane based lateral flow immunosensor which utilizes polyaniline (PANI) nanowires-based transducers to convert binding between target antigens and their specific antibodies into a measurable electrical signal. The principle was then extended to implement biomolecular logic circuits (AND and OR) and their functionality was experimentally verified.

Immunosensors (biosensors that use antibodies as the biomolecule) are of great interest recently because of their applicability (any compound can be analyzed as long as specific antibodies are available) and high selectivity. In particular, immunosensors with electrical readouts offer several advantages over their optical counterparts due to their reduced cost, reduced form factor and ease of signal acquisition. One such immunosensor, which is used in this paper was introduced in [120, 121, 122], and can achieve a detection limit of 80 colony forming units CFU/mL for bacteria and 103 cell culture infective dose per milliliter (CCID/mL) of bovine viral diarrhea virus (BVDV) antigens in approximately 6 minutes. The immunosensor uses conductive polyaniline as a transducer and a molecular switch that is triggered by the presence of target pathogen in the analyte. The use of polyaniline as a switch (yielding "on" and "off" responses) has been previously demonstrated using dual gold film electrodes [123]. In some biosensor configurations, polyaniline has also been used as an amplifier to improve the detection process [124, 125]. In the next section, we will describe basic properties of the PANI and discuss the application PANI in biosensors.

5.3.1 Conducting Polymer: Polyaniline (PANI)

Conducting polymers were first discovered in 1976 by Alan MacDiarmid, Hideki Shirakawa, and Alan Heeger, when it was found that the conductivity of polyacetylene increased by up to 6 orders of magnitude when reacted with iodine (from 10^{-4} S/cm to 10^{2} S/cm) [126]. The phenomenon, known as doping, is a result of the formation of charge carriers. It was discovered that conducting polymers can exhibit different electrical properties from insulator, to semi-conductor, to mental. The presences of π-electron backbone in the conducting polymers result in their electronic properties, such as electrical conductivity, low ionization potential, and high electron affinity. Doping can be a control element for varying conductivity of the conducting polymers. This ability to tailor the polymer's electrical properties exemplifies the versatility of conducting polymers. There are a number of methods known to effect doping of conjugated polymers including chemical, electrochemical, photo-doping, charge-injection doping, and non-redox doping [127]. The most common method of doping is known as oxidative doping, where π electrons are removed from the conjugated π-systems via either chemical or electrochemical oxidation. The method results in a positively charged backbone with counter-ions in close proximity, held by Coulombic interactions. This method is also called as p-doping. N-doping, instead, injects electrons into π systems and increases the number of π electrons leading a negatively charged polymer. However, the oxidation doping is more stable than n-doping.

Polyaniline

Polyaniline is well-known as an environmentally stable and highly tunable conducting polymer. It exists in a variety of forms differing in electrical conductivity and color. The general chemical structure of polyaniline is shown in Fig.5.3. There are three distinct oxidation states of the polymer, namely, "leucoemeraldine", "emeraldine", and "pernigraniline". The fully reduced form of polyaniline is "leucoemeraldine" (n = 1,

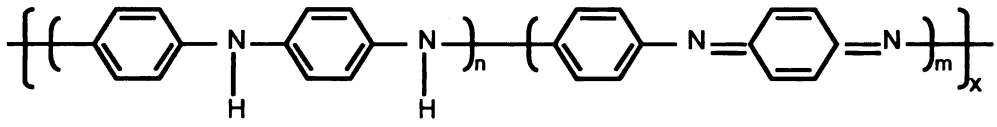

Figure 5.3: Structure of polyaniline, x = degree of polymerization, n + m = 1.

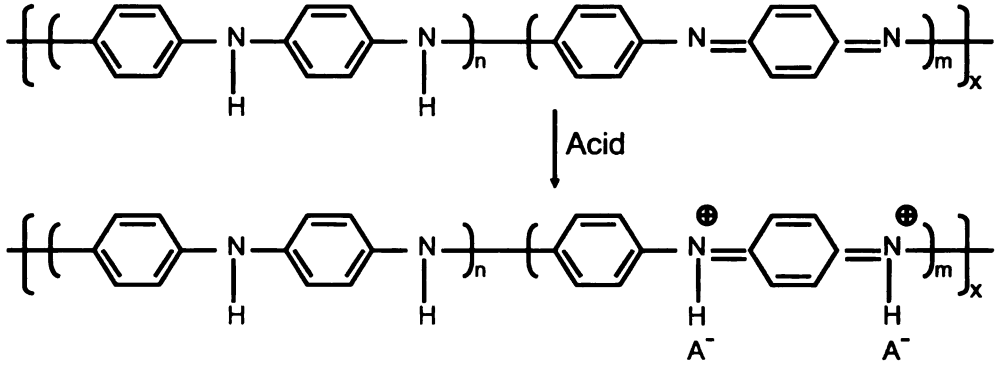

Figure 5.4: Neutral and doped polyaniline. A^- is an arbitrary anion, e.g., chloride.

m = 0), while "pernigraniline" (n = 0, m = 1) is the fully oxidized form of polyaniline and "emeraldine" (n = m = 0.5) is the 50% oxidized form of polyaniline [128]. Each oxidation state of the polymer can exist in its base form or its protonated form (salt) by treatment of the base with acid.

A more common method of producing doped polyaniline is known as acid-doping (or proton-doping). This method is a non-redox in the sense that the number of π electrons in the backbone chain is unchanged. As with the oxidative doping process, doped polyaniline may be produced in one step. The presence of the acid treatment results in the protonation of nitrogen atoms. The polymer chain is positively charged and has associated counter-anions once protonated. The degree of protonation depends on the oxidation state of the polymer and the pH of the acid solution [129]. The relative number of imine and amine nitrogen atoms depends on the oxidation state of the polyaniline (see Fig.5.4), and being more basic, the imine sites are more readily protonated than the amine sites.

Undoped polyaniline exhibits conductivity on the order of 10^{-10} S/cm; as with

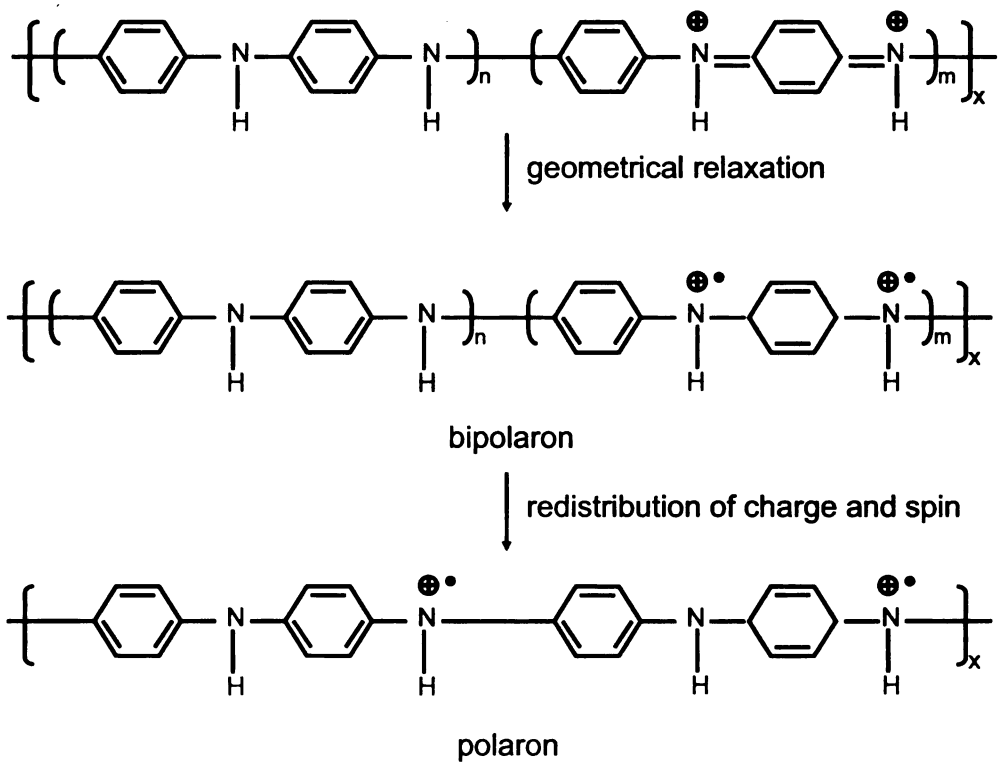

Figure 5.5: Polyaniline Charge Carriers: Bipolarons and Polarons.

oxidative doping, protonic, or acid, doping can result in a significant increase in conductivity (up to 10 S/cm - 11 orders of magnitude) [130]. The actual charge carriers are not as depicted in Fig.5.4. Once protonation of the imine nitrogen atoms has occurred, geometrical relaxation quickly follows and results in a quinoid to benzenoid transition (see Fig.5.5), yielding what is known as a bipolaron. The bipolaron charge carrier is of higher energy, and thus is short-lived. Redistribution of charge and spin yields a polaron as the more stable charge carrier [126]. The relative stability of the polaronic structure is attributed to a number of factors including charge separation (reduction in Coulombic repulsions) [131], and gain of resonance energy [132].

The most common synthesis of polyaniline involves oxidative polymerization, in which the polymerization and doping occur concurrently. There are two basic methods of polyaniline synthesis: chemical synthesis and electrochemical synthesis. The

chemical synthesis involves step-growth polymerization of an aqueous solution of the monomer in the presence of an oxidizing agent and a protonating acid. In the aqueous acidic media, aniline cation radical is the first product of the oxidation. The aniline cation radicals then recombine into benzidine and N-phenyl-p-phenylenediamine, or, participate in the growth of polyaniline chains in the pernigraniline form. Electrochemical synthesis of polyaniline is carried out in a typical electrochemical bath by adopting a standard three-electrode configuration. The standard three-electrode system usually comprises of a working electrode, a counter electrode and the reference electrode. The electrochemical polymerization generally employs a constant current or galvanostatic, constant potential or potentiostatic or potential scanning/cycling methods. The commonly used working electrodes are chromium, nickel, gold, platinum, palladium and glass coated with tin oxide or indium tin oxide. Electrochemical methods tend to have lower yields than chemical yields [133].

PANI Based Biosensors

Conducting polymers such as polyaniline have gained popularity in biosensor applications because of the following reasons: first, conducting polymers have flexibility in their chemical structure which allows modulation of the required electronic and mechanical properties of the polymer. Second, conducting polymers act as suitable substrate for biomolecules immobilization providing suitable environment [134]. PANI nanofibril networks have been reported to be employed as highly sensitive single cell biodetectors [135]. Third, conducting polymers can be deposited onto electrode surfaces which provide them with the versatility of being used in diverse biosensor platforms. Lastly, conducting polymers have been associated with efficient transfer of electric charge produced by biochemical reaction to electronic circuits [136]. Recently, conducting polymers have been used in numerous biosensing applications, such amperometric, potentiometric, conductometric, optical, calorimetric and piezo-

electric biosensors. Literature also shows the use of a wide variety of biomolecules in the conducting polymer based biosensors which range from enzymes, microorganisms, antibodies to nucleic acids [137]. Conducting polymer based biosensors can also serve the pressing requirements of in vivo sensing, multi-analyte assays, continuous drug monitoring, and high information-density biosensing. Beside those advantages mentioned above, conductive polyaniline nanowires based immunosensors are also relatively inexpensive to fabricate and easy to operate which makes it an ideal candidate for multi-array architecture.

5.3.2 Membrane based Lateral Flow Immunoassay (LFI)

Lateral flow immunochromatographic (LFI) assay is our first modified platform to discover FEC biosensor encoder, so we first describe its basic structure and principle. LFI is a user-friendly biosensor format that has following advantages: short diagnostic time, long-term stability, and relatively inexpensive to make. These features make strip tests ideal for applications such as home testing, rapid point of care testing, and testing in the field for various environmental and agricultural analytes. The principle behind the test is straightforward and will be discussed in great depth below.

Fig. 5.6 shows a popular sandwich format on a LFI assay and it is used when testing for larger analytes with multiple antigenic sites. In this case, less than an excess of sample analyte is desired, so that some of the microspheres complex will not be captured at the capture line, and will continue to flow toward the second line of immobilized antibodies, the control line. This control line uses species-specific anti-immunoglobulin antibodies, specific for the conjugate antibodies on the microspheres.

Normally, the membranes used to hold the antibodies in place are made up of primarily hydrophobic materials, such as nitrocellulose. Both the microspheres used as the solid phase supports and the conjugate antibodies are hydrophobic, and their interaction with the membrane allows them to be effectively dried onto the membrane.

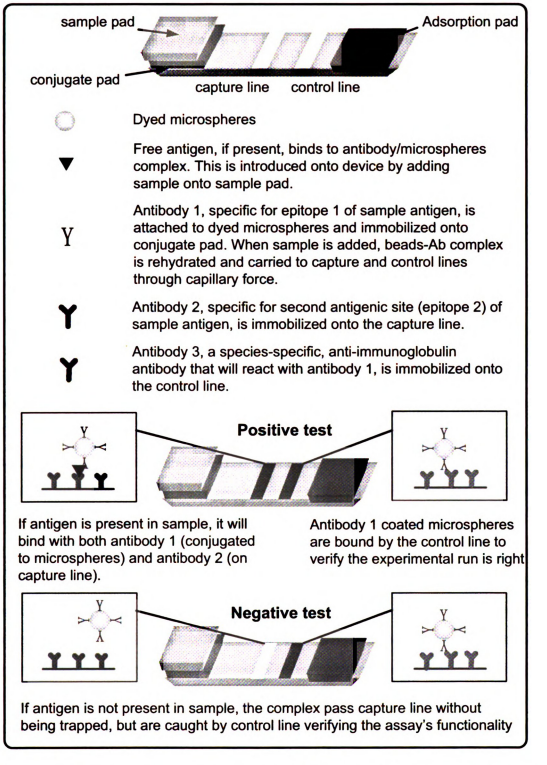

Figure 5.6: The structure and operating principle of a lateral flow immunochromatographic assay.

For lateral flow test strips, the membrane must irreversibly bind capture reagents at the capture and control lines. The polymer from which the membrane is made determines most of its binding characteristics. If the membrane undergoes a secondary process that chemically alters the polymer or buries it under a second polymer, protein binding properties may be dramatically altered [138]. Typical polymers and their binding properties are presented in Table. 5.1.

Table 5.1: Binding properties of different membrane polymers

Membrane Polymer	Primary Binding Mechanism
Nitrocellulose	Electrostatic and hydrophobic
Polyvinylidene fluoride	Hydrophobic
(Charge-modified) nylon	(Ionic) electrostatic
Polyethersulfone	Hydrophobic

A membrane's protein binding capacity is determined by the amount of polymer surface area available for immobilization. The membrane's surface area is determined by pore size, porosity (amount of air in the three dimensional structure), thickness, and, to a minor extent, structural characteristics unique to the polymer. All other parameters being equal, surface area decreases nonlinearly with pore size, increases linearly with thickness, and increases nonlinearly with porosity [138].

Nitrocellulose membrane may be the most popular membrane used in lateral flow devices and it will be adopted by our study. Nitrocellulose membranes bind proteins electrostatically through interaction of the strong dipole of the nitrate ester with the strong dipole of the peptide bonds of the protein. Nitrocellulose membranes are completely neutral with no acidic protons. Although their ability to adsorb protein is independent of the pH of the immobilization solution, pH can affect the immobilization efficiency of a particular protein by altering its properties in solution. Proteins maybe lost from the membrane during processing particularly if buffer contains nonionic detergents. It is important to check the surface treatment used for fixation

(e.g., glutaraldehyde and cross-linking) do not destroy the antigenic epitope. These treatments can also attribute to the brittleness of nitrocellulose membrane. We will discuss those fabrication considerations in detail in the next sections.

Protein Binding

In immunochromatographic assays, the main function of a protein applied to a membrane is to act as a capture reagent for the target analyte in a sample. The importance of achieving a high and consistent level of protein binding cannot be over-stressed because the device performance is totally dependent on achieving a good binding of the capture reagent to the membrane. It has been known that a number of forces are at work during the binding between protein and the membrane-specifically, hydrophobic interactions, hydrogen bonding, and electrostatic interactions. There are two reasonable models have been proposed to explain the interaction force involved during the binding event.

The first model states that proteins are initially attracted to a membrane surface by electrostatic interaction, while long-term attachment is accomplished by a combination of hydrogen bonding and hydrophobic interactions [139]. A second model suggests that the initial attachment of the protein is by hydrophobic interactions, with long-term binding accomplished by electrostatic forces [138]. Both models agree with much of published data. However, the first model is often the widely accepted mode while the second model may not provide a full explanation for the long-term stability conferred on protein attachment by drying or the use of an alcohol fixation step.

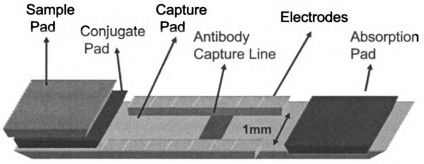

Figure 5.7: The structure of a PANI based lateral flow immunosensor.

5.3.3 Polyaniline Based LFI

Structure and Principle

The architecture of a PANI based lateral flow immunosensor is shown in Fig. 5.7. We can see that it is a modification from a typical LFI. In the modified structure, antibody 1 and antibody 2 are same and the control line is omitted for simplicity. In typical lateral flow immunochromatographic assay, dyed microspheres are used as a transducer for optical detector. In our study, we will use polyaniline nanowire as a transducer and then modify the LFI as a conductometric biosensor. It is also composed of four different pads: sample pad, conjugate pad, capture pad, and absorption pad. The antibody region (capture pad) constitutes a biomolecular switch triggered by specific antigens present in the analyte. The principle of operation of a single biomolecular switch is illustrated in Fig. 5.8, which shows a cross-sectional view of the immunosensor. Before the sample solution is applied, the gap between the electrodes in the capture pad is open. Immediately after the sample solution is applied to the sample pad, the solution containing the antigen flows to the conjugate pad, dissolves with the polyaniline-labeled antibody (Ab-P) and forms an antigen-antibody-polyaniline complex. The complex is transported using capillary action into the capture pad containing the immobilized antibodies. A second antibody-antigen reaction occurs and forms a sandwich. Polyaniline in the sandwich then forms a molecular wire and

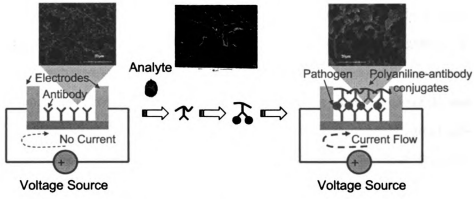

Figure 5.8: The operation principle of polyaniline based lateral flow immunosensor.

bridges two electrodes. The polymer structures extend out to bridge adjacent cells and leads to conductance change between the electrodes. The conductance change is determined by the number of antigen-antibody bindings, which is related to the antigen concentration in the sample. The unbound non-target organisms are subsequently separated by capillary flow to the absorption membrane. The conductance change is sensed as an electrical signal (current) across the electrodes. In Fig. 5.8 we also show SEM images of the capture pad before and after the analyte with pathogen has been applied. The change in material texture can be observed in Fig. 5.8, which is attributed to the formation of the antibody-antigen-antibody-polyaniline complex connecting the electrodes.

Fabrication

Purified rabbit polyclonal antibodies against *B. cereus* and *E. coli* were obtained from Meridian Life Science (Saco, ME, USA). The antibodies were suspended in phosphate buffer solution (pH 7.4) and stored at 4^oC. *B. cereus* and *E. coli* strains were obtained from the National Food Safety and Toxicology Center (Michigan State University) and the Michigan Department of Community Health (East Lansing, MI, USA). A 10 μL loop of each isolate was cultured in 10 mL of nutrient broth and incubated for 24

hours at 37^oC to prepare stock cultures. The stock cultures were serially diluted with 0.1% peptone water to obtain varying concentrations of each microorganism. Polyaniline was purchased from Sigma-Aldrich (St. Louis, MO, USA). All experiments were carried out in a certified Biological Safety Label II laboratory. The sample pads (size: 15mm x 5mm) and absorption pads (size: 20mm x 5mm) were made of nitrocellulose membrane (flow rate: 135s/4cm) and the conjugate pads (size: 10mm x 5mm) were made of fiberglass membrane (grade G6). The porous nitrocellulose substrate ensures good adsorption properties for immobilized antibodies and allows non-target antigens to flow through. The electrodes were patterned using aluminium paste and provided electrical connection between the nitrocellulose membrane and a data acquisition system. The conjugate pad was designed to allow maximal adsorption and flow of polyaniline-conjugated antibodies. Antibody concentration used for conjugate pad was 150 μg/ml and for the capture pad was 500 μg/ml. The polyaniline concentration in the conjugate pad was 1 mg/ml. All these values were found to be optimal, resulting in the highest ratio between the number of captured cells and the actual cell concentration tested. The immunosensors were then attached to an etched copper printed circuit board (PCB) which was used to connect to the multi-channel potentiostat array.

The polyaniline-multi-variate antibodies (PMA) conjugates were prepared by suspending 800 μL of polyclonal antibodies against *B. cereus* and *E.coli* (concentration 150 μg/mL) in a 4 ml of polyaniline solution in phosphate buffer (pH 7.4) containing 10 % dimethylformamide (DMF) (v/v) and 0.1 % LiCl (w/v). LiCl can maintain the stability of polyaniline while too much ionic strength can hurt the protein binding in the membrane. So we have to choose minimum ionic strength as sufficient stabilizer and we will discuss those issues in detail in next section. The solution was incubated at room temperature for 1 hour to allow binding of the antibodies with polyaniline and then treated with a blocking reagent (Tris buffer containing 0.1%

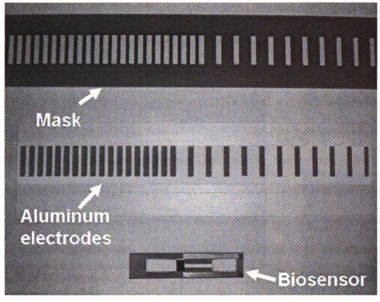

Figure 5.9: The prototype of polyaniline based immunosensor and the mask for making electrodes.

casein). The polyaniline-multi-variate antibody conjugates were then precipitated by centrifugation at 12,000 rpm for 5 min. The supernatant fluid was discarded and the pellets were mixed with the blocking reagent and centrifuged again. The centrifugation step was repeated three times. The conjugates were finally suspended in phosphate buffer solution containing 0.1 % LiCl (w/v) and 10 % DMF (v/v) and stored at 4^oC until used. The conjugate pads were prepared by soaking the fiberglass strip into the PMA solution until a homogenous dispersion is achieved. Extensive characterization of a single strip, single pathogen biosensor has been performed elsewhere [120, 140, 141, 142]. We have tried different methods for patterning silver electrodes onto the membrane. The simplest method is to use silver dispenser pen to hand draw two electrode line along the substrate. But it is time consuming and it suffer inconsistent performance. Another methods we have used is metal evaporation and Fig. 5.9 shows the mask for patterning electrodes on the nitrocellulose membrane using metal evaporation and a prototype of the fabricated immunosensor.

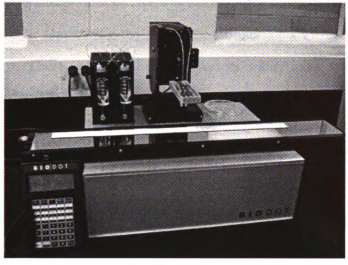

(a)

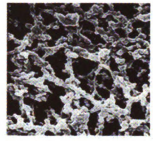

(b)

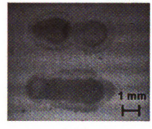

(c)

Figure 5.10: (a). Biodot dispersing machine for dispersing antibody onto the nitrocellulose membrane. (b). the SEM image of nitrocellulose matrix. (c). The dispersed antibody on the membrane.

With tapped the mask onto the membrane, evaporated silver will deposit onto the uncovered places on the membrane using metal evaporation machine, leading to a desired electrode pattern. The advantages of this method include automated procedure resulting in smaller variance, time-saving, and configurable format. After patterning silver electrodes on the nitrocellulose membrane, antibodies are dispersed onto the membrane to form the capture line using Biodot dispersing machine, which is shown in Fig. 5.10(a). Also shown in the figure are the SEM image of the nitrocellulose matrix (Fig. 5.10(b)) and the patterned antibody drop (in dyed green color) on the membrane (Fig. 5.10(c)).

Development Considerations

Fabricating good lateral flow immunoassay is a difficult task although the principle is simple. There are many factors which are involved to affect the performance of

lateral flow devices. We will discuss some of key factors and solutions in this section.

1. Optimizing the Application Buffer

There are several critical factors which have an effect on the protein binding onto the nitrocellulose membranes. Developers of lateral flow device often ignore the importance of optimizing reagents, which can greatly affect the protein binding. The proteins used as capture reagents vary from test to test. The optimization is straightforward if monoclonal antibodies are used while the process is more difficult in the case of polyclonal antibodies due to the presence of many epitopes. During the process of optimizing application buffer, we have to make sure solubility of the protein and the stability of the protein molecules are both well maintained. In some cases, adding some ions into the application buffer can promote solubility of the protein. However, strong ionic strength in the buffer could interferes with electrostatic interactions of protein binding [138]. As the molarity of the capture reagent solution increases, the amount of solid residue left on the membrane also increases, which affect wetting property of the membrane. We will discuss with this issue later on. Typically, the molarity of the buffer should be lowered to the minimum required to maintain a stable pH (<10 mM). As suggested in [138], the use of buffered saline solution is generally not recommended. Also, the increase of ionic strength can cause precipitation of proteins thus affecting the sensitivity and stability of the test [143, 144, 145, 146]. Choosing an optimal application buffer with proper ionic strength is a key for the device's performance.

Surfactants and detergents can affect protein adsorption if their concentration in the membrane is too high. Tween 20, Triton X-100, glycerin, polyvinyl glycol (PEG) can reduce protein binding by adsorpting to the membrane preferentially or forming a complex with a protein molecule before it adsorbs [138]. The concentration of those reagents should be kept as low as possible(<0.05% v/v for Tween and Triton, <0.1% v/v for glycerin).

Choosing pH in the capture reagent buffer is also crucial. Most antibodies have isoelectric points between pH 5.5 and 7.5. Using a buffer at pH 7.0-7.5 is close to optimal and practically the choose of pH is empirical.

The addition of a small amount of alcohol (1% to 10% v/v methanol, ethanol or isopropanol) can be helpful to improve the consistency of reagent application by lowering solution viscosity because it lowers surface tension. It can also enhance the drying and protein fixation process.

2. Non-specific Binding

Nonspecific binding can happen if non-target proteins bind with probes or nitrocellulose substrate. To reduce the non-specific binding with the membrane substrate, blocking agents such as bovine serum albumin (BSA) and some surfactant (Tween 20, Triton X-100, or sodium dodecyl sulfate (SDS)) have been used [147]. After the membrane has been blocked using blocking agents, it is important to remove unadsorbed blocking agent by washing with a weak buffer (e.g., 5 mM Na_2HPO_4, pH 7.5).

3. Optimizing Membrane Flow

The capillary flow rate is the speed at which a sample front moves along a membrane strip when liquid is introduced at one end [138]. The sensitivity of lateral flow immunoassay increases with the decrease flow rate. Also, the apparent concentration of the analyte increases as the flow rate decreases. Because nitrocellulose membranes are naturally hydrophobic and the wicking of water into a nitrocellulose membrane is due to the presence of interstatial moisture [148], the hydrophobicity of the membrane can cause the following problems: First, nonspecific interaction of a hydrophobic analyte with the membrane can generate significant nonspecific signal. Second, wetting technique is needed because the rate of rewetting and lateral flow can be too low for rapid test. Third, loss of interstatial moisture can cause long-term storage difficulties. Blocking agent is one of solutions to reduce or eliminate these problems.

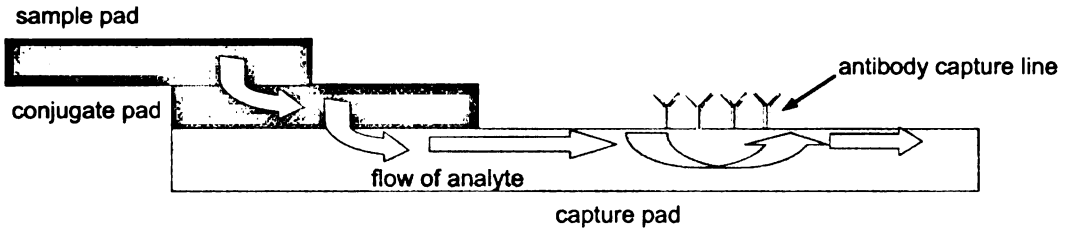

Figure 5.11: Illustration submarine phenomena due to uneven capture line wetting.

Ideally, they should simultaneously reduce the level of nonspecific background staining, remain bound to the membrane during prolonged storage, and achieve even and consistent rewetting upon sample application at a rate appropriate to the assay being developed [149].

4. Membrane Wetting

One of problems during the LFI fabrication is uneven hydrophobicity of the membrane. During the test, different solutions might flow through the membrane and the distribution of water-soluble residues may not be even. Any variations in the character or concentration of these residues will affect the rewetting rate of the membrane. The uneven rewetting of the capture line can greatly affect the performance of lateral flow immunoassays. We have met this problem during our research and one phenomena called "submarining" occurs. Because capture line is more hydrophobic than the surrounding membrane, so the sample solution by the capillary force was stopped by the capture line. Some of analyte may then run along the plastic support of the membrane (which is more hydrophilic) and then reenter the membrane above the capture line where the membrane is more hydrophilic. Fig. 5.11 describes this phenomena and it results in a capture line that has no or very little sample penetration, which affects test sensitivity and selectivity.

The solution to uneven hydrophobicity is to introduce a rewetting agent, a hydrophilic material added during process. Studies have shown that pretreating a nitrocellulose membrane with carefully selected rewetting agents can efficiently solve

problems caused by hydrophobicity and membrane storage [150]. Introduction of a certain surfactant to the buffer can also ensure the capture line is in an evenly hydrophilic environment. A low-concentration (0.1%) SDS or sodium dodecylbenzolylsulfonate solution is a typical one. In [150], blocking agents have been used as a method to even membrane rewetting.

5.3.4 Characterization of Single Biomolecular Transistor on a PANI based LFI

We have fabricated and characterized the response of a single biosensor (biomolecular transistor) using *B. cereus* antibody with respect to different pathogen concentrations. Data acquisition card NI-6221 was used to record continuous conductance across the two electrodes of biosensor. Fig. 5.12 shows the measured conductance across the biosensor electrodes as the concentration of pathogen (*B. cereus*) in the sample is varied. The measured conductance is normalized with respect to the "control" conductance (measured when a sample containing no pathogens is applied) and shows a clear discrimination between pathogenic and non-pathogenic cases. The plot in Fig. 5.12 also shows a monotonic increase in conductance with an increase in pathogen concentration (given in colony forming units per milliliter-CFU/mL). This response can be approximated using a log-linear model (shown by a dotted line in Fig. 5.12) and the regression error is used to approximate the systematic error. The Fig. 5.12 also shows error bars computed using multiple experimental runs and they are used for estimating the random errors.

A log-linear model is given by

$$G(X_B) = G_0 + \kappa \log \frac{X_B}{X_0} + G_n \tag{5.2}$$

where X_B represents the concentration of the pathogen *B. cereus* in CFU/ml, G_0

represents the "control" transconductance, κ represents sensitivity factor, and X_0 is a detection constant. Note that equation 5.2 is valid only for $X_B \geq X_0$, which is a reasonable assumption. The systematic and random errors are included as the additive noise component G_n in the equivalent circuit model of the biomolecular transistor (shown in Fig. 5.13). Based on this large signal model, it can be shown that a single biosensor acts like a "pathogen concentration" controlled resistor that is similar to an operation of a MOSFET transistor biased in weak-inversion [151]. The circuit model is important because we use setup a library of circuit models to mimic the behavior of biomolecular transistors. Another application of the biomolecular circuit model could be the development of computer-aided design (CAD) tools which can assist biosystem engineers to pattern and test biosensors in a virtual environment. Traditionally biosensor experiments are very time consuming, labor extensive, and are expensive. With our developed computational and electrical models, the building blocks can be configured, connected in arbitrary fashion and tested using computer simulations.

Limitations of the log-linear model in equation 5.2 in predicting the pathogen concentration will arise due the "hook effect", a common phenomenon observed in most biosensors where the conductance decreases with increase in pathogen concentration. The "hook effect" is typically attributed to the presence of large concentration of pathogens, leading to saturation of binding sites and obstructing charge transfer within the conductive polyaniline structure. For instance, in [121] the "hook effect" was observed at concentrations above 10^4 CFU/mL for biosensor electrode spacing of approximately 0.5 mm. In our experiments, the electrodes are spaced approximately at 1 mm which therefore the "hook effect" was not observed, possibly at the expense of reduced sensitivity factor.

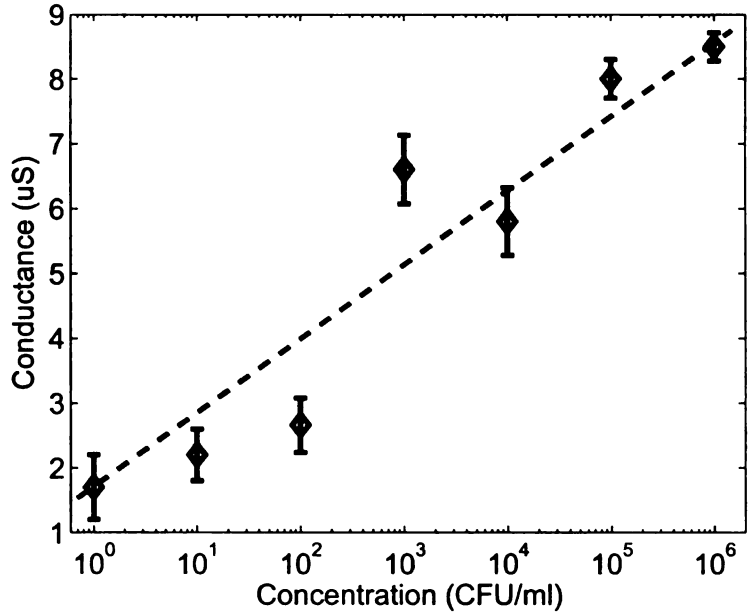

Figure 5.12: Conductance measurement of *B. cereus* single biomolecular transistor.

5.3.5 Fabrication and Characterization of Logic Gates

The biosensor principle was then extended to implement two variants of logical operations (AND and OR) in [140]. Fig. 5.14 shows the structure of an AND gate (marked by 1) and and OR gate (marked by 2) constructed using the antigen-antibody-polyaniline complex. An AND operation is achieved by cascading two different antibodies in between the biosensor electrodes. Thus, in an ideal condition, conduction between the electrodes occurs only when both of pathogens are present in the sample (for completing the polyaniline bridge as shown in Fig. 5.14 (1)). An OR operation is achieved by immobilizing a mixture of antibodies between the electrodes. Thus, in an ideal condition a polyaniline nanowire bridge is formed when either one of the antigen is present. We have successfully fabricated and characterized biomolecular logic gates based on the principles described above [140].

Fig. 5.15 and 5.16 show the transient responses measured using the fabricated AND and OR logic gates. They measure four different states when only *E. coli*,

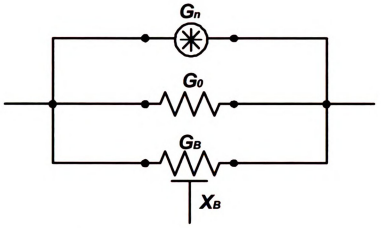

Figure 5.13: The circuit model of single biomolecular transistor.

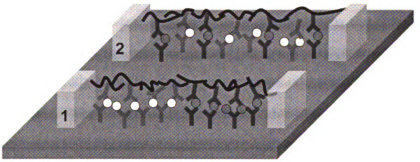

Figure 5.14: Schematic illustration of biomolecular logic gates. (AND gate (marked by 1), OR gate (2)).

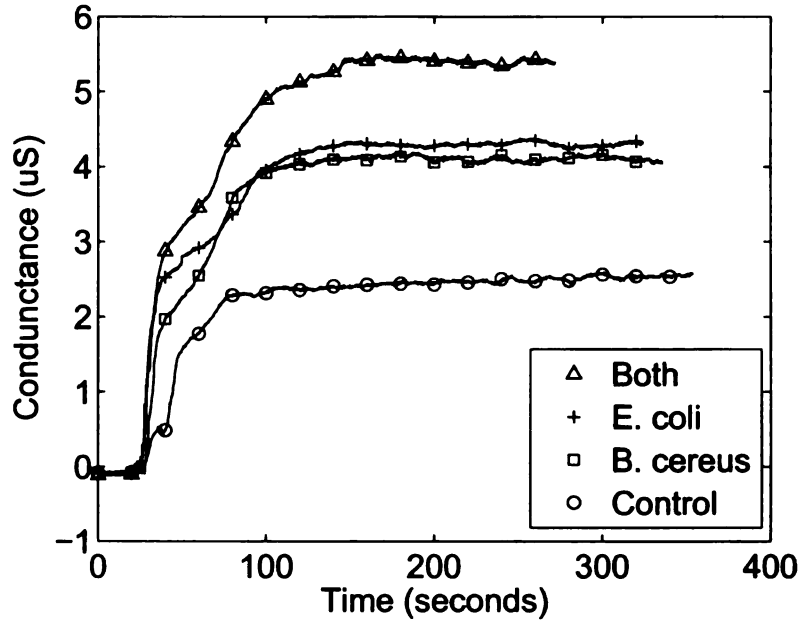

Figure 5.15: Typical transient response of AND gate.

only *B. cereus*, both pathogens, and no pathogens (control) exist. The calibrated concentration of *E. coli* and *B. cereus* are 6.3×10^7 CFU/mL and 5.03×10^7 CFU/mL respectively. The conductance measured across the electrodes stabilizes around 100 seconds after the application of the analyte and it constitutes the steady-state of the biosensor logic gate. The transient behavior is attributed to the dynamics of the polyaniline sandwich in the presence of analyte flow, adhesion and capillary force. However, in this study only the steady-state conductance will be used for modeling and derivation of transient models is deferred for future publications.

Fig. 5.17 shows the response of an AND gate corresponding to different pathogen concentrations, where E represents *E. coli* and B represents *B. cereus*. The conductance of biosensor is measured for two sets of pathogen concentration and for four possible logic conditions (E = 0, 1 and B= 0, 1) where a binary state represents the absence or presence of a pathogen. The measured conductance are compared against a "control" response that represents the logic condition E=0, B=0. It can be seen

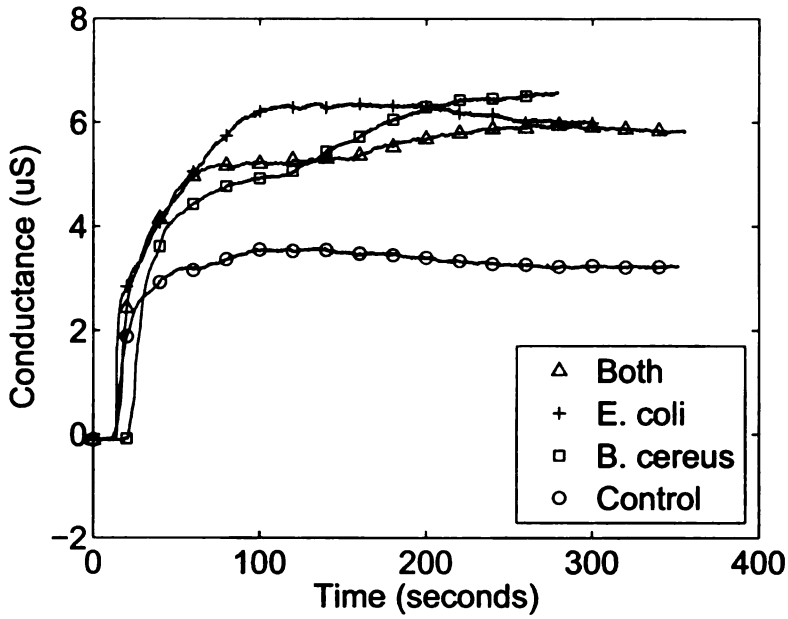

Figure 5.16: Typical transient response of OR gate.

from Fig. 5.17 that the measured conductance for logical condition (E = 1, B = 1) is higher than all other cases (irrespective of pathogen concentration) which corresponds to a soft AND operation. However, Fig. 5.17 also shows that the measured conductance, when only *B. cereus* is present, is close to the condition when both *B. cereus* and *E. coli* are present. This artifact could be attributed to the imperfect antibody masking in the fabrication procedure which led to signal leakage across the electrodes. Fig. 5.18 shows the measured conductance for a biosensor acting as an OR logic gate. The plot shows that for both pathogen concentration levels, the "control" condition (E=0, B=0) leads to a lower conductance as compared to other logical states. Therefore the response of the biosensor is equivalent to an OR logic. Also note that OR logic is easy to pattern (no masking required), therefore leading to near ideal operation as compared to an equivalent AND gate. The response of the logic gates for different concentration of pathogens is shown in Fig. 5.17- 5.18 and have been used to derive their equivalent circuit models that incorporate the inherent

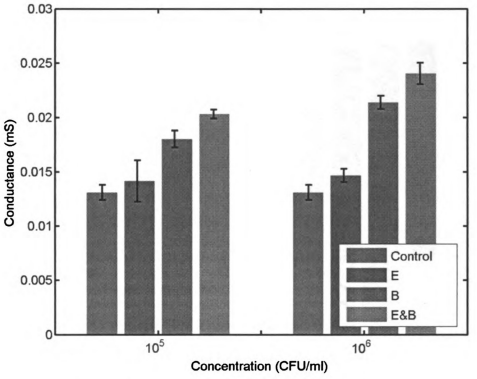

Figure 5.17: Conductance measurement of AND gate.

noise sources.

The corresponding circuit models for OR and AND gates are shown in Fig. 5.19 and their respective mathematical responses are provided below.

$$G(X_B, X_E) = G_{OR} + \kappa_B^{OR} \log \frac{X_B}{X_{0B}^{OR}} + \kappa_E^{OR} \log \frac{X_E}{X_{0E}^{OR}} + G_n \tag{5.3}$$

$$G(X_B, X_E) = G_{AND} + \kappa_B^{AND} \log \frac{X_B}{X_{0B}^{AND}} + \kappa_E^{AND} \log \frac{X_E}{X_{0E}^{AND}} + \kappa_{EB}^{AND} \log \frac{X_E + X_B}{X_{0EB}^{AND}} + G_n \tag{5.4}$$

Table 5.2 summarizes the meaning and typical values of the model parameters that have been extracted using the measured results and have been used for simulations

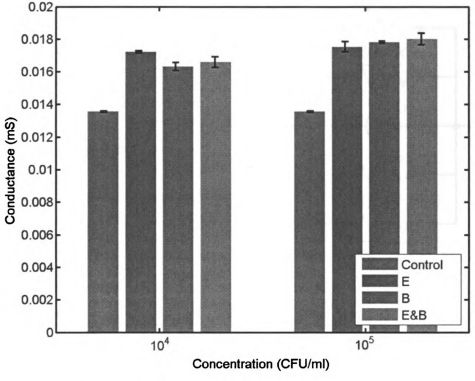

Figure 5.18: Conductance measurement of OR gate.

presented in next following chapters.

We have shown that LFI can be modified to fabricate biomolecular logic gates, which will be used in a biosensor encoder. However, fabricating AND gate is a pain due to the constraints of the biosensor structure and principle. In the next study, we will discover another biosensor platform that greatly improve the performance of biomolecular logic gates.

5.3.6 Membrane based LFI Biosensor Encoder

As the Fig. 5.1 shows, the biomolecular encoder has to be constructed in the biosensor structure, being able to provide redundant information. However, it depends on the types of logic functions that can be achieved by bimolecular logic gates. We will first

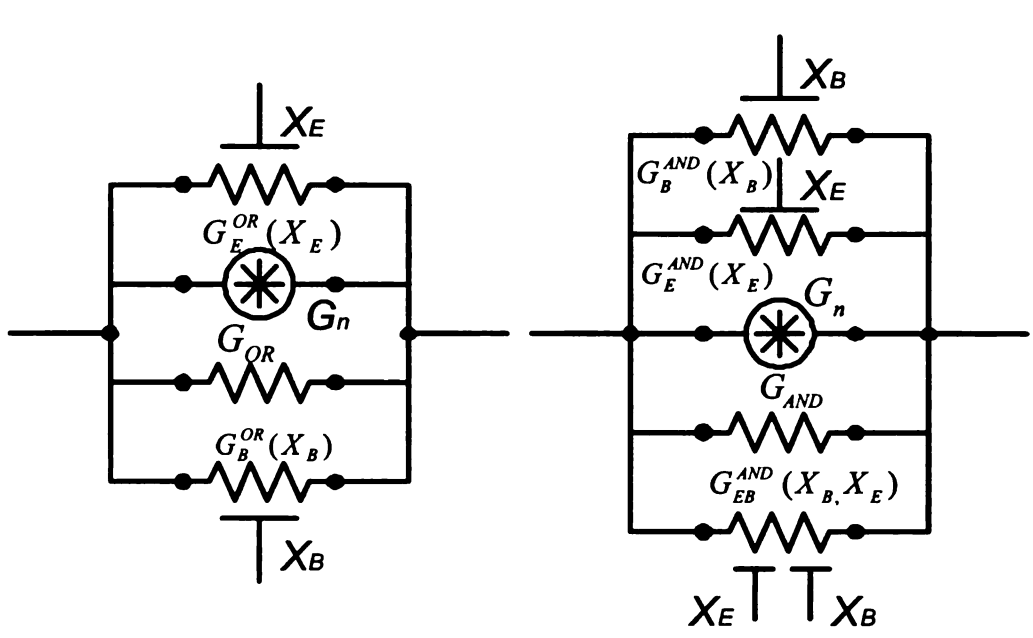

Figure 5.19: The circuit model of OR and AND gates.

discuss possible encoding methods that can be applied in biosensors. The simplest encoding method is the "repetition" code where biomolecular transistors that detect single pathogen are replicated multiple times. One could get more accurate estimation when using majority voting rule. For example, biomolecular transistors specific to two model pathogens *B. cereus*and *E. coli* are replicated three times respectively. In this case, $X_1, .., X_6$ will be used to represent the boolean variables corresponding to output of each of the biomolecular transistor. The resulting encoder function $f(X_1, X_2, .., X_6)$ is summarized in Table 5.3. This encoder is denoted as a (6,2) repetition code which implies that six measurements are independently performed (sequentially or in parallel) to detect two possible pathogens.

Another form of the encoding function that will be the focus of this study uses the biomolecular OR and AND logic circuits. In conventional FEC codes used in communications and storage systems, a XOR operation is utilized to obtain linear codes which by construction are symmetric. Unfortunately, XOR logic using the proposed biosensor principle is un-realizable and hence our encoding (also referred to

Table 5.2: Parameter meaning and typical values of formula 3.1-3.3

Parameter	Meaning	Value
G_0	"control" transconductance	1.24 μS
κ	sensitivity factor	1.2 μS
X_0	detection constant	0.1 CFU/mL
G_OR	"control" transconductance	13.6 μS
κ_B^{OR}	sensitivity factor of *B. cereus*	0.15 μS
X_{0B}^{OR}	detection constant for *B. cereus*	0.76 μS
κ_E^{OR}	sensitivity factor of *E. coli*	0.09 μS
X_{0E}^{OR}	detection constant for *E. coli*	8.5×10^{-4} CFU/mL
G_{AND}	"control" transconductance	13.1 μS
κ_B^{AND}	sensitivity factor of *B. cereus*	3.4 μS
X_{0B}^{AND}	detection constant for *B. cereus*	$10^3 CFU/mL$
κ_E^{AND}	sensitivity factor of *E. coli*	0.45 μS
X_{0E}^{AND}	detection constant for *E. coli*	4.6×10^2 CFU/mL
κ_{EB}^{AND}	sensitivity factor of coupling effect	0.4 μS
X_{0EB}^{AND}	detection constant of coupling effect	1.2×10^3 CFU/mL
G_n	conductance induced by noise	variable

as an asymmetric code) function will only be based on OR and AND biomolecular circuits. We will discuss asymmetric code in detail in next chapter. One specific instance of a (6,2) encoder function is summarized in Table 5.4, where X_1, X_2 are boolean variables corresponding to the absence or presence of *B. cereus* and *E. coli*. The variable X_3 represents a logical OR operation between X_1 and X_2 and variable X_4 corresponds to a logical AND operation. The variables X_5 and X_6 are repetition of variables X_1 and X_2.

For the lateral flow immunoassay which was taken as a model biosensor in this study, the encoder can be realized by adding redundant paths for flow of analyte to-

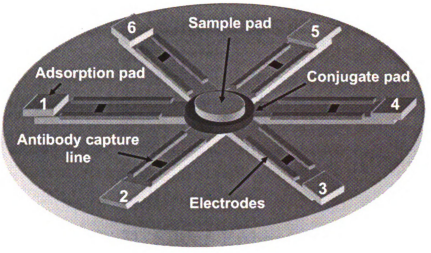

Figure 5.20: A visualization of multi-pathogen biosensor CD that could implement the encoding methods.

Table 5.3: (6,2) Repetition code

X_1	X_2	X_3	X_4	X_5	X_6
0	0	0	0	0	0
0	1	0	1	0	1
1	0	1	0	1	0
1	1	1	1	1	1

wards the biomolecular logic gates. One possible realization is illustrated in Fig. 5.20, where the sample is first applied to a sample pad and a conjugate pad where the pathogen-antibody-polyaniline complex is formed. The complex then splits into parallel flow paths and propagates to different antibody capture lines where the biomolecular logic gates/transistors are immobilized. Conductometric potentiostats [152, 153] are then used to measure the conductance across the electrodes of the biomolecular circuits. The measured conductance is then processed by a digital signal processor or analog decoder chip, which implements the factor graph decoding algorithm and flags the presence or absence of target pathogens.

Table 5.4: (6,2) Asymmetric code

X_1	X_2	X_3	X_4	X_5	X_6
0	0	0	0	0	0
0	1	1	0	0	1
1	0	1	0	1	0
1	1	1	1	1	1

5.4 Case Study II: Silver-Enhanced Gold Nanoparticle Based Biosensor Logic Gates

One of biggest challenges of designing FEC biosensors is to construct encoder into biosensor structure. During our experiments, there are some main problems in our first model logic gates. One is low signal-to-noise ratio due to the operation principle of lateral flow immunosensor coupled with the principle of conductometric measurement. Another big challenge is to pattern AND logic gate in the lateral flow immunosensor, which require that two cascaded antibody drops are within a 1 mm electrode gap. That turns out to be a difficult task since antibody solution will spread out on the nitrocellulose membrane. Those problems lead to experiment results with large variations. We now reported to explore gold nanoparticle based biochip, which can be used as an alternative platform for the FEC biosensor encoder. We have successfully functionalized and characterized a gold nanoparticle based biochip, and it has more sound principle and more repeatable results. Here we introduce the principle and some preliminary results. The structure of biochip is also easy to be modified to construct logic gates, which is shown in the following sections.

5.4.1 Introduction to Silver-Enhanced Gold Nanoparticle based Biochip

One of popular methods engaged in immunoassays is based on gold nanoparticles that are used as a label and a signal generator. However, the sensitivity of this approach is limited by resolution of the optical detector especially when the concentration of gold nanoparticles is very low [154]. However, the sensitivity of detection can be increased dramatically by using a procedure called "silver enhancement" where silver deposition occurs around nucleic sites formed by the gold nanoparticles. The core principle behind this technique is to grow silver micro-particles around nucleation sites formed by gold nanoparticles. The micro-particles can then be easily interrogated using optical techniques. Some examples of immunoassays using gold nanoparticles combined with silver enhancement have been demonstrated in [154, 155, 156, 157]. For instance, in [155] gold nanoparticle and silver enhancer solution have been employed in the immunoassay for detecting ricin with a detection limit of 100 pg/mL.

The silver enhancement principle, however, is ideal for conductometric biosensors which offer several advantages over their optical counterparts due to their reduced cost, reduced form factor and the ease of signal acquisition [158]. Silver enhancement can significantly improve the signal-to-noise ratio in a conductometric biosensor by suppressing the background interference and in the process can achieve detection sensitivities comparable or better than an optical based system. The conductometric biosensor reported in this study uses a biomolecular transistor that is constructed using functionalized gold nanoparticle on the high-density interdigitated microelectrode array. The interdigitated electrodes provide a large active area to facilitate binding between the analyte and the detection probe and hence have several advantages over non-interdigitated electrode arrays [156, 160]. We show that the response of the biomolecular transistor comprises of three distinct regions depending on the

formation of the conductive path between the electrodes. These three regions provide different modalities to measure and detect target analytes at different concentration levels. We then extend the functionality of the biomolecular transistor to construct logic gates (AND and OR) by patterning target specific antibodies at different spatial locations on the interdigitated microelectrode array.

5.4.2 Gold Nanoparticles

Gold nanoparticles typically have dimensions ranging from 1-100 nm and they generally are produced in a liquid by reduction of chloroauric acid ($H[AuCl_4]$), although more advanced and precise methods do exist. Fig. 5.21 shows the SEM image of synthesized gold nanoparticles in our lab. Gold nanoparticles display many interesting electrical and optical properties. First, they are good conductors and they are widely used in electronics and wiring. Second, gold nanoparticles can experience surface plasmon resonance in the visible portion of the spectrum. This means that a certain portion of visible wavelengths will be absorbed, while another portion will be reflected. The portion reflected will lend the material a certain color. Small gold nanoparticles absorb light in the blue-green portion of the spectrum (400-500 nm) while red light (700 nm) is reflected, yielding a dark red color. The wavelength of surface plasmon resonance related absorption shifts to longer wavelengths when the particle size increases. Red light is then now adsorbed, and bluer light is reflected, yielding particles with a pale blue or purple color. As particle size continues to increase toward the bulk limit, surface plasmon resonance wavelengths move into the IR portion of the spectrum and most visible wavelengths are reflected. This gives the nanoparticles clear or translucent color [161].

Those interesting properties enable gold nanoparticles become as drug carriers [162] and useful tool for cancer research. In [163], gold nanoparticles have been reported to be used for tumor detection. To specifically target tumor cells, the pegylated gold

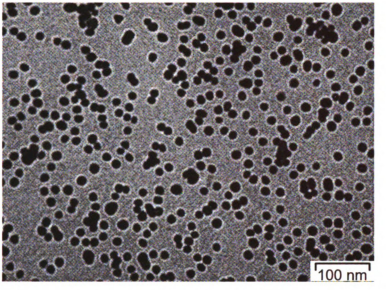

Figure 5.21: The SEM image of gold nanoparticles.

particles are conjugated with an antibody against epidermal growth factor receptor (EGFR). Using Surface Enhanced Raman Spectroscopy (SERS), these pegylated gold nanoparticles can then detect the location of the tumor.

5.4.3 Principle of Silver Enhancement

The principle of conductometric detection is shown in Fig. 5.22 where initially probes specific to the target molecules are immobilized in the regions between two electrodes. When the analyte is applied, the target biomolecules hybridize with the specific probes. The secondary antibodies conjugated with gold (Au) nanoparticles are then applied to the biochip, which leads to the formation of a sandwich array as shown in Fig. 5.22 (A). This configuration is denoted as the "cut-off" region since the current measured between the electrodes (for a fixed potential difference) is small. In the next step of the silver enhancement procedure, the active component (with gold nanoparticles) of the biochip is exposed to a solution of Ag(I) and hydroquinone (photographic developing solution). The gold nanoparticles act as a catalyst and reduce

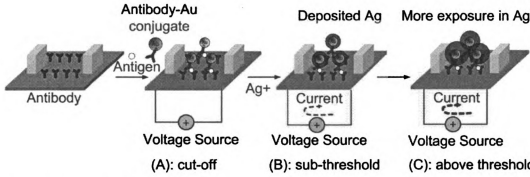

Figure 5.22: The operation principle of silver enhanced gold nanoparticle based biochip.

silver ions into metallic silver in the presence of a reducing agent (hydroquinone). The reduced silver then deposits on the gold surface, thus enlarging the size of the gold nanoparticles. As the size of the silver islands grow, they provide shorter paths for electrons to hop between the electodes. The region of operation when the distance between the elecrodes has not been fully bridged by the silver islands is the sub-threshold region (see Fig. 5.22 (B)). With the increase in enhancement time, the consistent growth of silver-enhanced particles completely bridges the area between the electrodes. Under this condition, the device enters the above threshold region of operation where a flow of current can be measured when a fixed potential is applied between the electrodes (Fig. 5.22 (C)). The time required for the device to reach the threshold from the cut-off region is known as the transition time. In this paper, we use the sub-threshold and above-threshold characteristics of the device for conductometric measurement of the concentration of the target biomolecules.

5.4.4 Biochip Fabrication and Surface Modification

The procedure for fabricating high-density interdigitated microelectrodes is described in detail in this section. The biochips were fabricated from 4″ silicon wafers (p-type 100, thickness 500-550 μm). A 2 μm thick layer of thermal oxide was grown

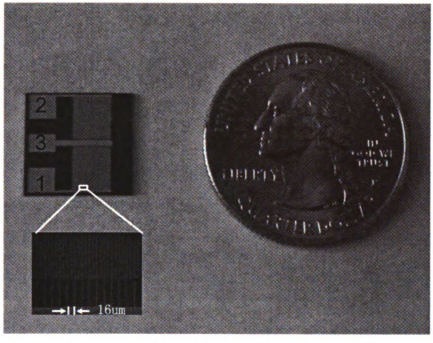

Figure 5.23: The high-density interdigital microelectrode biochip.

over the silicon to serve as an insulator between the electrodes and the substrate. Photolithography was used to pattern photoresist, metal electrodes were deposited by the evaporation of 10 nm of chrome under 100 nm of gold and a lift-off process was used to develop the interdigitated electrode array. Fig.5.23 shows the high-density interdigitated electrodes biochip fabricated using a standard MEMS technology. Each electrode finger has a length of 5000 μm, a width of 5 μm and an inter-electrode spacing of 6 μm.

The surface of biochips was then modified for immobilizing the antibody. The chips were first immersed in acetone in a crystallizing dish for 10 min to dissolve away the protective PR layer. The chips were then treated with 1:1 mixture of concentrated methonal and hydrochloric acid for 30 min followed by immersion into boiling distilled water for 30 min. The biochips were allowed to air dry completely. The cleaning and drying of the biochips are now ready for silanization where it occurred in an anaerobic glove box. The biochips were immersed in a crystallizing dish containing a solution

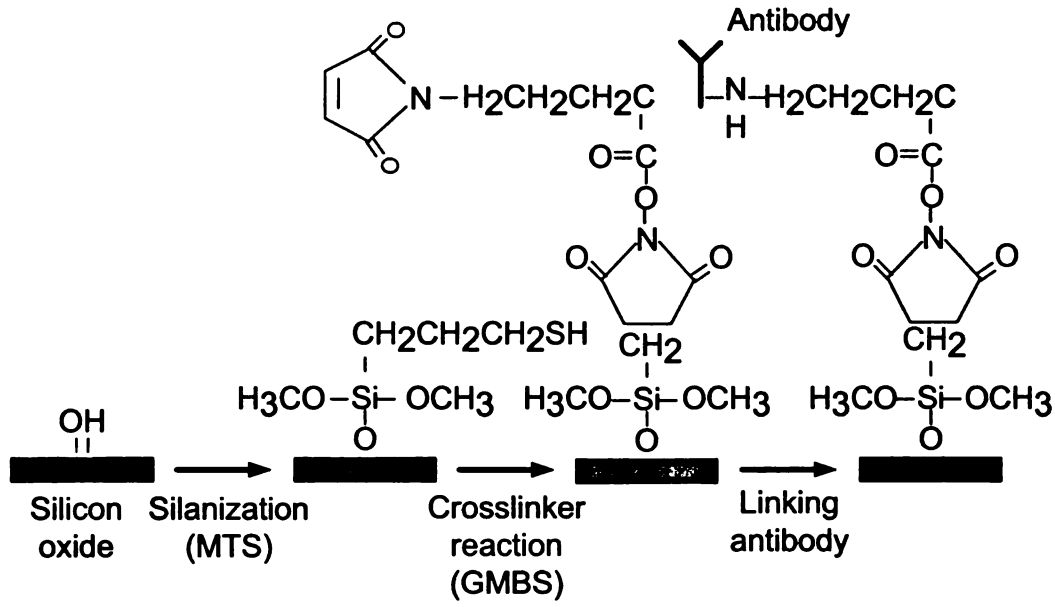

Figure 5.24: The process of gold anti-IgG conjugate immobilization to the silicon oxide.

of 2 % 3-Mercaptopropytrimethyloxysilane (MTS) (Sigma; St.Louis, MS) for 2 h. The chips were then rinsed in toluene and allowed to dry completely. After silanization, N-y-maleimidobutyryloxy succinimide ester (GMBS) (Sigma; St.Louis, MA) was choosen as crosslinkers to avoid multi-protein complex [164]. The crosslinking reagent was dissolved in a minimum amount of dimethylformamide (DMF) and then diluted with ethanol to a final concentration of 2 mM. The silanized substrate was treated with crosslinker for 1 h and washed in phosphate buffered saline (PBS, pH 7.4). After the application of the crosslinker, goat anti-rabbit IgG (Sigma; St.Louis, MA) was immobilized onto the biochip active surface. The biochips were placed in a petri dish, sealed with parafilm and allowed to incubate at 37^oC for 1 h. Fig. 5.24 summarize the process of biochip surface functionalization. The biochips were then treated with 2 mg/mL bovine serum albumin (BSA) (Sigma; St.Louis, MA) for 45 min. After incubation, the biochip surface was rinsed with PBS (pH 7.4) and allowed to air dry. In order to simplify the procedure and reduce the incubation time for the entire pro-

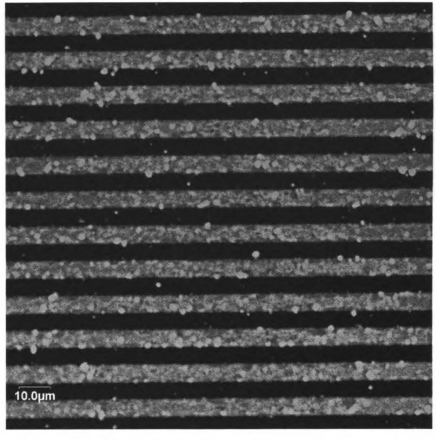

Figure 5.25: Confocal laser scanning microscopy image of electrodes showing FITC-labeled bovine IgG only immobilized to silicon dioxide surfaces (black areas are the electrodes where no IgG are present).

cess, subsequent experiments were performed in which BSA and the anti-IgG were combined in the same solution. We noticed the results obtained using this method were equivalent to those obtained by adding the blocking agent and anti-IgG separately. The confocal laser scanning microscopy image was used to validate antibody immobilization and determine where it occurred (Fig. 5.25). The image shows that the antibody immobilization was only occurring on the silicon dioxide area between the electrodes, thus proving the effectiveness of the surface functionalization.

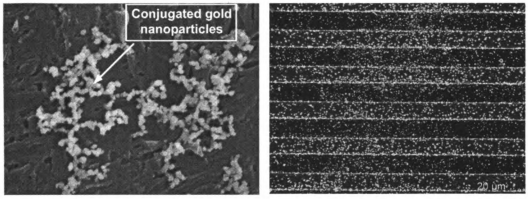

Figure 5.26: The comparison of SEM images showing the importance of proper washing during biochip fabrications.

5.4.5 Fabrication Considerations

In some steps during the process of surface modification, aggressive washing steps are needed to remove chemical residues from last steps. Fig. 5.26 shows two SEM images of biochips after surface modification. Fig. 5.26 (a) shows the biochip with insufficient washing, thus leaving lots of chemical residues before immobilizing gold nanoparticles. We can tell the big difference from Fig. 5.26 (a) to Fig. 5.26 (b), which adopt aggressive washing to get rid of chemical residues. Too strong washing force will affect chemical covalent binding and protein binding while weak strong one might not be enough for removing chemical residuals. Actual washing time and washing force should be adjusted according to experimental trials.

5.4.6 Experimental Results of Single Biochip

Verification of the Operating Principle

The first step in verifying the silver enhancement principle is to measure the size of the silver-enhanced gold nanoparticles with respect to the silver enhancing time.

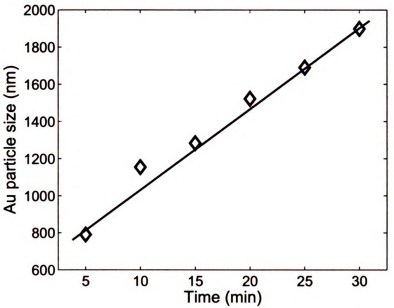

Figure 5.27: The relationship between the gold particle size and the silver enhancing time.

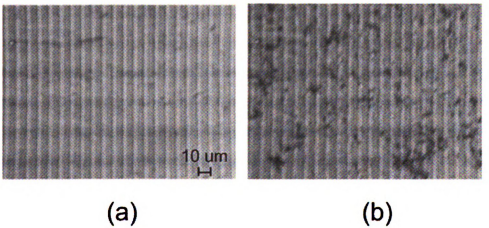

Figure 5.28: Microphotographs for the biochip active surface. (a) before silver enhancement (b) 35 min after silver enhancement.

For this experiment, Zetasizer Nano (Malvern Instruments Ltd, UK) was used to characterize the particle size. Fig. 5.27 shows the linear relationship between the silver enhancing time and the size of gold particles. We have observed that the 40 nm gold nanoparticles will reach average size of 1.2 μm when exposed to the silver enhancer for approximately 10 min. This interesting property makes the silver-enhancement principle suitable for signal amplification in conductimetric biosensors.

To evaluate the detection capabilities of the biochip, we dispense 2.5 mM/mL gold anti-IgG conjugate onto the biochip surface for 2 h and then treat the biochip with silver enhancer solution (Ted Pella, Inc.,CA). To stop silver enhancement, the biochip was rinsed with distilled water and was dried with N_2. Fig. 5.28 shows the microscopic observations before and after 35 min silver enhancing time . Because gold nanoparticles are 40 nm size and they can not be observed by in Fig 5.28(a), where as they can be clearly observed after silver enhancement (see Fig. 5.28(b)). It can also be seen that the silver-enhanced gold particle form a bridge between the interdigital electrodes. Fig.5.29 shows the SEM image of the bridge formed by silver-enhanced gold particles and then verifies the operating principle.

IgG Detection

Based on the principle of silver enhancement, we conduct IgG detection by first applying rabbit IgG onto the active area of the anti-rabbit IgG biochip allowing incubation for 30 min. Goat anti-rabbit IgG and gold conjugates were then applied and were incubated for 30 min. Excess gold conjugates were washed with PBS solution. Electrical measurements are conducted after each treatment of the biochip with the silver enhancer solution and the conductance between the electrodes was measured with a BK multimeter Model AK-2880A (Worchester, MA).

Fig. 5.30 shows the conductance between the electrodes increases with the increasing exposure to the silver enhancer solution while Fig. 5.31 shows the conduc-

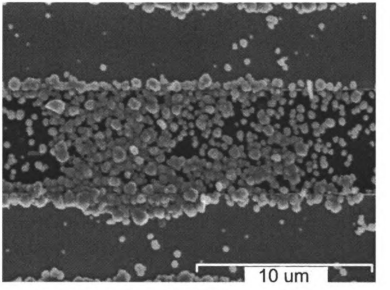

Figure 5.29: SEM image of the bridge formed by enlarged gold particles.

tance measurement in the logarithmic domain. The conductance increases when the biochip is exposed more in the silver enhancer solution as expected. It clearly shows the response has three distinct operation region (A, B, and C), which verifies the operating principle of the silver-enhanced gold nanoparticle based biochip. During the sub-threshold region (labeled as B) of the operation, gold nanoparticles grow in the presence of silver enhancer solution thus leading to a shorter path for electron transport. But during this stage, enhanced gold particles have not formed the bridge to short the electrodes. With the increase in enhancement time, the consistent growth of silver-enhanced particles completely bridges the area between the electrodes and there is immediate transition from state B to C when it happened (shown a step from B to C in Fig. 5.31). In the stage C, more bridges formed by gold nanoparticles are building up in parallel, thus leading to more conductance increase until it become to a more stable state. Bovine IgG biochips were used as negative control experiments and we have observed that the conductance of "control" biochip start to increase at 10 min. It means that the non-specific binding actually occurred but the number of

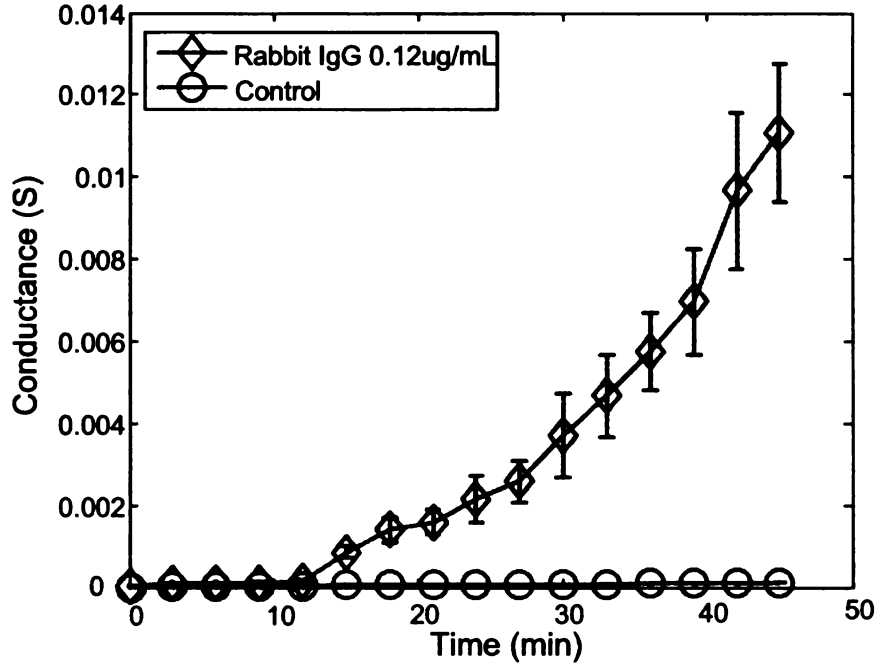

Figure 5.30: Conductance of the rabbit IgG biochip measured as a function of silver enhancing time.

such events is much smaller than the number of specific binding events. Thus, the biochip is able to detect target IgG in the presence of background noise. We have seen that the measurement results are stable several days after the experiments have been conducted. Also, the results in Fig. 5.31 show that the detection range that can be achieved by proposed biosensor is 40 dB with respect to the control conductance. Fig. 5.32 and Fig. 5.33 show the conductance measurement of the mouse IgG biochips as a function of silver enhancing time and it has the same trend with the Fig. 5.30 and Fig. 5.31, thus showing the consistent behavior of fabricated biochips.

We also conducted rabbit IgG detection using different IgG concentrations and Fig. 5.34 shows the conductance measurements at 45 min with three IgG concentrations and the control experiment. For each concentration, the experiment is repeated three times and the standard deviation is also shown in the graph. It clearly shows that pathogenic and non-pathogenic cases can be easily distinguished even with low

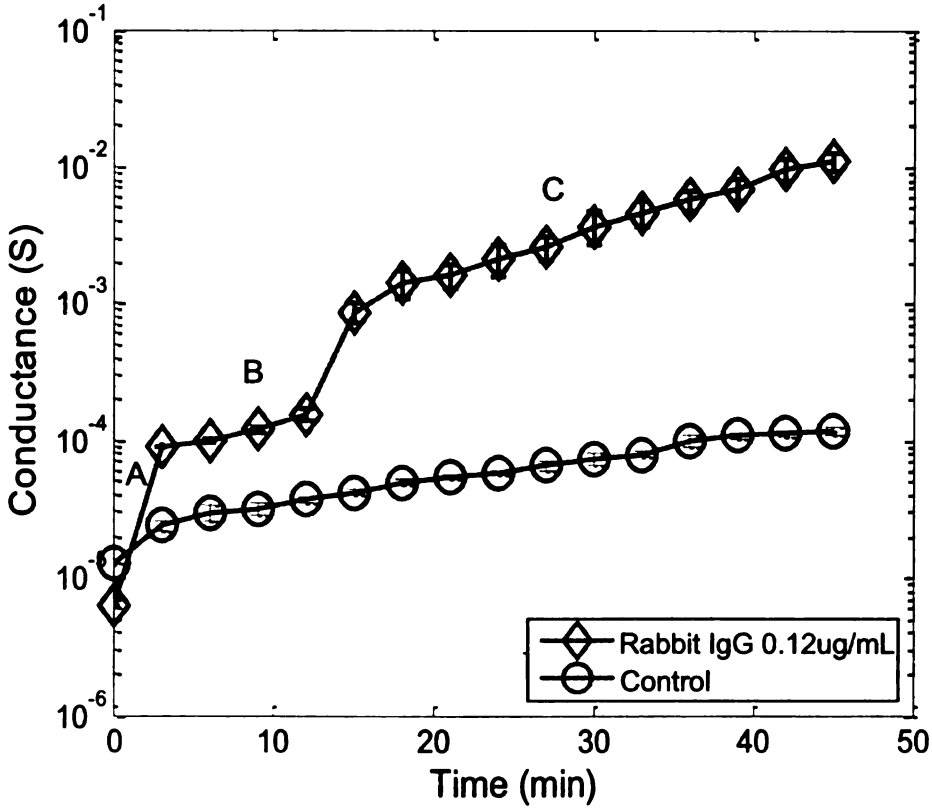

Figure 5.31: Conductance measurement of the rabbit IgG biochip in logarithmic domain, which can clearly show that the biomolecular transistor exhibits 3 different types of responses (labeled as A, B, and C) based on the nature of the conductive path across the electrodes. A: cut-off region; B: sub-threshold region when the formation of the conductive bridge between the electrodes is incomplete; C: above-threshold region where the bridge is completely formed by silver-enhanced gold nanoparticles leading to a step increase in conductance and conductance slope.

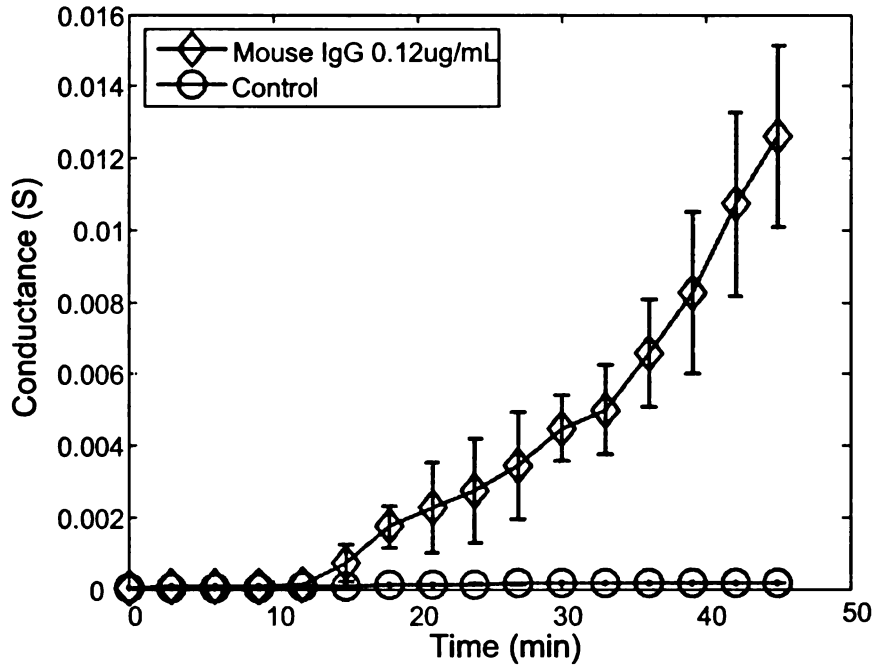

Figure 5.32: Conductance of the mouse IgG biochip measured as a function of silver enhancing time.

concentration of IgG. As seen in the graph, the conductance of biochip decrease with the decrease of the IgG concentration level, implying a decreasing of the signal-to-noise ratio. Similar experiments have been performed using anti-mouse IgG biochip with the mouse IgG detection and the results are shown in the Fig. 5.35. These repeated and controlled experimental results verify the functionality of proposed biochip to detect biomolecules.

Some researchers have argued that the conductivity-based silver-enhanced detection is not applicable to quantitative concentration assays because the electrodes are short circuited above a certain density of the silver-enhanced gold particles [156]. In the next experiment we will show that the quantitative analysis can be achieved by adjusting silver enhancing time. Fig. 5.36 shows the relation of the silver enhancing time required to reach a conductance range of 3.8-5 mS as a function of rabbit IgG concentration. It is interesting to note that 240 pg/mL rabbit IgG can be detected

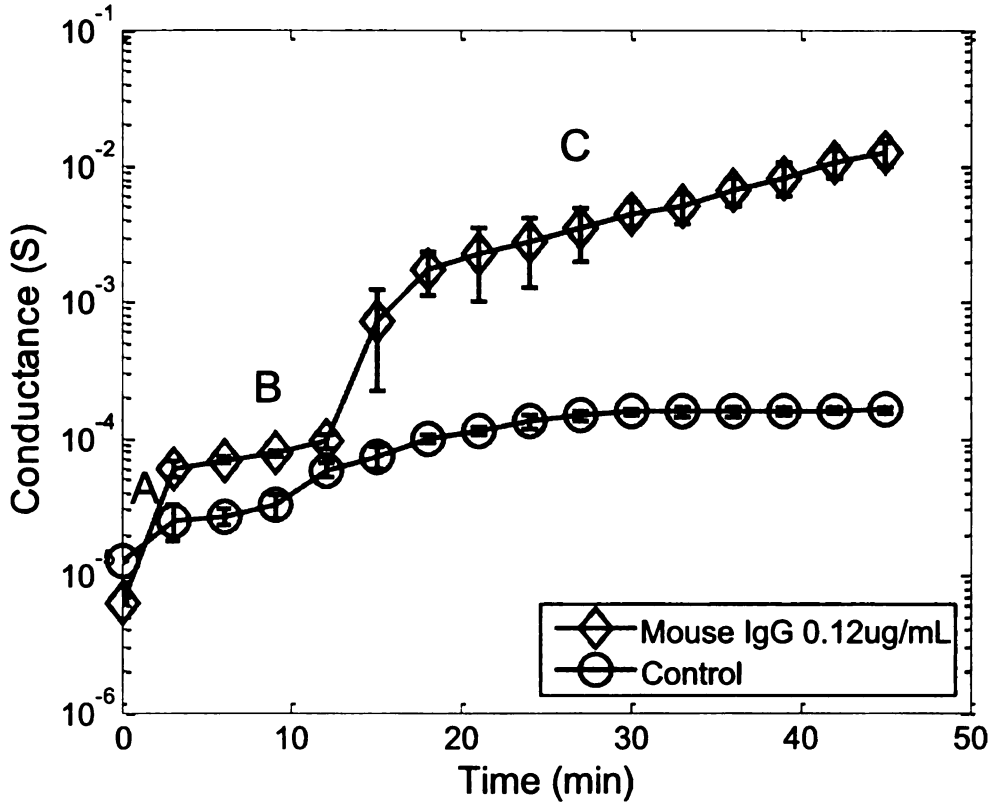

Figure 5.33: Conductance measurement of the mouse IgG biochip in logarithmic domain, which can clearly show that the biomolecular transistor exhibits 3 different types of responses (labeled as A, B, and C) based on the nature of the conductive path across the electrodes. A: cut-off region; B: sub-threshold region when the formation of the conductive bridge between the electrodes is incomplete; C: above-threshold region where the bridge is completely formed by silver-enhanced gold nanoparticles leading to a step increase in conductance and conductance slope.

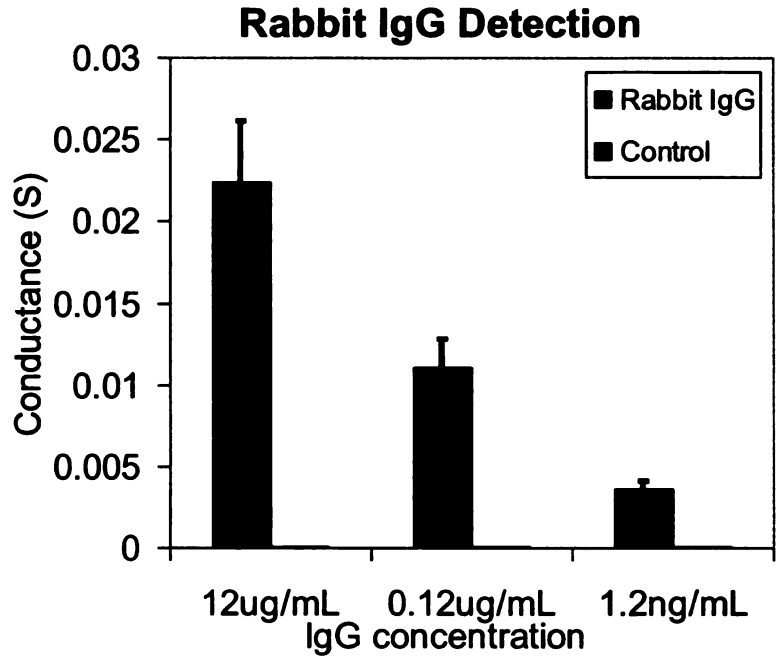

Figure 5.34: Steady state conductance measurement of rabbit IgG detection.

when the conductance increases to 3.8 mS at the silver enhancing time of 42 min.

We have shown the experiments to verify the principle of silver-enhanced electrical detection of biomolecules using rabbit IgG as model antigen. One issue that other researchers have not addressed in the silver enhancement method is the accuracy and possible false positive errors. Due to the sensitivity of the presence of gold nanoparticles when exposing to silver, it might have a high level of false positive results. The typical method of prevention is to extensively wash the biochips to alleviate non-specific binding. The gold nanoparticles serve as nucleation sites about which a reduction reaction deposits silver and hence enlarges the size of the gold nanoparticle. Using silver enhancer solution, the gold antiparticles can grow into a micro size particle and ultimately can bridge the gap between electrodes, leading a measurable change in conductance. Comprehensive experiments have verified the effectiveness of surface functionalization and the functionality of biochip. The proposed biochip in

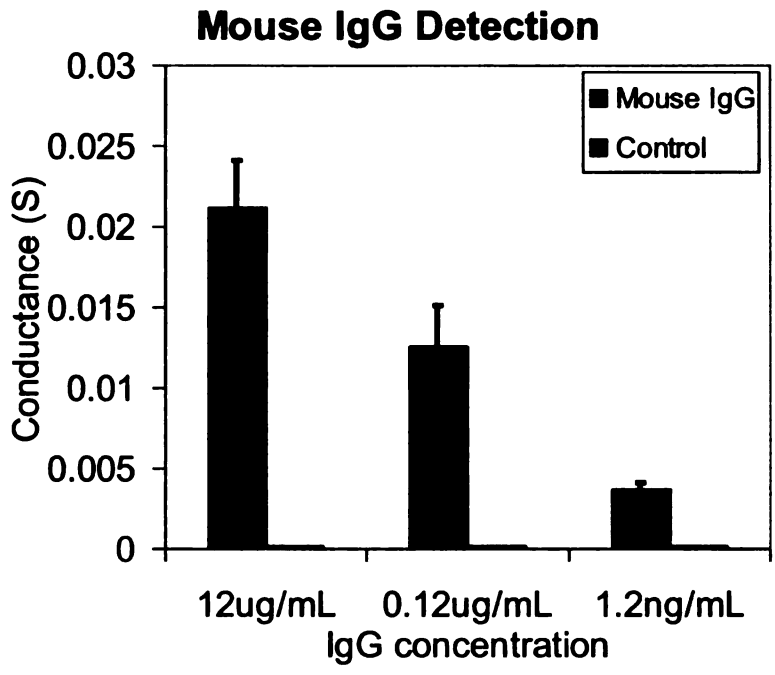

Figure 5.35: Steady state conductance measurement of mouse IgG detection.

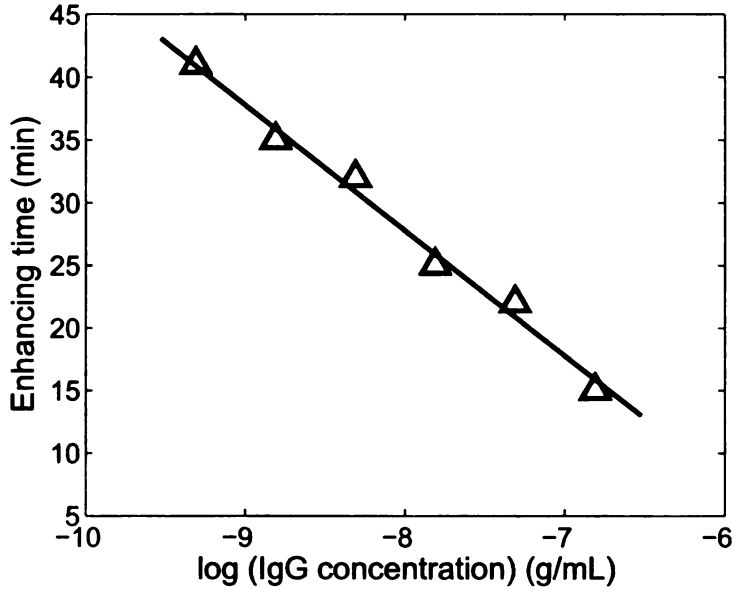

Figure 5.36: Quantitative analysis: the silver enhancing time required to reach a conductance range of 3.8-5 mS as a function of rabbit IgG concentration.

conjunction with silver enhancement provides a simple, effective, and sensitive way of detecting trace quantity of biomolecules.

5.4.7 Silver-enhanced Gold Nanoparticle based Biomolecular Logic Gates

We have demonstrated the feasibility of detecting model biomolecules (rabbit and mouse IgG) by using siver-enhanced gold nanoparticle based biochip. Also we mentioned that large variability and leakage in membrane based biomolecular circuits severely limited the performance of the FEC technique. Next step will be fabricating the biochip logic gates to form biosensor encoder. As we described before, biomolecular logic AND and OR gates are enough to construct biosensor encoder. Due to the structure of this biochip, we only need to change the antibody pattern to cater for the structure of biomolecular logic gates. In this section, we report the design and fabrication of the fundamental logic gates using a silver enhancement technique that is used for amplifying the signals at the biomolecular level. The biomolecular level amplification improves the sensitivity as well as the reliability of the logic circuits which has been verified using measured results from fabricated prototypes. The improved reliability and leakage of the resulting logic circuits makes the proposed approach ideal for integration into the FEC biosensor.

Fabrication of AND and OR logic gates

We have shown that the biomolecular logic gates can be constructed by using lateral flow immunoassays but the performance of these logic gates is far from ideal [140]. In this study, we extend and optimize the logic gates principle to the gold nanoparticle based biochip. The principle of logic gates can be illustrated in Fig. 5.37 where the schematics of AND and OR logic gates have been shown. Based on the biochip

platform we described above, these logic gates can be achieved by patterning desired antibody onto different spatial locations of biochip active surface. Taking the detection of two model pathogens (rabbit IgG and mouse IgG) as an example, we would need to dispense two different specific antibodies onto the biochip. However, there will be a little modification for different logic gates. For preparing the OR gates on the biochip, a mixture of goat anti-rabbit IgG and goat anti-mouse IgG (concentration 0.05 mg/ml) was dispensed onto the surface of biochip (shown in Fig. 5.37). AND gates were fabricated on the biochip by dispensing anti-rabbit IgG and anti-mouse IgG in a cascaded pattern. The immobilization patterns are based on our hypothesis regarding the operating principle of silver-enhanced gold nanoparticles. In the case of OR gate, when either one of model pathogens (rabbit IgG or mouse IgG) exists, the silver-enhanced gold nanoparticles will ultimately bridge the two electrodes assuming the antibody density is large enough. While in the case of AND gate, the condition of shorting the two electrodes is the presence of both of two pathogens (rabbit IgG and mouse IgG in our case). When either one of them exists, the bridge can only be partially formed leading to a weak conductance change. We have conducted repeated and controlled experiments to verify our hypothesis. For the AND gate, the fabrication challenge remains due to the size limitation of two electrodes. Typically the OR gate is easy to fabricate while the AND gate is harder because the cascaded pattern between the narrow gap of two electrodes. To solve this problem, we adopt the biochip structure where additional electrode (the electrode marked with 3 in the Fig.5.23) is located in-between two electrodes to isolate two electrodes (marked with 1 and 2 in the Fig.5.23). The experimental results presented below verify the efficacy of proposed logic gate fabrication methods.

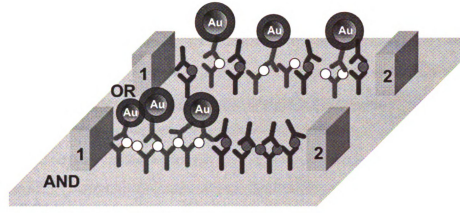

Figure 5.37: The schematics illustration of logic gates patterned on the biochip.

Characterization of AND and OR logic gates

Goat anti-mouse and Goat anti-rabbit IgG were used to fabricate OR and AND gates using the procedure described above. Fig. 5.38 and Fig. 5.39 show the conductance response of logic gates with the respect of silver enhancement time. From the graph, we observed that the conductance is increased with the increasing exposure to the silver enhancer solution. We treat the logic gates with difference IgG solutions to simulate different logic states. When solution contains only rabbit IgG or mouse IgG, it simulates the logic state (0,1) or (1,0). Logic state (1,1) is represented when the solution contains both IgG and mouse IgG. In the case of AND gate (Fig. 5.38), the steady state conductance of (1,1) is much higher than (0,1) and (1,0) and it verify the functionality of AND gate. While in the case of OR gate (Fig. 5.39), the response of these three states are almost same, thus verifying the function of the OR gate.

The logic gates were then characterized to determine their variation with 3 different IgG concentrations. Pure cultures of rabbit IgG and mouse IgG were serially diluted using PBS to prepare 100-fold dilutions representing IgG concentrations ranging from 12 ug/mL-1.2 ng/mL. Each of the tests was repeated three times and the results were measured every 3 minutes after the replacement of new silver enhancer

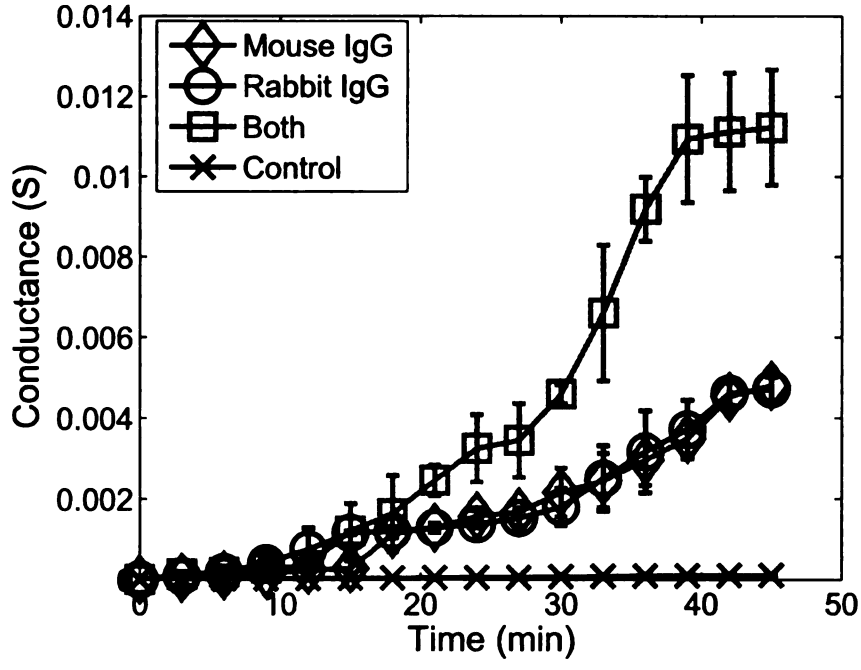

Figure 5.38: Conductance measurement of AND logic gate with respect to the silver enhancement time. The conductance with the presence of both IgG (mimic the (1,1) scenario) is highest showing the soft-AND logic property.

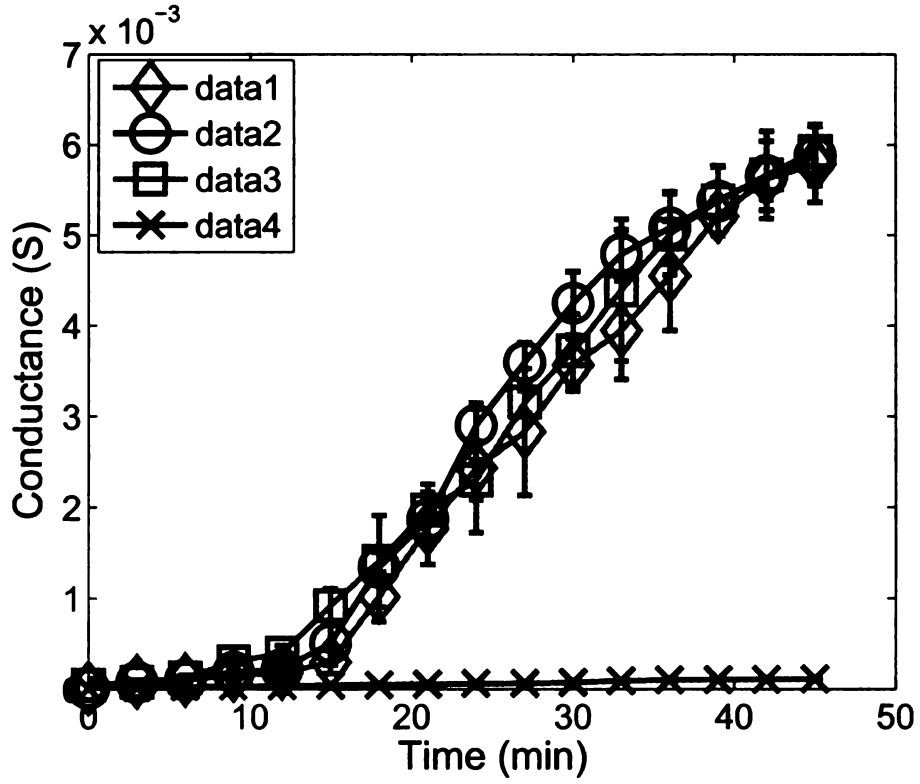

Figure 5.39: Conductance measurement of OR logic gate with respect to the silver enhancement time. The responses expect that of control are almost similar showing the soft-OR logic property.

solution onto biochips. "Control" for all the experiments were obtained using bovine IgG as a negative control. Fig. 5.40 and Fig. 5.41 plot the response of AND and OR gates for these 3 different IgG concentration. It can be seen from Fig. 5.40 that the measured conductance for logical condition "both" (1, 1) is higher than all other cases (irrespective of pathogen concentration) which corresponds to a true AND operation. The plot also shows that for both IgG concentration levels, the "control" condition (0, 0) leads to a much lower conductance as compared to other logical states. That also means the biochip can detect as low as 1.2 ng/mL IgG. Fig. 5.41 shows the measured conductance for a biochip acting as an OR logic gate. The plot shows that for both IgG concentration levels, the "control" condition (0, 0) leads to a much lower conductance as compared to other logical states and the responses of other 3 logical states are almost similar. Therefore the response of the biochip is equivalent to an OR logic. Fig. 5.40 and Fig. 5.41 also show that the responses of logic gates are very consistent across different IgG concentrations, thus verifying the functionality of the logic gates. Also as expected, the conductance responses of logic gates decrease almost linearly with the decrease of the IgG concentration. Compared to our past work (shown in Fig. 5.17 and Fig. 5.18), significant improvement has been achieved thanks to the principle and robust measurement of silver-enhanced gold nanoparticle based biochip.

Logic Gates Circuits Models

We have presented the circuit model of biomolecular logic gates fabricated by lateral flow immunosensors and explained the benefit of using circuit models. Since we have discovered a more robust biosensor platform for fabricating logic gates, we now derive a modified biomolecular circuit model based on experimental data of gold nanoparticle based biochips.

A log-linear model of single biomolecular transistor is the same with the equa-

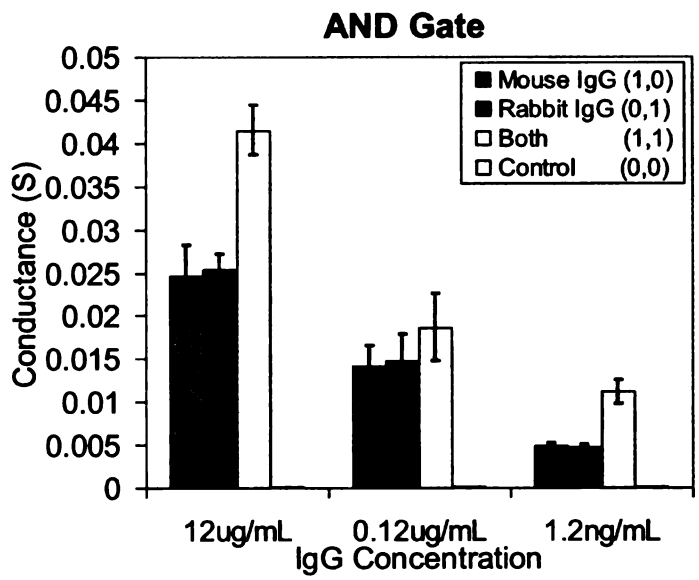

Figure 5.40: Conductance measurements obtained from biochips configured as AND logic for three different IgG concentrations.

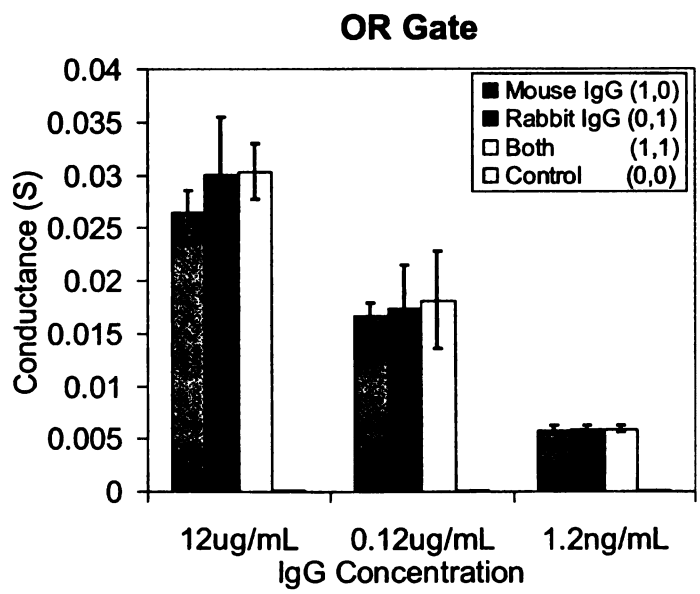

Figure 5.41: Conductance measurements obtained from biochips configured as OR logic for three different IgG concentrations.

tion 5.2 and is given by

$$G(X) = G_0 + \kappa \log \frac{X}{X_0} + G_n \tag{5.5}$$

where X represents the concentration of the biomolecules (IgG in this study) in μg/mL, G_0 represents the "control" transconductance, κ represents sensitivity factor, and X_0 is a detection constant. The systematic and random errors are included as the additive noise component G_n in the equivalent circuit model of the biomolecular transistor. For fabricated mouse IgG biochip: G_0=0.16 mS; κ=4.4 mS; X_0=190 pg/mL. In the case of rabbit IgG biochip, G_0=0.16 mS; κ=4.4 mS; X_0=195 pg/mL.

In this study, we modify the logic gate circuit models and make a unified circuit model for both AND and OR logic gates. Taking mouse IgG and rabbit IgG as two model biomolecules, the corresponding circuit model for OR and AND gates is shown in Fig. 5.42 and its mathematical responses are provided below.

$$G(X_m, X_r) = G_0 + \kappa_m \log \frac{X_m}{X_{0m}} + \kappa_r \log \frac{X_r}{X_{0r}} + \kappa_{mr} \log \frac{X_m + X_r}{X_{0mr}} + G_n \tag{5.6}$$

The parameters for OR and AND logic gates are shown below: For OR logic gate: G_0=0.12 mS; κ_m=-0.3 mS; κ_r=1 mS; κ_{mr}=5.3 mS; X_{0m}=57.4 pg/mL; X_{0r}= 1 ng/mL; X_{0mr}= 63 pg/mL. For AND logic gate: G_0=0.11 mS; κ_m=2.4 mS; κ_r=2.7 mS; κ_{mr}=2.6 mS; X_{0m}=4.6 pg/mL; X_{0r}=24 pg/mL; X_{0mr}=1.2 ng/mL.

In this section we have shown the feasibility of constructing basic logic gates (AND and OR) based on the silver-enhanced gold nanoparticle based biochip. AND logic gates have been constructed by cascading two model anit-IgG, whereas OR logic gates have been fabricated by homogenously mixing and dispensing of anti-IgG. The biochip utilizes the gold nanoparticle as label and signal transducer in conjunction with specific antigen-antibody binding and it use silver enhancement as

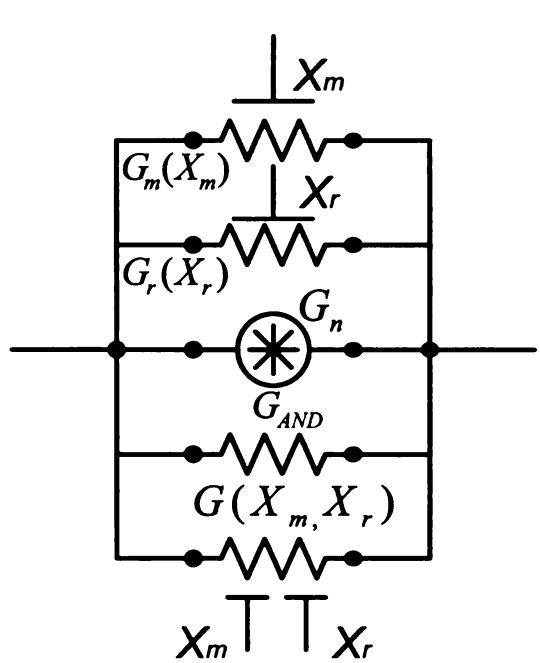

Figure 5.42: Circuit model for AND and OR logic gates fabricated by gold nanoparticle biochip.

biomolecular level signal amplification. The functionality of the AND and OR logic gates have been validated using repeated conductance measurements for different pathogen concentrations. The proposed biochip logic gates will play a key role in designing a FEC biosensor.

Chapter 6

Design of Forward Error Correction Biosensors: Biosensor Decoder

As shown in Fig. 5.2, the decoder can be implemented on silicon circuits and could be integrated in proximity with the biomolecular encoder. In this section, we will focus on the decoding algorithm design and then we introduce an asymmetric code, which only uses AND and OR logic functions to efficiently transmit computational capabilities. We also describe the factor graph based soft decoding and message passing algorithm operating on the graph.

6.1 Introduction to Factor Graph Model

6.1.1 Factor Graph Model

This section introduces basic information about the factor graph and the associated summary propagation algorithms, which operate by passing messages along the edges of the graph. The origins of factor graphs come from coding theory, but they offer an

attractive approach for a wide variety of signal processing problems. In particular, many practical algorithms for a wide variety of detection and estimation problems can be derived as summary propagation algorithms [165]. According to the definition in [166], a factor graph is a biparticle graph that represents factorization of a global function graph that expresses how a "global" function of many variables factors into a product of "local" functions. A factor graph has a variable node for each variable x_i, a factor node for each local function f_j, and an edge-connecting variable node x_i to factor node f_j if and only if x_i is an argument of f_j. A factor graph is thus a standard bipartite graphical representation that depicts a dependence relation between variables and local functions.

To introduce the factor-graph concept, let us start with a simple example. Take a five variable function as an example, $G(x_1, x_2, x_3, x_4, x_5)$ can be written as the product

$$G(x_1, x_2, x_3, x_4, x_5) = f_A(x_1, x_2) f_B(x_2) f_C(x_1, x_3) f_D(x_3, x_4) f_E(x_2, x_3, x_5) \quad (6.1)$$

The factor graph corresponding to equation 6.1 is shown in Fig. 6.1. We can identify a circle for each variable x_i representing variable nodes and a filled rectangle for each factor f representing function nodes, respectively. The variable nodes for x_i are connected to the function node for f by means of edges if and only if x_i is an argument of f.

The original definition of factor graphs allows only the connection of nodes of different types [167]. In [168], Forney applied modifications to original definition of factor graph and the new factor graphs allow direct connections of function nodes. He define the convention that the degree of a variable node has to be less or equal to 2. In doing this, external variables are separated from internal variables or state variables. So external variable nodes have only one degree and internal variable have

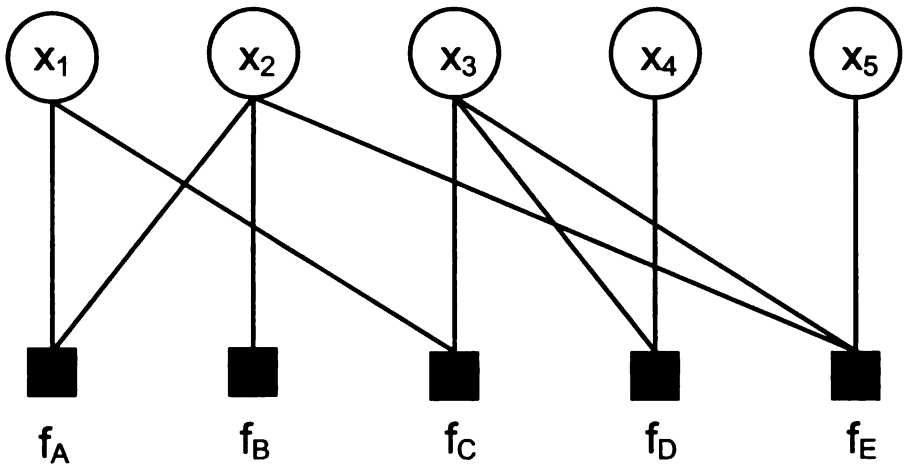

Figure 6.1: A factor graph expressing that a global function $G(x_1, x_2, x_3, x_4, x_5)$ factors as the product of the local functions $f_A(x_1, x_2)$, $f_B(x_2)$, $f_C(x_1, x_3)$, $f_D(x_3, x_4)$, $f_E(x_2, x_3, x_5)$.

degree two. Internal nodes can be removed since they have no explicit meanings.

6.1.2 The Sum-Product Algorithm

The sum-product algorithm is a generic algorithm that operates on a factor graph via a sequence of local computations at every factor-graph node [166]. Before we introduce the sum-product algorithm, we would like to describe marginal function first.

Marginal Function

In many cases, we are interested in determining the marginal function from a global function. There is an important operation called "summary" or "marginal", where instead of indicating the variables being summed over, we indicate those variables not being summed over. For example, if g is a function of three variables x_1, x_2, and x_3,

then "summary for x_1" is denoted by

$$\sum_{\sim x_1} g(x_1, x_2, x_3) = \sum_{x2} \sum_{x3} g(x_1, x_2, x_3) \tag{6.2}$$

We need sum over all possible configurations of g other than x_1 to get the marginal function (summary) for x_1 of g. We also can factor a general function $g(x_1, x_2, ...x_n)$ into a product of several local functions, each having some subset of $x_1, x_2, ...x_n$ as arguments.

$$g(x_1, x_2, ..., x_n) = \prod_{j \in J} f_j(X_j) \tag{6.3}$$

So the marginal function for x_i of g can be derived as followed:

$$g_i(x_i) = \sum_{\sim x_i} g(x_1, x_2, ..., x_n) = \sum_{\sim x_i} (\prod_{j \in J} f_j(X_j)) \tag{6.4}$$

So if we want to calculate the marginal function, the first operation is generating the product and the next operation is summing the product terms.

The Sum-Product Update Rule

In many circumstances, we may be interested in computing for more than one marginal functions. The computation can be accomplished one by one using a single marginal function computation described above. However, it is not efficient since some of computed messages can be reused by other marginal functions. Ideally, all of interested marginal functions can be computed at the same time.

The sum-product algorithm uses a simple update rule and it can efficiently compute all marginal functions simultaneously. It is described as follows [166]:

The message sent from a node v on an edge e is the product of the local function at v (or the unit function if v is a variable node) with all messages received at v on edges other than e, summarized for the variable

associated with e.

A summary function is applied after calculating the product of all incoming messages including the local function. Let $\mu_{x\to f}(x)$ denotes the message sent from node x to node f in the operation of the sum-product algorithm, let $\mu_{f\to x}(x)$ denotes the message sent from node f to node x. Also, let $n(v)$ denotes the set of neighbors of a given node in a factor graph. Then, as illustrated in Fig. 6.2, the message computations performed by the sum-product algorithm can be classified as two update rules: variable to function; function to variable, as expressed as follows:

variable to function update:

$$\mu_{x\to f}(x) = \prod_{h\in n(x)\setminus\{f\}} \mu_{h\to x}(x) \tag{6.5}$$

function to variable update:

$$\mu_{f\to x}(x) = \sum_{\sim\{x\}} ((f(X_{n(f)}) \prod_{y\in n(f)\setminus\{x\}} \mu_{y\to f}(y)) \tag{6.6}$$

The set $n(v)$ denotes the neighbours of node v, i.e., $n(f) = \{x, y_1, y_2, ..., y_m\}$ and $n(x) = \{f, h_1, h_2, ..., h_n\}$.

The update rule at a variable node takes on the particularly simple form given by equation 6.5 because there are no local functions to include, and the summary for x of a product of functions of x is simply the product itself. Equation 6.6, on the other hand, involves multiplication function followed by an application of the summary operator. Variable nodes of degree two perform no computation and a message arriving on one incoming edge is simply transmitted to the outgoing edge.

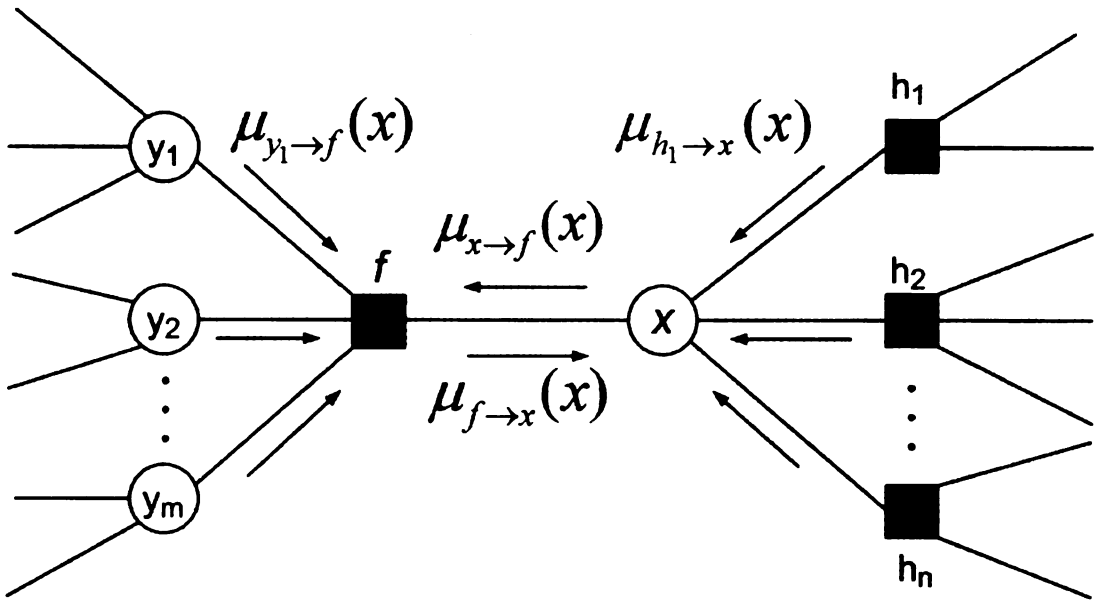

Figure 6.2: The sum-product algorithm update rules illustrated in a fragment of a factor graph.

A Detailed Example

Let's take look at a simple example that uses the sum-product update rules described above to calculate posteriori probabilities. Consider a simple binary code C={(0, 0, 0, 0), (0, 1, 1, 1), (1, 0, 1, 1), (1, 1, 0, 0)}, which is represented by the FFG in Fig. 6.3 (a) and (b). We also assume that a codeword (X_1, X_2, X_3, X_4) is transmitted over a binary symmetric channel with crossover probability ε=0.15 and assume that (Y_1, Y_2, Y_3, Y_4)=(0, 1, 0, 1) is received. The third data bit is corrupted due to the channel noise. In this case, the length of the simple code n=4 and the dimension k=2. Fig. 6.4 shows the message passing rules for two logic functions: Equality and XOR. The message μ are represented as ($\mu(0)$, $\mu(1)$) scaled such that $\mu(0)+\mu(1)=1$. In Fig. 6.3 (c), the FFG is extened to a joint code/channle mode where the codeword is transmitted over a binary symmetric channel. The channel outputs represent the measurements and what we are interested in are the posteriori probabilities $p(x_1, x_2, x_3, x_4|y_1, y_2, y_3, y_4)$. Fig. 6.3 (d)-(g) show that the messages as

computed according to the sum-product rule (equation 6.5 and equation 6.6). Fig. 6.3 (d) computes a initial message according to the measurement vector $\{y_1, y_2, y_3, y_4\}$. Then the messages from 4 variables to two function nodes (XOR and Equality) are updated which is shown in Fig. 6.3 (e). In Fig. 6.3 (f), the messages from the function nodes to variable nodes are obtained based on equation 6.6. The final result (shown in Fig. 6.3 (h)) is the per-symbol a posteriori probability $p(x_i|y_1, y_2, y_3, y_4)$ for i=1,2,3,4. It is obtained as the product of two message along the edge X_i, which is shown in Fig. 6.3 (g). We can see that the final decision of the codeword is (0, 1, 1, 1) and the third data bit is corrected due to error-correction function of this simple code.

6.1.3 Message Passing Schedules

We have discussed the sum-product message passing rule and we know exactly how to calculate the message. However, we have not discussed how to initiate the updates and how to pass the messages. Finding an optimal message passing schedule with least iteration number is a nontrivial problem. Since a message depends on other messages on the graph, it has not been clear how those messages are initiated. There are several methods to initiate the messages [170, 171, 172, 173]. A good option is to initially assign unit message on every edge on the graph and every node has sent a unit function to all of its neighbors. This method can guarantee that every node is in a position to send a message at any time starting from its equilibrium state. We also need to assume the message passing is synchronized with a global clock. This is a reasonable assumption although it is not practical in the analog circuit implementation. With this method, only one message can be passed on any edge in any given direction during one clock and other previous messages will be replaced by this message. If multiple messages are generated at the same time, they will be passed simultaneously.

A factor graph with no cycles can be viewed as a tree structure. If flooding

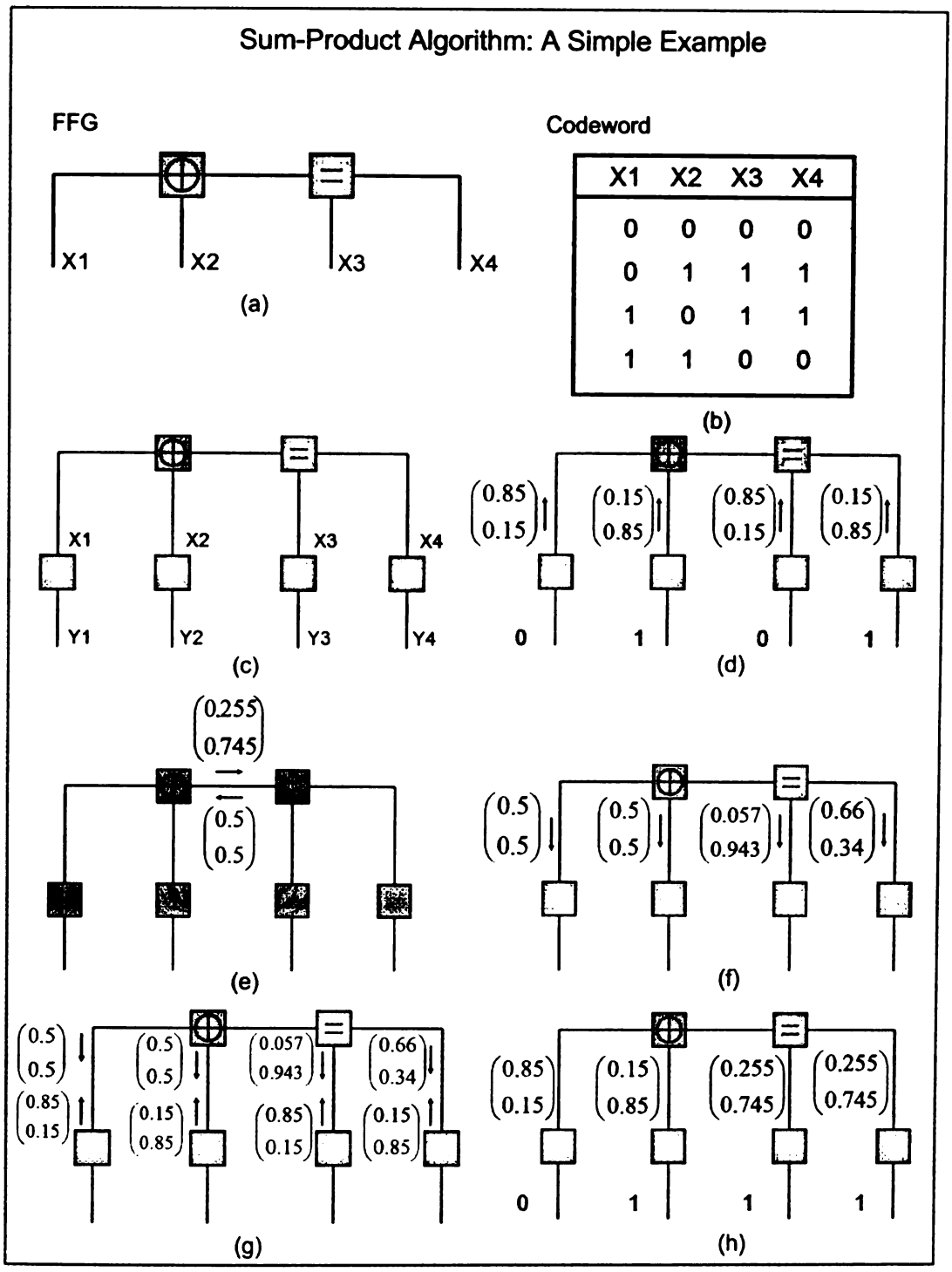

Figure 6.3: A simple example of FFG that employs the sum-product algorithm update rules to calculate interested posteriori probabilities.

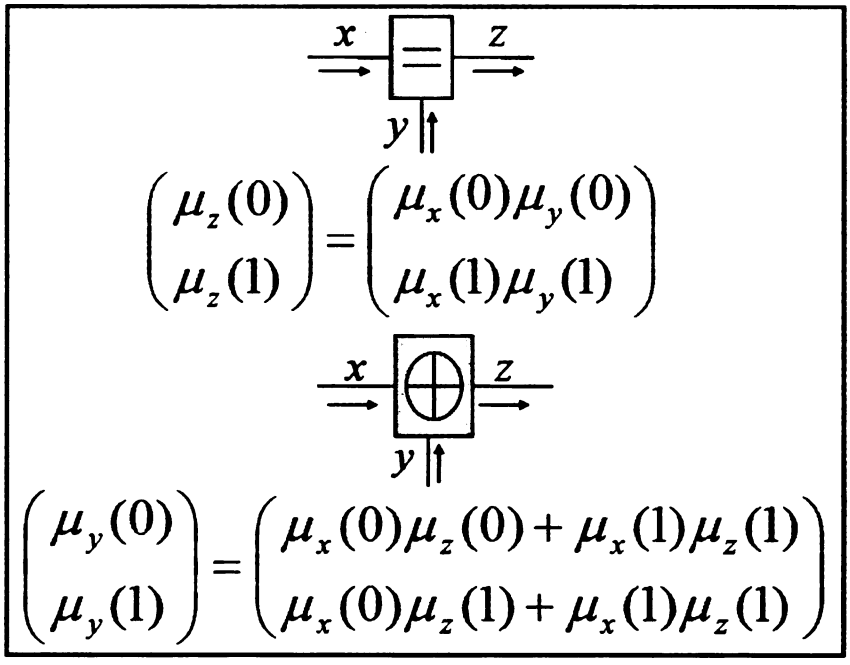

Figure 6.4: The message passing rules for two logic functions: Equality and XOR in Fig. 6.3.

schedule is used, the messages are all absorbed in a finite time and the graph reaches a final stable state, so we can calculate the marginal functions. However, graphs with cycles never have a nowhere-idle message passing schedule and there might be some messages passing on the graph. The termination of the calculations can be done in these cases arbitrarily by some predetermined steps. The degree of converge depends on how close the value generated by the new message to the value of the old message on the edge. For a general treatment of message passing algorithms, the readers can refer to [165].

6.2 Factor Graph Based Soft Decoding Algorithm and Asymmetric Code

In a traditional algebraic decoding, we determine whether or not the received information bit as a '0' or '1'. Then, we use the certain decoding algorithm to find out what the original information bits should be. The first step of deciding whether the information is '0' or '1' is called a hard decision. The hard decision, however, lose some information because it can not determine how close the information bit is close to a '0' or '1'. While in soft decoding treatment, probability is interested measurement to decide how close the information bit is near to a '1' or '0'. Soft decision is superior to hard decision in terms of lower error rate, but is typically requires a more complex decoder. In this section, we reported a soft decoding scheme based on a Forney-style factor graph.

When the encoded information of biomolecular circuits is available, appropriate and efficient decoding algorithm will be applied to decipher the original biological information. Unfortunately, some popular codes in communication systems such as Hamming code and LDPC code can not be directly applied in FEC biosensors because of the uniqueness of biomolecular logic functions. In our study, we proposed a biosensor asymmetric code that only uses computation capability from AND and OR logic functions. The name of asymmetric code comes from the asymmetric nature of decoding message passing rules, which will be described below. We then presented detailed factor graph based decoding algorithm based on a asymmetric code. The factor graph representations are used for efficient computation of the aposteriori probabilities by marginalizing variables according to equation 5.1. Computation on factor graphs proceeds using distributed algorithms which in literature are known as the "sum-product" algorithms described in [169]. The structure of different biosensor codes can be conveniently represented as a factor graph (shown in Fig. 6.5 and 6.6).

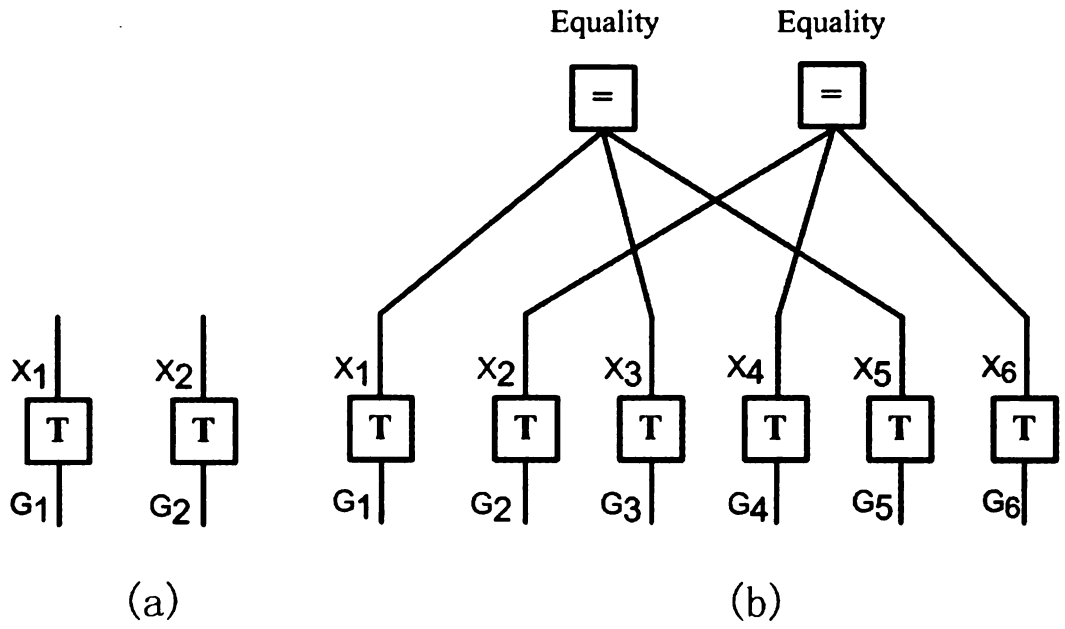

Figure 6.5: Factor graph model of FEC Biosensor (a) Uncoded biosensor; (b) (6,2) biosensor repetition code.

In this section we will describe the "sum-product" message passing algorithm for factor graphs corresponding to the biomolecular circuits.

A Forney-style factor graph [168] corresponding to an uncoded biosensor, a (6,2) repetition code biosensor is shown in Fig. 6.5, and a (6,2) asymmetric code biosensor is shown in Fig. 6.6. For the uncoded case, the factor graph in Fig. 6.5 (a) consists of two transducer nodes (T) whose inputs are the conductance measured from two biosensors specific to two model pathogens: *E. coli* and *B. cereus*. The transducer node captures the relationship between the measured conductances $G_1, ..., G_N$ and the indicator variables $X_1, ..., X_N$. Because estimations of the presence of pathogens are directly based on the measurement, so there is no coupling between the two transducer nodes implying that the detection of pathogens (*E. coli* and *B. cereus*) is performed independently of each other. For the (6,2) repetition code factor graph shown in Fig. 6.5 (b) the transducer nodes corresponding to each of the two pathogens

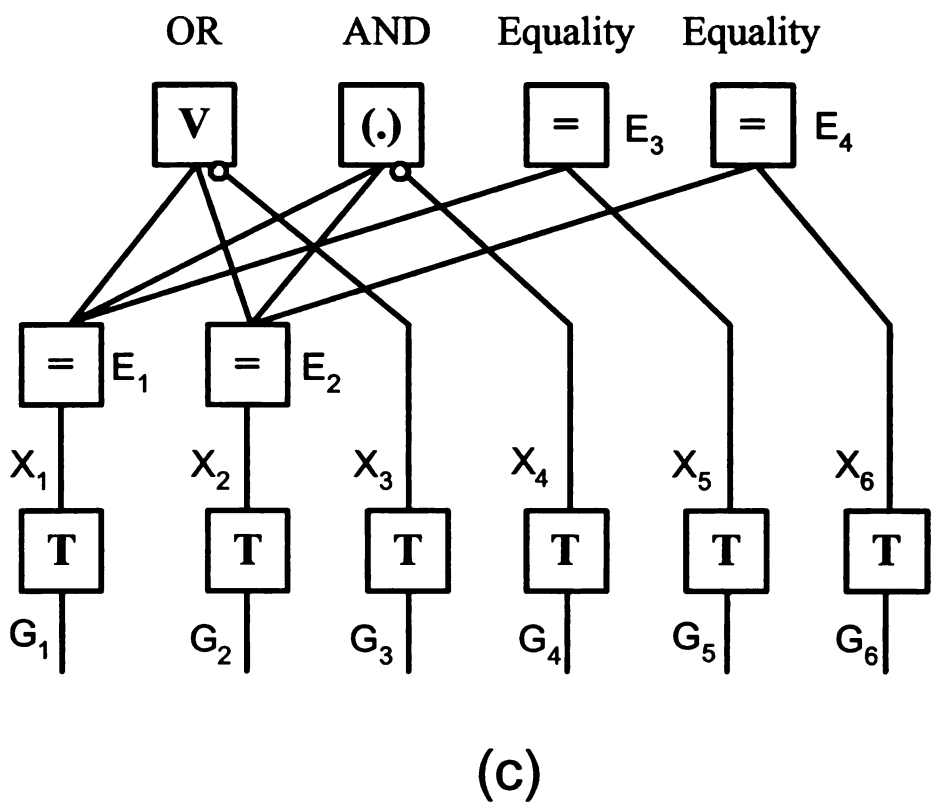

Figure 6.6: Factor graph model of FEC Biosensor (c) (6,2) biosensor asymmetric **code**.

are repeated twice. In this case, however, the measurements are coupled and the dependency is depicted in the factor graph using the Equality nodes (=). In an (6,2) asymmetric code factor graph shown in Fig. 6.6 (c) some of the transducer nodes also models the biomolecular OR and AND circuits. Therefore, the edges in the factor graph which represent the functional dependencies between the nodes connect the pathogen indicator variables $(X_1, .., X_6)$ using the AND, OR and Equality nodes. Note that the AND and OR nodes are connected to exactly three edges, where as the equality nodes are connected to at least two edges.

In the biomolecular factor graph decoding algorithm, each of the nodes propagates messages along the edges to each of its immediate neighbors. These messages take the form of probability estimates that the node to which the message is being sent to is in state 0 or 1. For example consider an equality node E that is connected to three adjacent nodes x, y, z (shown in Fig. 6.7). The node E receives messages from nodes x and y denoted by $(\mu_{x\to E}(0), \mu_{x\to E}(1))^T$ and $(\mu_{y\to E}(0), \mu_{y\to E}(1))^T$. It then computes the message sent to node z, denoted by $(\mu_{E\to z}(0), \mu_{E\to z}(1))^T$ according to the equality constraints which ensure that there are only two valid states $(x, y, z) = (0, 0, 0), (1, 1, 1)$. The corresponding message passing rules for the equality node are summarized in Fig. 6.7. Fig. 6.8 summarized message passing rules corresponding to the OR and AND node. Because OR and AND operations are asymmetric (as opposed to an XOR operation that is symmetric) with respective to their inputs, the figure describes two sets of rules based on the direction of the message flow. The asymmetric message schedule is unique to the proposed FEC biosensor as it only uses AND, OR and Equality logic functions for computation.

Decoding using the factor graph model in Fig. 6.5 and 6.6 begins by initializing the transducer nodes using the conductance measurements obtained from the biomolec-

ular circuits. The transducer nodes first normalize the measurements according to:

$$\mu_{G_k \to X_k}(1) = \frac{\exp^{\beta_k (G_k - G_0)}}{1 + \exp^{\beta_k (G_k - G_0)}} \tag{6.7}$$

where $\beta_k \in [0, 1]$ is a scaling factor that is heuristically chosen for the transducer element k. These normalized measurements are used as messages which are sent to the neighboring Equality, AND and OR nodes. The Equality, AND and OR nodes also compute messages locally and transmit them to their neighbors. Messages are propagated back and forth between the nodes for a pre-determined number of iterations before a decision on the boolean variables $X_1, .., X_6$ is made [165]. In algorithm 1. we summarize the complete message passing algorithm which is specific to the factor graph model in Fig. 6.6 (c).

Algorithm 1 Calculate $P(X_1|G_1, .., G_6)$, $P(X_2|G_1, .., G_6)$

Require: Factor graph containing nodes X_1, X_2 and $G_1, .., G_6$.
Require: Measured conductances $G_1, .., G_6$.
Ensure: For each pair of node (i, j) connected by an edge in the factor graph initializes the messages from node i to j according to $(\mu_{i \to j}(0), \mu_{i \to j}(1)) = (0.5, 0.5)$ except for messages from G_k to X_k which is initialized as $(\mu_{G_k \to X_k}(0), \mu_{G_k \to X_k}(1)) = (1 - P(X_k|G_k), P(X_k|G_k))$ according to equation 6.7. No messages are passed from X_k to G_k.
Ensure: Number of iterations $N = 1$
  while $N \leq TotalIterations$ **do**
    For each direction along the edge of the factor graph calculate the messages according to the Figure 6.7.
  end while
  $P(X_1 = 1|G_1, .., G6) \leftarrow \mu_{G_1 \to X_1}(1) \mu_{E_1 \to X_1}(1)$
  return Normalized $P(X_1 = 1|G_1, .., G_6)$.
  $P(X_2 = 1|G_1, .., G6) \leftarrow \mu_{G_2 \to X_2}(1) \mu_{E_2 \to X_2}(1)$
  return Normalized $P(X_2 = 1|G_1, .., G_6)$.

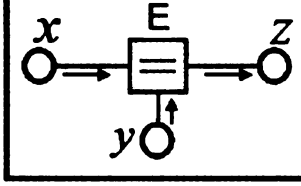

$$\begin{pmatrix} \mu_{E\to z}(0) \\ \mu_{E\to z}(1) \end{pmatrix} = \begin{pmatrix} \mu_{x\to E}(0)\mu_{y\to E}(0) \\ \mu_{x\to E}(1)\mu_{y\to E}(1) \end{pmatrix}$$

Figure 6.7: Sum-product message updated rules for the Equality function node.

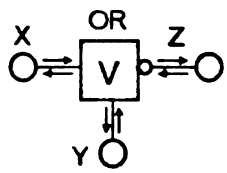

$$\begin{pmatrix} \mu_{OR\to X}(0) \\ \mu_{OR\to X}(1) \end{pmatrix} = \begin{pmatrix} \mu_{Y\to OR}(0)\mu_{Z\to OR}(0) + \mu_{Y\to OR}(1)\mu_{Z\to OR}(1) \\ \mu_{Y\to OR}(0)\mu_{Z\to OR}(1) + \mu_{Y\to OR}(1)\mu_{Z\to OR}(1) \end{pmatrix}$$

$$\begin{pmatrix} \mu_{OR\to Y}(0) \\ \mu_{OR\to Y}(1) \end{pmatrix} = \begin{pmatrix} \mu_{Z\to OR}(0)\mu_{X\to OR}(0) + \mu_{Z\to OR}(1)\mu_{X\to OR}(1) \\ \mu_{Z\to OR}(0)\mu_{X\to OR}(1) + \mu_{Z\to OR}(1)\mu_{X\to OR}(1) \end{pmatrix}$$

$$\begin{pmatrix} \mu_{OR\to Z}(0) \\ \mu_{OR\to Z}(1) \end{pmatrix} = \begin{pmatrix} \mu_{X\to OR}(0)\mu_{Y\to OR}(0) \\ \mu_{X\to OR}(0)\mu_{Y\to OR}(1) + \mu_{X\to OR}(1)\mu_{Y\to OR}(0) + \mu_{X\to OR}(1)\mu_{Y\to OR}(1) \end{pmatrix}$$

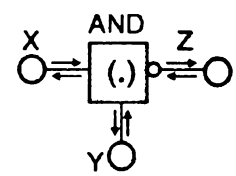

$$\begin{pmatrix} \mu_{AND\to X}(0) \\ \mu_{AND\to X}(1) \end{pmatrix} = \begin{pmatrix} \mu_{Y\to AND}(0)\mu_{Z\to AND}(0) + \mu_{Y\to AND}(1)\mu_{Z\to AND}(0) \\ \mu_{Y\to AND}(0)\mu_{Z\to AND}(0) + \mu_{Y\to AND}(1)\mu_{Z\to AND}(1) \end{pmatrix}$$

$$\begin{pmatrix} \mu_{AND\to Y}(0) \\ \mu_{AND\to Y}(1) \end{pmatrix} = \begin{pmatrix} \mu_{X\to AND}(0)\mu_{Z\to AND}(0) + \mu_{X\to AND}(1)\mu_{Z\to AND}(0) \\ \mu_{X\to AND}(0)\mu_{Z\to AND}(0) + \mu_{X\to AND}(1)\mu_{Z\to AND}(1) \end{pmatrix}$$

$$\begin{pmatrix} \mu_{AND\to Z}(0) \\ \mu_{AND\to Z}(1) \end{pmatrix} = \begin{pmatrix} \mu_{X\to AND}(0)\mu_{Y\to AND}(0) + \mu_{X\to AND}(0)\mu_{Y\to AND}(1) + \mu_{X\to AND}(1)\mu_{Y\to AND}(0) \\ \mu_{X\to AND}(1)\mu_{Y\to AND}(1) \end{pmatrix}$$

Figure 6.8: Sum-product message updated rules for the OR and AND function nodes.

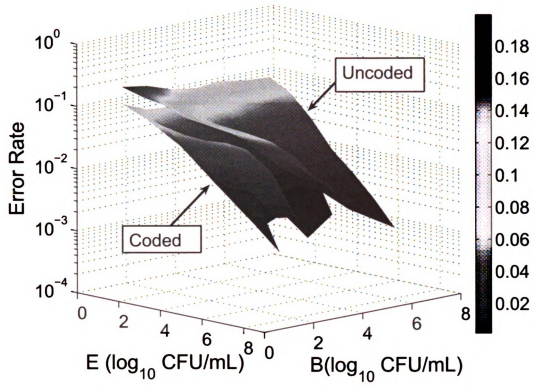

Figure 6.9: DER curve of (6,2) repetition code. Each point in the error curve is based on multiple biosensor experiments for a given pathogen (*B. cereus* and *E. coli*) concentration.

6.3 Behaviorial Simulation of FEC Biosensors

6.3.1 LFI based FEC Biosensor

In this section we present behavioral simulation results that were obtained using the algorithm 1 when applied to the factor graphs shown in Fig. 6.5 and 6.6. The biosensor encoder was simulated using the biomolecular circuit models of LFI based FEC biosensor summarized in chapter 3. For different concentration of pathogens (*B. cereus* and *E. coli*), these models produced conductance parameters that were then corrupted by measurement noise. The noise was modeled as a zero-mean additive white Gaussian noise (AWGN) whose variance was experimentally determined according to the

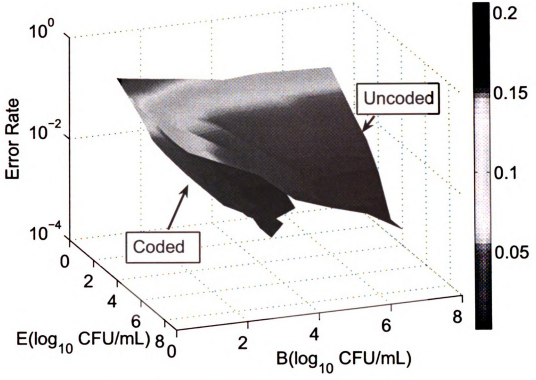

Figure 6.10: DER curve of (6,2) asymmetric code.

procedure described before. The noisy conductance parameters $G_1, .., G_k$ were then presented as an input to the factor graph model and the probability of the presence of *B. cereus* and *E. coli* was estimated using the message passing algorithm 1. The estimated probability was compared against a pre-determined threshold (0.5) to obtain a yes/no answer indicating the presence or absence of pathogens in the sample. The simulation experiment was repeated 1000 times for each pathogen concentration and the detection error rate (DER) was determined by the occurrence of false rejection and false acceptance.

First, we want to simulate the performance of a FEC biosensor using membrane based lateral flow immunosensor, which is described in section 5.4. Fig. 6.9 shows two-dimensional DER (error rate for *E. coli* + error rate for *B. cereus*) curves ob-

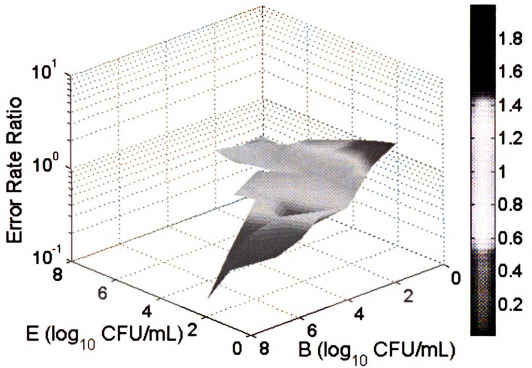

Figure 6.11: The comparison of (6,2) asymmetric code and (6,2) repetition code. The error curve shows the ratio of the DER corresponding to the asymmetric code with the repetition code.

tained for a (6,2) biosensor repetition code (represented by the factor graph model in Figure 6.5 (b)) and compares it against the DER curve obtained for the uncoded case (represented by the factor graph model in Fig. 6.5 (a)). As expected, the DER reduces when the concentration of pathogen (represented in CFU/mL) increases. Also as expected, the DER for the repetition code (due to larger redundancy) is lower than that of uncoded case. That explain the benefit of adding redundancy in biosensors to improve the reliability. Similar improvement is also obtained when a (6,2) biosensor asymmetric code (represented by the factor graph model in Fig. 6.6) is compared against the uncoded case and is shown in Fig. 6.10. Fig. 6.11 compares the ratio of the DER corresponding to the asymmetric code with the repetition code and demon-

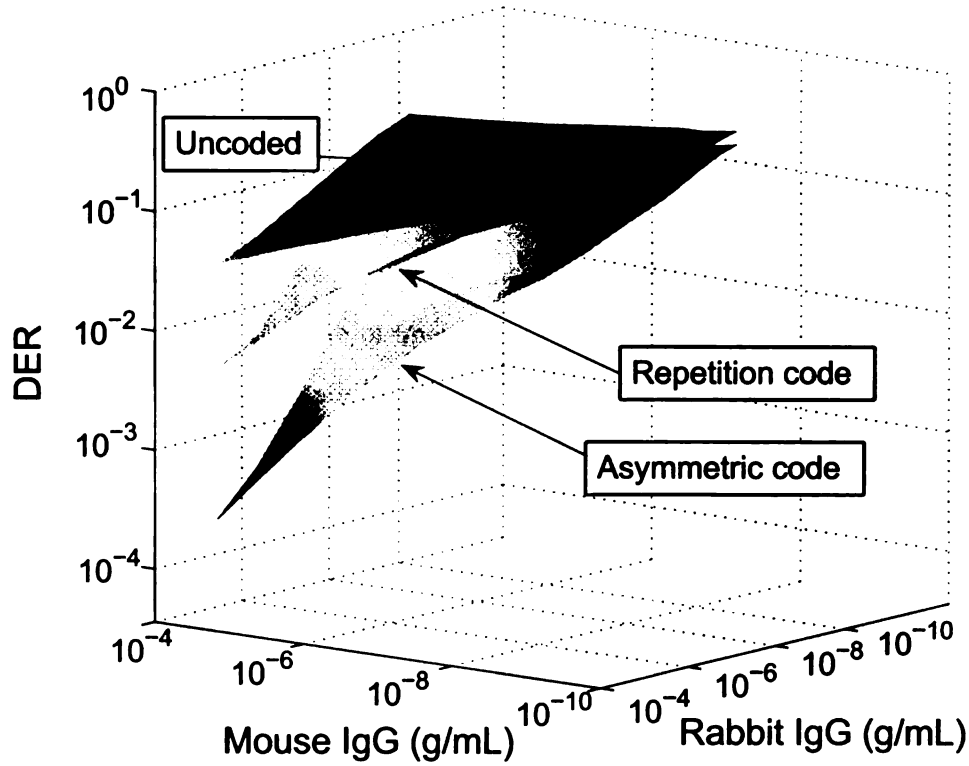

Figure 6.12: DER curve of (6,2) asymmetric code using gold nanoparticle biochip based FEC biosensor.

strates that except for ultra-low pathogen concentration levels, the performance of the biosensor asymmetric code is superior to that of the biosensor repetition code by a factor of 5. The un-ideal of logic gates attribute to the reason of the exception at ultra-low concentration and we will show the significant improvement in our second biosensor platform: silver-enhanced gold nanoparticle based biochip.

6.3.2 Gold Nanoparticle based FEC Biosensor

We also simulate the DER of FEC biosensor based on gold nanoparticle biochip. Biomolecular circuits are simulated using derived circuit models. "Control" experiments for all the experiments were obtained using bovine IgG. The responses from logic gates and single biomolecular transistors are sent to the decoder that give a aposteriori probabilities based on the "sum-product" message passing algorithm.

Fig. 6.12 shows the DER curve of uncoded case, (6,2) repetition code, and (6,2) asymmetric code using gold nanoparticle biochip based FEC biosensor. It clearly show that proposed asymmetric code outperforms the repetition code. It can greatly improve the reliability of biosensors in terms of reduced detection error rate. The result also coincides with the DER curve from lateral flow immunosensor based FEC biosensor, thus verifying the functionality of (6,2) biosensor asymmetric code.

6.4 "Co-Detection" Principle

Compared to the repetition code, asymmetric code exhibits a novel detection principle which we label as "co-detection". The principle can be clearly seen if the DER (Fig. 6.9 and Fig. 6.10) for each of the pathogens (instead of total DER) are separately projected on a 2-D plot. This is shown in Fig. 6.13 (a) and (b) for a repetition code and in Fig. 6.13 (c) and (d) for the asymmetric code. Fig. 6.13 (a) shows the colormap of the DER corresponding to *B. cereus* illustrating that the DER is independent of the *E. coli* concentration which is expected since there is no coupling between the two detection mechanisms. Similar DER plot for the *E.coli* is shown in Fig. 6.13 (b). However, equivalents plots for the asymmetric code shown in Fig. 6.13 (c) and (d) demonstrate a strong coupling between the concentration of *E. coli*/*B. cereus* in the input sample and the DER corresponding to *B. cereus*/*E. coli*. This suggests that for the asymmetric code, one pathogen with large concentration could in fact improve

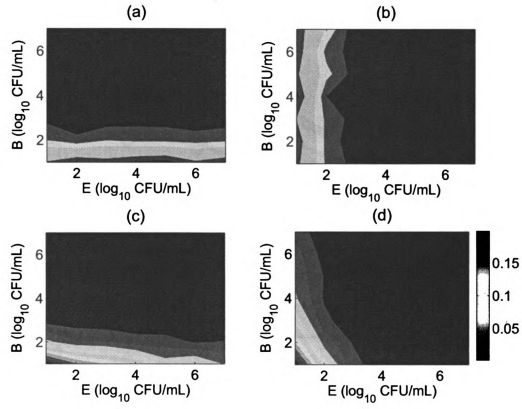

Figure 6.13: Separate DER curve for *B. cereus* and *E. coli*: (a,b) Repetition code; (c,d) Asymmetric code. (a) and (c) represent the detection error rate of pathogen *B. cereus* where nonlinear detection relationship between two pathogens is revealed in (c). (b) and (d) represent the detection error rate of pathogen *E. coli* where nonlinear detection relationship between two pathogens is revealed in (d).

the detection performance of trace quantities of another pathogen. We refer to this mutual coupling as the "co-detection" principle and represents one of benefits of developed simulation environment where the different encoding-decoding techniques could yield novel methods of improving the reliability of biosensors.

We also verified the "co-detection" principle using behavioral simulation model of gold nanoparticle based biochip. In Fig. 6.14, the concentration of rabbit IgG is increased which as expected leads to the decrease in its DER. However as shown in Fig. 6.14, the increase in concentration of mouse IgG also leads to the decrease in

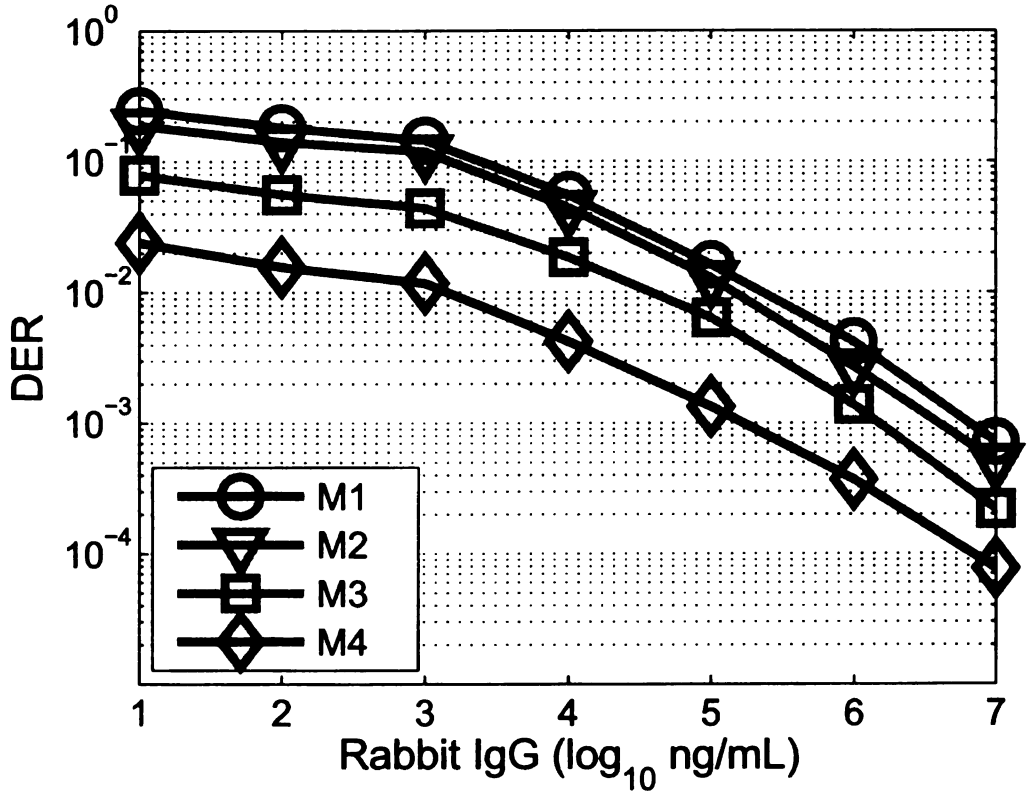

Figure 6.14: Rabbit IgG detection error-rate (DER) curves obtained using described behavioral models. It shows "co-detection" when the presence of higher concentration of mouse IgG enhances the detection reliability of rabbit IgG. M1 represents mouse IgG concentration: 1 ng/mL; M2 represents mouse IgG concentration: 100 ng/mL; M3 represents mouse IgG concentration: 10 ug/mL; M4 represents mouse IgG concentration: 1 mg/mL.

DER, clearly indicating the "co-detection" principle. A similar behavior was also observed for the DER of mouse IgG as shown in Fig. 6.16. For comparison purposes, Fig. 6.15 and Fig. 6.17 show the DER curves that were obtained if six independent rabbit and mouse IgG biochips are used for detection. This scenario replicates the testing strategy commonly employed in diagnostics where repeated experiments followed by majority voting are performed to obtain reliable detection results. The plots in Fig. 6.15 and Fig. 6.17 clearly show the absence of "co-detection" which is expected as there is very little coupling between different detection tests.

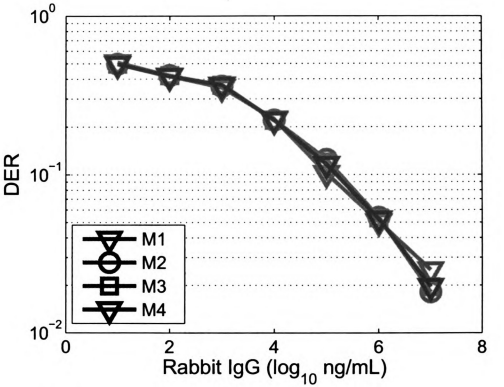

Figure 6.15: DER curve of rabbit IgG detection using (6,2) repetition code where "co-detection" principle does not hold.

6.5 "Co-Detection" Principle Verification using Markov Chain Model

We have developed a general Markov chain model to simulate the stochastic nature of biomolecular interaction. Using the model, we explain how biological noise (non-specific binding) will affect biosensor performance in terms of SNR. Here, we use this general Markov model to simulate FEC biosensor, and to verify if the "co-detection" principle is theoretically sound. Same assumption is made as the Chapter 4, and the probability of specific binding of a biomolecule target with its probe is assumed to be P^b= 0.9, while the probability of non-specific binding P^c is assumed to be 0.01. For simplicity, these probabilities are assumed to be the same for all types of

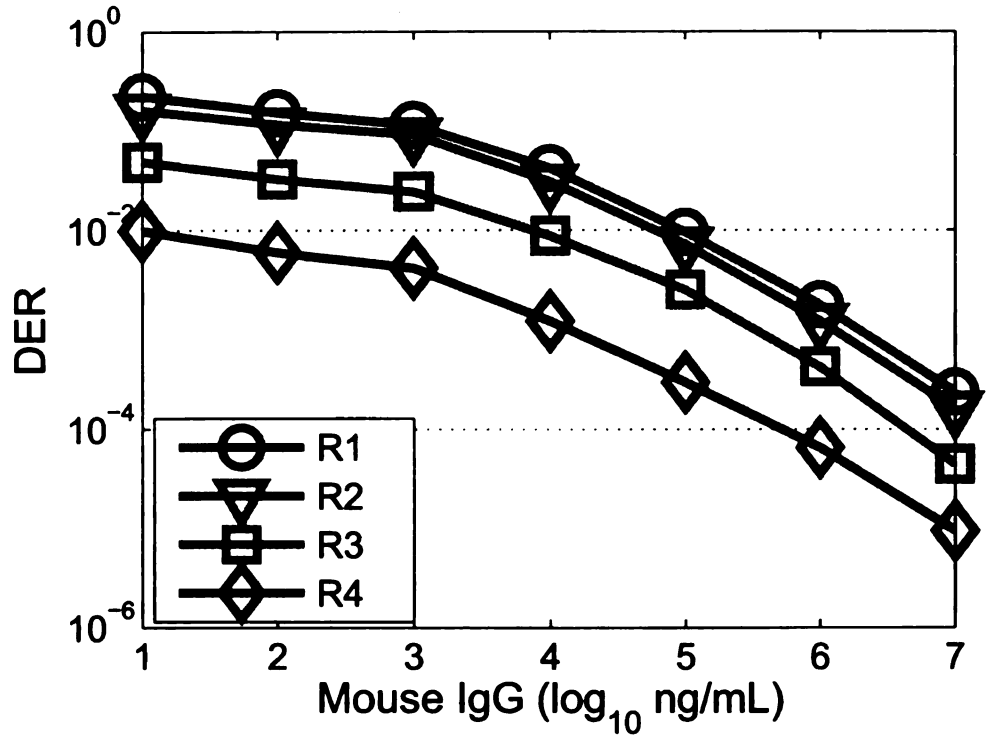

Figure 6.16: DER curve of mouse IgG detection using (6,2) asymmetric code. The presence of higher concentration of rabbit IgG enhances the detection reliability of mouse IgG; R1-R4 hold similar meaning and same value as M1-M4.

the probes. The free target biomolecules perform a random walk within the reaction chamber. At each time step of the random walk, the bounded target biomolecules may be released, upon which they resume the random walk. The release probabilities of from both specific and the non-specific states for all targets are P^r=P^{rc}= 0.02.

Also, we will simulate gold nanoparticle based biochip based on the Markov chain model of biomolecular interaction. To illustrate the simulation, as shown in Fig. 6.18, "AND" and "OR" gates are constructed using silver-enhanced gold nanoparticles. To facilitate the modeling process, the reaction chamber is equally divided into two sub-chamber (A and B), as shown in Fig. 6.18. Also for simplicity, we will make the following assumptions: first, the probes are enough to bind with target biomolecules,

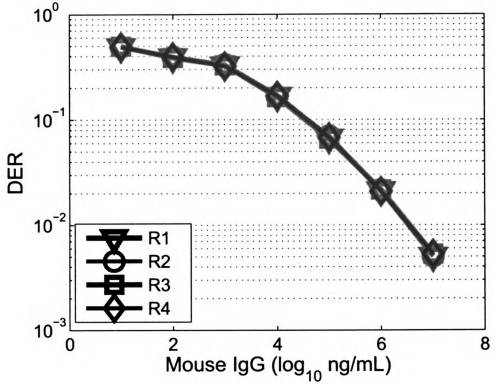

Figure 6.17: DER curve of mouse IgG detection using (6,2) repetition code. the absence of "co-detection" in the conventional repetitive tests where rabbit IgG does not affect the detection reliability of mouse IgG;

in other words, the condition of saturation is never reached. Second, assume the growth rate of gold nanoparticles R is constant and the process of growth is homogeneous. In reality, the rate can be obtained by calibration experiments. The enhancing time for chamber A is t_1 while the enhancing time for chamber B is t_2. The length of the chamber is L. Due to the homogenous growing process of gold nanoparticles, the enhancing time of sub-chamber A can be approximated by $t_1 = \frac{L/2}{N_1 R}$, where N_1 is the captured biomolecule numbers that is same as the number of gold nanoparticles. Similarly, the enhancing time of sub-chamber B can be approximated by $t_2 = \frac{L/2}{N_2 R}$, where N_2 is the captured biomolecule numbers in sub-chamber B. So the total enhancing

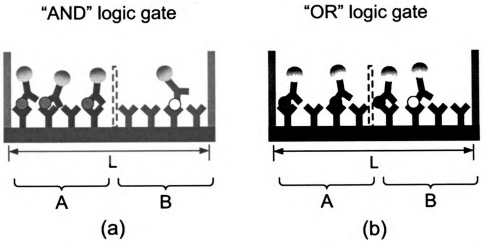

Figure 6.18: Schematic illustrations of Au nanoparticle based logic gates for Markov chain model.

time is given by

$$t = t_1 + t_2 = \frac{L}{2R}(\frac{1}{N_1} + \frac{1}{N_2}) \tag{6.8}$$

The mean value and variance of the number of captured biomolecules (gold nanoparticles) can be obtained from the equation 4.12 and 4.13 by using Markov model. So the total silver enhancing time is related to the number of captured target biomolecules and then it is an indicator of interested target biomolecular concentration. The measurement input to the FFG of (6,2) asymmetric code can be obtained by normalizing the enhancing time using equation 6.7. These normalized measurements are used as input messages that are sent to the the neighboring Equality, AND and OR nodes, which fulfill the described algorithm of the asymmetric code.

First, we want to verify the "co-detection" is theoretically correct. We simulate the (6,2) asymmetric code with the constructed Markov model of gold nanoparticle interactions. The simulation process is the same as that of behaviorial simulation. In the simulation, the conductance of the single biosensor is only related its only concentration and no background biomolecules are introduced. The log-linear model

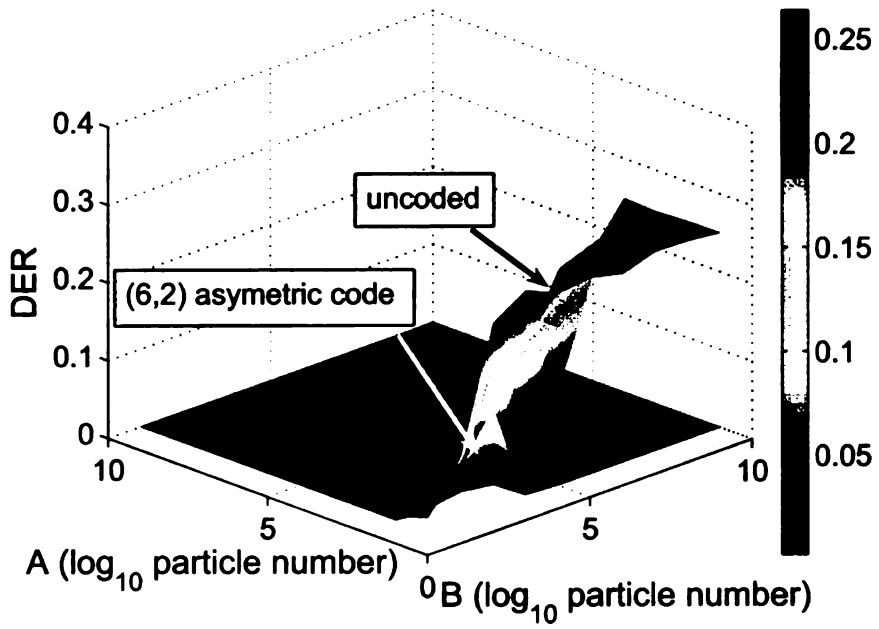

Figure 6.19: DER curve of biomolecule A and B detection using Markov model.

of the single biosensor satisfies the equation 5.2. If the biomolecular number is large enough, the process can be approximated by Gaussian process, so the noise can be modeled as a zero-mean additive white Gaussian noise (AWGN) whose variance was defined by equation 4.13 in chapter 4. The simulation experiment was repeated 1000 times for each biomolecular concentration levels and the detection error rate (DER) was determined by the occurrence of false rejection and false acceptance.

In the simulation study, we introduce a background biomolecule into the biosensor reaction chamber. That is, introduce a background biomolecule A into the detection of target biomolecule B while introducing background biomolecule B into the detection of target biomolecule A. The concentrations of biomolecule A and B are steadily increased during the simulation study. The 3D detection error rate of biomolecules A and B detection using the asymmetric code and without using decoding is compared and it is shown in Fig. 6.19. As shown from the figure, the reliability (in terms of detection rate) significantly increase with the use of the asymmetric code and the

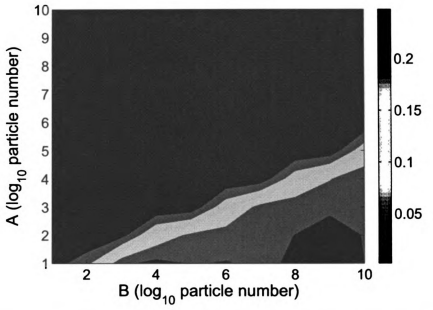

Figure 6.20: Detection of A biomolecule with background biomolecule B.

DER of the asymmetric code decreases, as expected. The interesting part in the DER curve of the asymmetric code is the presence of 3D triangle and the 2D projection of DER for detection of biomolecule A and B can clearly see its trend. Fig. 6.20 shows the detection error rate of biomolecule A in the presence of background biomolecule B. In this case, biomolecule B serves as a biological noise since non-specific binding will affect the detection of A. As evident from the figure, the detection error of biomolecule A is increased with the increase of B concentration. The result coincides with the Fig. 4.5 and demonstrate the contribution of non-specific binding to SNR degradation of biosensors. However, shown in Fig. 6.21, a remarkable reliability improvement can be achieved when the concentration of background biomolecule is large enough. Initially, when the concentration of background biomolecule is less than the target biomolecules, non-specific binding will become a biological noise. However, when the concentration of biomolecule becomes comparable to the concentration of target biomolecule or even larger, the "co-detection" begins its effect and turn the biological

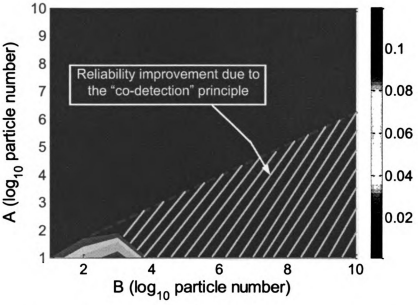

Figure 6.21: Detection of A biomolecule after decoding with background biomolecule B, where non-specific bindings of background biomolecule B serves as useful information for improving the reliability.

noise into a useful information to reduce the detection error rate (shown in the shadow grey area of Fig. 6.21). The reason why the nonlinearity of "co-detection" exhibits a triangle shape could be explained this way. The non-specific binding will becomes a biological noise and dominate the biosensor behavior in the low concentration of target biomolecules. Also, "AND" logic gate is main contributor for nonlinearity of "co-detection". The response of "AND" gate is noisy when the concentration of background biomolecule is not comparable to the target biomolecule. However, the increase of background biomolecules facilitate the bridge formation of electron transport, thus increasing the response of the 'AND" gate and resulting in a lower detection error rate of target biomolecules.

Similar conclusions can also be drawn from Fig. 6.22 and Fig. 6.23. In this section, we shows the simulation results from a general Markov model of (6,2) asymmetric code and simulation results coincide with the results from the derived biomolecular

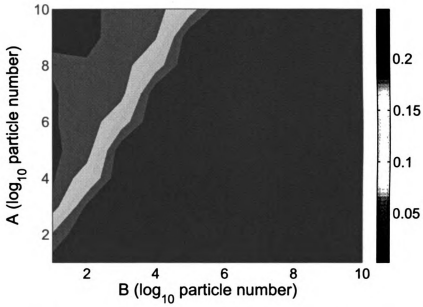

Figure 6.22: Detection of B biomolecule with background biomolecule A.

circuit model and previous biosensor research [14]. It proves "co-detection" principle theoretically exists. It also shows a general condition of triggering the "co-detection' principle, that is, the concentration of background biomolecules have to be larger or at least comparable to the concentration of target biomolecules.

6.6 Analysis and Discussions

We have also conducted experiments with different sizes of asymmetric code and demonstrated that the DER will consistently improve with the size of the code. This is illustrated in Fig. 6.24 which shows the DER obtained for a (10,2) extended asymmetric code with the structure shown in Table 6.1 and compares it with an uncoded case. This illustrates that consistent improvement could be obtained if the asymmetric code is applied to large scale immunoassays similar to DNA microarrays.

Several conclusions can be drawn from the simulation results presented above.

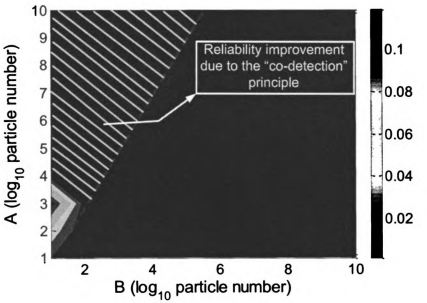

Figure 6.23: Detection of B biomolecule after decoding with background biomolecule A, where non-specific bindings of background biomolecule A serves as useful information for improving the reliability.

Table 6.1: (10,2) Asymmetric code

X_1	X_2	X_3	X_4	X_5	X_6	X_7	X_8	X_9	X_{10}
0	0	0	0	0	0	0	0	0	0
0	1	1	0	0	1	1	0	0	1
1	0	1	0	1	0	1	0	1	0
1	1	1	1	1	1	1	1	1	1

First, embedding an encoding scheme like a repetition code on the biosensor improves its reliability (given by DER) compared to the case when no encoding is used. However, an equivalent asymmetric code offers a better performance in terms of DER as shown in Fig. 6.11. The error rate of repetition code is higher than that of asymmetric code except of low concentration of both pathogens. The deviation can be attributed to imperfect modeling of the logic gates (AND and OR) due to limited experimental data, especially at low pathogen concentration levels. We also believe that improving the response of logic gates (AND and OR) would improve the performance

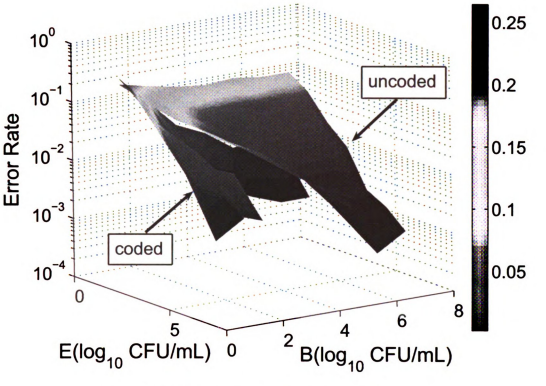

Figure 6.24: DER curve of (10,2) asymmetric code

of the asymmetric code.

The use of logic gates in biosensor encoder synthetically introduces coupling between multiple conductance measurements. In contrast to most biosensor designs, where the objective is to obtain independent measurements and in the process suppress any cross-reactive phenomena. In our prior work, we demonstrated that a non-linear classifier (support vector machine) can exploit the non-linear interaction between pathogens and their target/non-target antibodies to improve the detection performance. However, the training complexity significantly increases when the classifier has to model the side-information present at the output of the biosensor logic gates. We believe that incorporating cross-reactive principles in the FEC encoder would enhance the side-information available to the decoder to improve the detec-

tion reliability. The non-linear side information also leads to the previously referred principle called "co-detection". In the "co-detection" principle, a large concentration of known pathogen improves the detection of trace quantities of unknown pathogens. We attribute this effect to the non-linear properties of the AND/OR gate formed using antibodies corresponding to the known and unknown pathogen. When large quantity of known pathogens is added, the conductive polyaniline or gold nanoparticle bridge between the electrodes is partially formed. Thus, completion of the bridge could be achieved even when trace quantities of unknown pathogen is present. Also, the occurrence of false positive can be suppressed due to the principle of embedded encoding/decoding scheme.

The simulation study also show that the reliability of FEC biosensors improves as the size of the asymmetric code is increased. Thus, a trade-off exists between the reliability of the biosensor and redundant biomolecular circuit elements added, which is also related to biosensor area (cost). Future research will focus on optimizing the biosensor codes for achieving the optimal reliability, which is equivalent to deriving information theoretic bounds used in communication and storage systems. In this regard, the nature of biological channel needs to be investigated further to model and understand the stochastic protein-protein interaction and how it contributes to the biosensor noise.

Chapter 7

Experimental Verification and Discussion

A major challenge in the area of biomolecular detection is the capability to detect target biomolecules in the presence of large background interference [174]. Background interference could constitute the presence of non-target analytes which could not only produce non-specific binding events but also cause steric hindrance, preventing binding between target analytes with its specific recognition probes (antibody or DNA) [86]. Most of the reported methods in biosensors either aim to reduce the effect of background interference using pre-filtering techniques [7] or aim to boost the concentration of the target analyte using pre-concentration [8] or target-amplification (e.g. polymerase chain reaction or PCR). However, in our behavioral simulation, we showed that background interference created by the presence of non-specific analytes can be exploited to amplify and improve the reliability of detection of the target analyte.

The technique we described called "co-detection" exploits the non-linear redundancy amongst synthetically patterned biomolecular logic circuits for deciphering the presence or absence of target biomolecules in a sample. In this section, we experimen-

tally verify the "co-detection" principle on a gold-nanoparticle based conductometric soft-logic circuits which uses a silver-enhancement technique for signal amplification. "Co-detection" is similar in spirit to many noise exploitation techniques like stochastic resonance which has been reported in physics [175] and biology [21, 176], where it has been shown that addition of random noise into a non-linear system in fact improves the system sensitivity. However, the key towards implementing co-detection in biosensors is to effectively control the coupling (or interference) between different analytes and to effectively exploit the non-linear response of the biosensor. In this study we report that background interference created by the presence of non-specific analytes can be exploited to amplify and improve the reliability of detection of the target analyte. Ideally, the detection error-rate (DER) or the sum of false-positive or false-negative errors decreases with the increase in target biomolecules concentration and the DER is largely unaffected or is increased with higher concentration of background biomolecules. However in "co-detection", addition of background biomolecules (background interference) can actually reduces the DER for target biomolecules, and hence enhances the reliability of detection.

7.1 Experiment Design

To demonstrate the "co-detection" principle, a total of six different biochips (they are representing (6,2) asymmetric code) were used: two single analyte biochip specific to mouse IgG, two single analyte biochips specific to rabbit IgG, one soft-AND biochip and one soft-OR biochip. Those six biochip measurements constitute the input for a asymmetric code, which is evaluated for "co-detection" principle. The experimental procedure involved the following steps: (a) a sample was applied to the six biochips; (b) the measured conductance X_i were presented as inputs to the biosensor model, whose outputs were normalized to generate posterior probabilities.

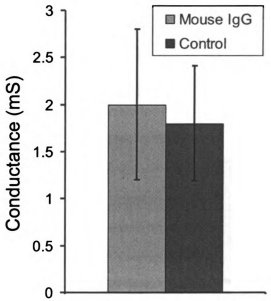

Figure 7.1: Experimental result from a mouse IgG biochip when 100 pg/mL target mouse IgG is applied.

For example, the soft-OR biochip model generated the posterior probability that either one of the analytes (rabbit or mouse IgG) is present $P(IgG_M + IgG_R|X_i)$ given the conductance measurement X_i. All of the posterior probabilities are combined together using described FFG decoding algorithm to compute the probability of the presence of target analytes $P(IgG_M|X_1,.,X_6)$, $P(IgG_R|X_1,..,X_6)$ given all the measured conductances X_1, X_2,...,X_6 (from six biochips). The probability scores are compared against a pre-determined threshold to make a positive identification of the target analyte.

7.2 Experimental Results

We now report results where the "co-detection" principle has been experimentally verified in the detection of a trace quantity of mouse IgG, which serves as a model

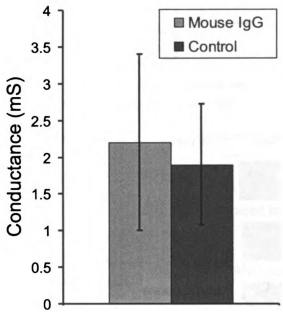

Figure 7.2: Experimental result from a mouse IgG biochip when 100 pg/mL target mouse IgG is used in the presence of 10 μg/ml of background rabbit IgG.

target biomolecule. In this experiment, we want to simulate a real scenario where targets biomolecules are often accompanied with other background biomolecules. Most nanobiosensor research demonstrate the biosensor superior sensitivity by only introducing pure target biomolecules [177], which is not a real scenario in biosensor detection especially in diagnostics application. For example, the real challenge in the HIV detection is to detect trace quantity of HIV antibody in the background of other biomolecules in blood serum.

In the first set of experiment, we first applied a sample only containing 100 pg/mL mouse IgG to a single mouse IgG biochip for calibration purposes. Bovine IgG is used as negative control experiment. Each experiments are repeated three times and the mean value and variance are plotted. Fig. 7.1 shows the detection result compared against the negative control. Even though the experiments show that on average

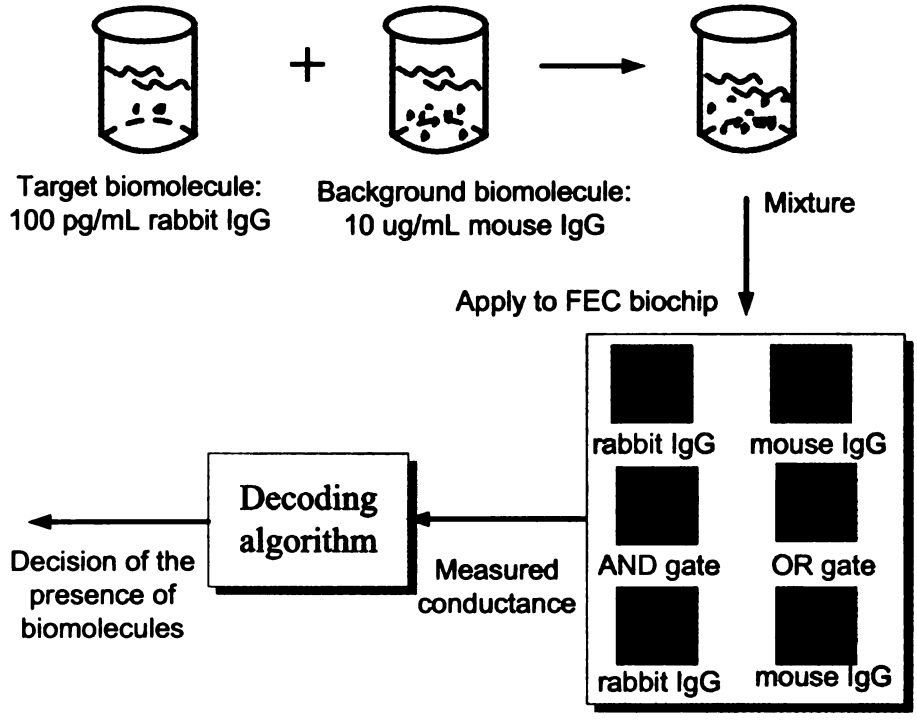

Figure 7.3: Experimental setup for "co-detection" verification.

the silver-enhancement technique can detect the trace quantity of mouse IgG, but the variance of the experiment (shown by the overlap between the error bars) is too large for reliable confirmation. It also shows that the low concentration of 100 pg/mL is beyond the detection limit of the designed mouse IgG biochip and it can not be reliably detected.

In the second set of experiment, 100 pg/mL mouse IgG (target biomolecule) is added to the solution of 10 μg/mL rabbit IgG that serves as the background interference. Fig. 7.2 shows the result obtained from the single mouse IgG biochip when a mixture of 100 pg/mL mouse IgG and 10 μg/mL rabbit IgG is applied. The mean value of detected mouse IgG is larger than that of mouse IgG without background rabbit IgG. It is due to the fact that some of non-target rabbit IgG bind with anti-rabbit IgG probes. However, the experimental result shows similar response as the previous experiment. The mean value of mouse IgG detection is larger than that of

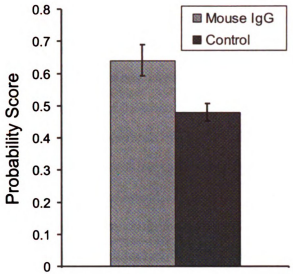

Figure 7.4: Result from the FEC biosensor decoder showing significant improvement in reliability of mouse IgG detection in the presence of background rabbit IgG.

the control experiment. But the variance is too large to confirmation the detection. In this case, rabbit IgG serves as non-specific binding noise to the mouse IgG detection and that verify that background biomolecules can often hinder the detection of target biomolecules.

In the last set of experiment, the mixture with similar composition was applied to the FEC biochip (six corresponding biochips) and the measured conductances were process by the described decoding algorithm. Fig. 7.3 shows the experimental setup for detecting trace quantity of mouse IgG in the background rabbit IgG in a FEC biochip. Fig. 7.4 shows the response obtained from the decoder and compares it with results obtained for the negative control experiments. Note that the output of the decoder is the normalized score indicating the presence or absence of mouse IgG. It can be clearly seen from the figure that not only has the magnitude of the scores have increased significantly compared to the control, the variance of the results have also decreased by orders of magnitude. Since there is no overlap between

error bars, perfect detection of mouse IgG can be achieved in the presence of high background concentration of rabbit IgG. In this case, we experimentally verify that non-specific binding could be a useful information in the detection of trace quantity of biomolecules. Note that it not only can improve the reliability of biosensors, it also indeed improve the detection limit of biosensors.

We believe that the non-linear response of the FEC biochip in conjunction with "co-detection" is the primary reason behind the improvement in reliability. The presence of large background interferences introduces conduction sites which can be easily populated by the target analytes. The computational approach for co-detection bears similarity to DNA signature discovery techniques. However, the key difference in this work is exploitation of background noise instead of suppressing it. We would also like to point out that even though in our report, we have used only two analytes (mouse IgG and rabbit IgG) to demonstrate the "co-detection" principle, the approach is generic and can be extended to any kinds and any number of analytes. In fact we anticipate significant improvements in reliability as the number of analytes increases. This is because of the exponential increase in the side-information that is available through coupling between multiple binding events. One of the key applications where "co-detection" could be used in the future is in the early diagnosis of HIV. Early diagnosis of HIV requires detecting trace quantity of HIV biomolecules that are usually accompanied by other non-specific biomolecules that directly interfere in the detection process [178] and usually require several days for confirmation tests. Window period is an important parameter for HIV detection, which is an indication of time of the concentration of HIV antibody being sufficient to be detected. The improvement in reliability offered by "co-detection" could reduce the window period for positive or negative diagnosis and hence can facilitate rapid screening.

Chapter 8

Conclusions and Future Work

8.1 Summary

The objective of this research is to replicate the success of FEC principles in designing reliable computing and storage systems towards designing reliable biosensors. In this regard, the study addresses some of the key challenges in this long-term goal. The study presents a systematic framework of designing reliable biosensors with embedded error-correction functions. The first step involves deriving a general Markov chain model, which simulates the stochastic nature of biomolecular interaction. The second step involves mathematical abstraction where simulation models are developed to capture experimentally measured response of biomolecular circuits. These simulation models are then used to: (a) understand the behavior of the biomolecular circuits; (b) rapid design and evaluation of different FEC encoding and decoding algorithms without resorting to painstaking experimental procedures. We then have presented an analytic framework of FEC biosensors that have different encoder topologies. Two biosensor platforms (lateral flow immunoassay and silver-enhanced gold nanoparticle based biochip) have been adopted as model biosensor encoders that are synthetically patterned with redundant biological probes. Reliability analysis is performed

by exploiting probabilistic dependencies between the biomolecular circuit elements using a factor graph based decoding technique. Using the simulation framework, we demonstrated the efficacy of an asymmetric biosensor code as a potential candidate for improving the reliability of the FEC biosensor.

We also reported a novel "co-detection" principle based on the property of the asymmetric code. The principle exploits the non-linear coupling between different biomolecular circuits and prescribes an experimental protocol that could be used for trace detection of pathogens in a given sample. One of the key applications where "co-detection" could be used in the future is in the early diagnosis of HIV. Using derived Markov model, we prove that the "co-detection" principle theoretically exists and simulation results from the Markov model coincide with the ones from experimental results. We then reported experimental results where the "co-detection" principle has been successfully verified in the detection of trace quantity of mouse IgG in the presence of larger background of other biomolecules. We believe that the proposed analytical framework in this study will serve as an important design tool for circuit designers and information theorists for evaluating the performance of different encoding and decoding principles in biosensor systems.

8.2 Future Directions

This work demonstrates the design of forward error-correction biosensor, which can greatly improve the reliability and accuracy of biosensors. There are some promising research directions involved in the FEC biosensor design.

Biosensor computer-aided design (Bio-CAD) can be a valuable tool that can assist biosensor designers to pattern and test biosensors in a virtual environment and can be used for rapid evaluation of biological protocols. Traditionally biosensor experiments are very time-consuming, labor-intensive, and expensive. With the help of the

developed Bio-CAD model, different building blocks can be configured, connected in an arbitrary fashion and tested using computer simulations. It will help to shorten the development phase of engineered biological systems and the discovery of drugs. It is very promising to replicate the similar success in the VLSI industry because design can be standardized and simplified by using the standard design library.

There are many theoretical parts that can be developed in the regime of FEC biosensors. First, we need fully understand all the mechanisms involved in biological information transfer, we need to model the biological pathways in the detection process. Famous Shannon's theorem tells us information can be communicated over a noisy channel at a non-zero rate with arbitrarily small error probability. Information theory addresses both the limitations and the possibilities of communication. The noisy-channel coding theorem, which we will prove in asserts both that reliable communication at any rate beyond the capacity is impossible, and that reliable communication at all rates up to capacity is possible. We could establish an equivalent concept of "Shannon-Limit" that is applicable to biosensors. In this regard, there might exist a fundamental limit, namely "biosensor channel capacity", which could be a function of the detection technology being employed and determine the minimum amount of redundancy required to obtain perfect reliability.

In our study, we demonstrate the efficacy of the asymmetric code. The asymmetric code takes advantage of "non-linearity" of logic AND and OR gate to explore the "co-detection" principle. We have experimentally verified the principle using two model biomolecules. Another important issue is the optimization of biosensor codes when multiplex pathogens are needed to be screened.

Appendix A

FEC Biosensor Protocols

A.1 Fabrication of Membrane-based Lateral Flow Immunosensor

Polyaniline Conjugating with Antibodies

1. Add 800 μL of the polyclonal (150 μg/mL) of antibody in a 4 mL of polyaniline solution in phosphate buffer (pH 7.4) containing 10 % dimethylformamide (DMF) (v/v) and 0.1 % LiCl (w/v).

2. Leave to react for 1 hour.

3. Add 1 mL of blocking reagent (tris buffer) containing 0.1% of casein.

4. Leave to react for another 30 min.

5. The polyaniline-multi-variate antibody conjugates were then precipitated by centrifugation at 12,000 rpm for 5 min.

6. Discard the supernatant liquid.

7. The solution was mixed with the blocking reagent and centrifuged again.

8. Repeat the above procedure twice.

9. The conjugates were finally suspended in phosphate buffer solution containing 0.1 % LiCl (w/v) and 10 % DMF (v/v).

10. Store at 4^oC before use.

Capture Pad Preparation

1. Cut the nitrocellulose membranes (NC) into smaller pieces (30 cm/4) to fit into a petri dish.

2. Wash the membranes with distilled water three times and let dry for 30 min.

3. Immerse the membranes in 10% methanol. The membranes are left to air-dry for 30 min.

4. Apply 0.3 mL of 0.5 mg/mL of antibodies on membranes. Seal the petri dish with a parafilm and incubate at 37^oC for 60 min.

5. Wash the membrane with 0.3 ml of 100 mM tris buffer containing 0.1% (v/v) tween-20. Note: experimental results show that adding tween-20 might affect protein binding, so the concentration of tween-20 should keep as minimum as possible or even be omitted.

6. Dry the membrane for 30 min.

7. Store the prepared membranes at 4^o C.

A.2 Fabrication of Biochip

1. Thermally grow a 2 μm layer of silicon oxide on 4" (100) silicon wafers.

2. Wafers are cleaned in isopropyl alcohol solution followed by distilled water.

3. Wafers are placed on a photoresist (PR) spinner.

4. A small volume of photoresist is pipetted onto the center of the wafer and the spinner is actuated.

5. If photoresist cover entire wafer homogenously, wafers are transfered to the oven for soft bake at 90^o for 30 min.

6. Wafers are then transferred to the photomask aligner and the wafer is exposed to 2.2 seconds of UV light at a wavelength of 440 nm and the expose time can be adjusted a little bit after you inspect the wafer surface.

7. Wafers are immersed in PR developer solution for a time of 1-2 minutes to do the lithograph and wafers are dried under nitrogen stream.

8. Once examine the quality of PR mask, wafers are transferred to oven for hard bake at 135^oC for 1 hour.

9. Wafers are loaded into metal evaporation chamber, which includes chrome and gold pellets for use in the evaporation procedure.

10. A 10 nm think layer of chrome is evaporated over entire surface of the wafer.

11. A 100 nm thick layer of gold is evaporated over entire surface of the wafer above the chrome layer.

12. Wafers are immersed into crystallizing dish filled with acetone.

13. The crystallizing dish is sonicated for 2 min to promote lift-off process. We have to make sure the lift-off process is fast and smooth, otherwise, the metals are easy to rebuild onto the surface of wafers.

14. Wafers are cleaned with distilled wafer followed by isopropyl solution.

15. The quality of wafers should be inspected by microscope after dying under s stream of nitrogen.

16. A protective layer of PR is applied onto the surface of wafers to protect harsh process during dicing.

17. The fabrication process is completed once it was diced using dicing saw.

A.3 Operation Summary of Biochip MEMS Fabrication

Make Masker

1. Open software "Electromask II"

2. Click "PG"; choose parameter: Exposure: 250; LargeExp: 300; X(μm): -62230, Y(μm): -63500

3. On the menu "OP" and "Graph", choose expo: 1000 or 1200

4. Press "IG" button. From the "mode" menu, choose "IR" and decide step size; Choose "OP", then choose "Pass".

The Procedures of Developing and Cleaning Photomask (shown in Fig.A1

1. Use MF319 developer to do developing procedure.

2. Use etchant to remove the chrome.

3. Use PRS2000 to remove the photoresist (PR).

4. Put photomask into Acetone and swing gently.

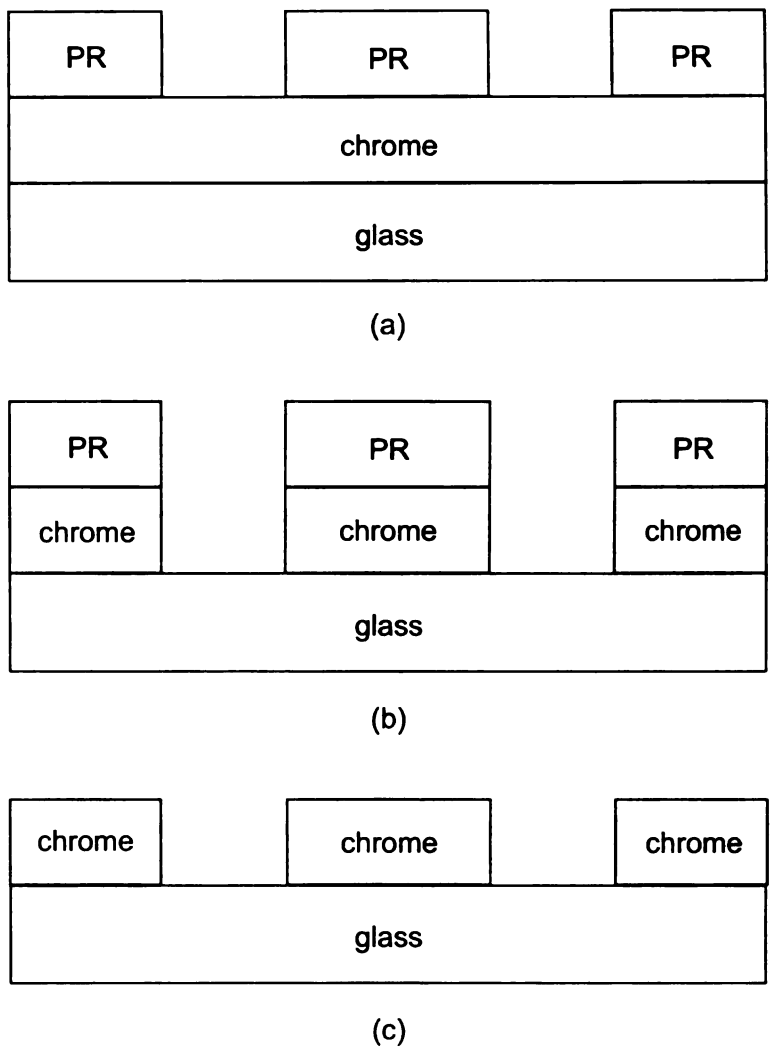

Figure A.1: Developing procedures for photomask.

5. Then put the photomask into IPA, swing gently. Put into secondary IPA.

6. Rinse the photomask with water and dry.

Operation of MA6 Mask Aligner

1. Use the on/off key to turn on the system. Make sure the channel 2 is on and the lamp is 405 nm (20 mW/cm^2) and 365 nm (11 mW/cm^2).

2. Press "Load" and ensure that the configuration is MA6 for lithograph.

3. Press "Enter". Make sure that the micrometer's setting is 10 mm. Ensure that the theta (white line on front of system) is lined up. Also ensure that the N_2 line for the mask holder is connected.

   Loading the mask:

4. In the menu, choose "Change mask" and slide the mask tray out. Place the mask to be used on the holder. (chrome side up). Use three alignment pins to enter the mask.

5. Press "Enter" to turn the vacuum on and push the silver tab down on the clip.

6. Use nitrogen gun to blow off any possible particles on the mask surface.

7. Slide the wafer chuck back into the system. Now load the mask by pressing "Change mask".

8. Edit parameter by pressing "Edit" button. Press it again when finish editing.

   Exposure:

9. Press "Exposure" to do exposure. In our experiments, we have chosen the exposure time to be 6 and 8 second. We found 8 second exposure time might be better for our application.

   Shut down:

10. Press "Change mask". Slide the mask tray out and place on the shelf. Release the spring clip. Press "Enter" to turn off the vacuum, and place the mask back into place.

11. Turn off the system.

Metallization

1. Open the chamber and put metals you want (Cr/Au in our case) on the holes. Put silicon wafers on the holder and the holder can host up to 9 wafers simultaneously.

2. Close the chamber and set parameters. We choose deposit Cr layer with 10 nm and Au layer with 100 nm.

3. Press "Prog" button to set parameters. Find appropriate thickness, then check the deposit rate. Press "Prog", "Stop", and "Reset" to save the program.

Lift-off Procedure

1. Prepare three crystallizing dishes for holding Acetone, Acetone, and Isopropyl alcohol (IPA).

2. Put wafers into Acetone for some time (maybe overnight). Use Acetone rinse their surface to remove any metal residuals. Note: we have to make sure the process is fast encough because Acetone evaporate very fast, and the metal is easy to deposit on the wafer surface again when the surface is dry.

3. Put wafers into Acetone solution again and sonicate it for 10-15 min.

4. Rinse again with Acetone and put another dish with Acetone, sonicate again for another 2-5 min.

5. Bring the wafers and put them into IPA dish and swing them gently.

6. Rinse with IPA and dry them with N_2 gun.

7. Inspect wafers using microscope.

A.4 Surface Functionalization of the Biochip

Surface Clean

1. Biochips are immersed in the Acetone to remove protective PR for 10 min.

2. Rinse Biochips with IPA or Methanol.

3. Biochips are cleaned by immersing in a 1:1 mixture of HCL and Methanol for 30 min followed by rinsing several times with distilled water.

4. Biochips were treated with concentrated sulfuric acid for 30 min and rinsed several times with distilled water. (This step can be optional!)

5. Biochips are immersed into the boiling water for 30 min.

6. Left to air dry.

Surface Silanization

7. Inside the glove box, biochips are immersed into a 2% MTS solution for 2h.

8. Biochips are rinsed with Toluene, and followed by rinsed with distilled water, and allow to air dry.

Surface Cross-Linking Treatment

9. GMBS are pipetted onto biochips active surface and incubate the biochips for 1 h, and washed with distilled water.

10. Antibody (anti-IgG) is pipetted onto biochip active surface using Biodot dispersing machine. Put biochips into Petri Dishes sealed with parafilm and incubate for 1 h at 37^oC. After which, biochips were rinsed with PBS. Be careful, wash the biochips before they are dry.

11. Biochips then were incubate with blocking agent (BSA) 2 mg/mL for 1 h, followed by washing with PBS. Left for dry.

12. Storage: biochips were put into the Petri Dishes sealed with parafilm and are placed under refrigerated conditions of 4^oC until use.

    Note: Washing step is more important than you thought. The washing time and force will affect the protein binding and the optimal washing time and force should be adjusted during the experiments. I adjusted the washing time by examining the SEM image of biochip to identify the surface of protein binding.

Testing

1. Apply IgG (model antigen) onto the biochip using Biodot dispensing machine or pipette. Incubate for 30 min. Wash with PBS to remove excessive IgG.

2. Apply Anti-IgG gold nanoparticle solution onto the biochips and incubate for 30 min. Wash with PBS to remove excessive conjugate.

3. Apply silver enhancement solution and measure the conductance of biochips. There are two modes to measure the conductance change of biochips: continues mode and discrete mode. We can use data acquisition card (NI 6221 DAQ) to continuously monitor the process. Another method is to stop the silver enhancement by drying with the nitrogen gas and to measure the conductance value. Then apply the silver enhancement solution and resume the process. We noticed the conductance value in the dry phase is higher than that of in aqueous phase, but both measurements have similar trend.

A.5 Reagent Preparation

0.1% (w/v) Peptone water

First, add 1 g of powder in 1 L of distilled water and autoclave the solution for 15 min at 121^oC.

0.1 M Sodium Phosphate Buffer

Weigh 8.62 g of dibasic sodium phosphate and 5.42 g monobasic sodium phosphate. Add 1 L distilled water and measure the pH. If the pH is below 7.4 adjust it by adding several drops of 1 M NaOH. If pH is above 8.3 adjust with several drops of 1 M HCl.

2% MTS (Silane)

(3-Mercaptopropyl) trimethyloxysilane (MTS) purchased from Sigma (St. Louis, MS) was diluted in toluene purchased from J.T. Baker (Phillipsburg, NJ).

50:50 Methanol:HCl

The 50:50 mixture contains equal parts of methanol purchased from CCI (Columbus, WI) and 1.0 M HCl purchased from Sigma (St. Louis, MS).

GMBS (Crosslinker)

4-maleimidobutyric acid N-hydroxysuccinimide (GMBS) was purchased from Sigma (St. Louis, MS) and diluted in N,N-Dimethylformamide purchased from Spectrum (New Brunswick, NJ). The solution was diluted to 2mM in ethanol purchased from Pharmco (Brookfield, CT).

Appendix B

Operating Protocols of BioDot XYZ3050 Dispensing Machine

B.1 Initialize the Equipment

1. The first step is to prime the liquid you want to dispense. From the menu, choose "Prime" and also choose "Group"; decide the prime cycles (I choose 6 for typical use). Press "Activate" to begin to prime the liquid.

   Choose program

2. Choose "Data storage"; Choose "Program" and select the program you want to run.

3. Then back to the main menu; choose "Pattern" and select the pattern.

4. When you finish using the machine, you can back to the main menu. Choose "Empty" and press "Activate" button to empty the liquid. So the liquid in the tubes begin to flow back into the container. Generally it is safe to reuse the proteins, which flow back to the container.

B.2 Procedure of Creating a New Program

1. Confirm that system electrical and pneumatic systems are energized.

2. Confirm that the handheld terminal is properly connected to the platform and the coiled cord for the terminal should be plugged into the outlet labeled Terminal located on the backside of the unit.

3. Press Enter to go to the terminal main menu.

4. From the terminal main menu, locate and select the menu option listed below:

   DATA STORAGE

5. This bring up the Data Storage, with the following options displayed:

   PROGRAMS

   SAVE DATA

   LOAD DATA

   then select the PROGRAMS menu option: use the up/down arrow keys to bring the arrow pointer to your choice, and press the enter key to select it.

6. The following menu options will be displayed:

   CREATE

   Select CREATE. A screen with a blinking cursor will appear, prompting you to enter a file name for your new program.

7. Using the terminal keypad, type a name for the new program and press ENTER.

8. Press the ESC key several times until you return to the main menu.

9. From the main menu, select the PATTERNS menu, which will bring up the following options:

CREATE

EDIT

SELECT

DELETE

10. Select the EDIT option, which displays the program parameters for the program name that you created above.

11. Enter the following parameters for your sample program.

12. To run the program, we just simply need to press the GO key to observe platform movement and the appearance of the dispensed line. We can press the ABORT button to suspend the program and stop platform movement.

    Note: please be sure to save the program before exiting. Otherwise, you might lose your new program.

B.3 Cleaning Protocols

To obtain optimum performance and maximum life from BioDot dispensers, it is important that the routine cleaning procedure listed below be followed after each period of use. The number of priming cycles used to move cleaning agents through the system should be adequate (about 10 cycles in our cases) to expose all channel components. This volume will depend on length of tubing and size of syringe. Required number of priming cycles can be established by introducing air into the inlet tubing, re-inserting inlet tubing into backing solution and observing the number of cycles required to eject liquid at the tip.

1. Purge supply lines of reagent with de-ionized water.

2. Clean and refill the supply reservoir with deionized water containing 1% Jet Wash II. The actual concentration of this non-ionic surfactant-containing detergent should be scaled to the amount and nature of reagents dispensed. Protein and nucleic acid concentrations in excess of 1 mg/mL require elevated amounts of detergent. Prime dispensers to fill system.

3. Repeat steps 1 and 2 with deionized water.

4. If introduction of air is observed during cleaning, the system can be de-gassed with 100% EtOH, MeOH or IPA (2-propanol). Prime with alcohol followed by (vacuum degassed) deionized water or backing solution.

5. With frequent cleaning, the reagent reservoirs and feed lines can be reusable.

Weekly cleaning. After prolonged dispensing of reagents, some buildup of protein and salts may occur. We do the following cleaning steps be followed on a weekly basis to dissolve any accumulated materials.

1. Purge supply lines of fluids and complete Daily Procedure.

2. Clean and refill the supply reservoir with a dilute acid (0.1N HCI). Prime through and allow to sit for 10 minutes.

3. Prime using deionized water as in step 1 above.

4. Clean and refill the supply reservoir with a dilute base (0.1N NaOH). Prime and allow to sit for 10 minutes.

5. Purge the supply lines and prime using deionized water.

6. De-gas with alcohol if needed and follow with backing solution or leave system dry if instrument is powered off for an extended period.

B.4 Instructions for Use of JetWash II

JetWash II is a powerful cationic detergent and should be treated as a potentially hazardous substance. It is used as washing reagent for BioDot 3050. Here is a brief summary of the use of JetWash II.

1. JetWash II is diluted in water (deionized grade or better). For most routine cleaning procedures, it can be used at 0.05% (50 μL into 100 mL water).

2. If the dilute concentration fails to dissolve biologicals, more concentrated solutions up to 10% can be used. Dried blood or concentrated protein solutions, when dehydrated, can usually be dissolved with JetWash II diluted to 2%.

3. Diluted JetWash II can be used in BioJet instruments in In-Line or Aspirate-Dispense modes to clean reservoir bottles, syringes, tubing, valves and ceramic tips. Always rinse thoroughly with deionized water following treatment with JetWash II.

BIBLIOGRAPHY

[1] Food and Drug Administration, "Bacteriological Analytical Manual. 8th ed.," Arlington, VA: Association of Analytical Chemists, 2000.

[2] L. J. Kricka, "Interferences in Immunoassay Still a Threat," *Clin. Chem.*, 46:10378, 2000.

[3] W. Preiser, N. S. Brink, A. Hayman, J. Waite, P. Balfe, R. S. Tedder, "False-Negative HIV Antibody Test Results,", *J. Med. Virol.*, pp. 600-437. 2000.

[4] C. Selby, "Interference in Immunoassay," *Ann. Clin. Biochem.*, Vol. 36, pp. 70421, 1999.

[5] S. Rotmensch, L. A. Cole, "False Diagnosis and Needless Therapy of Presumed Malignant Disease in Women with False-Positive Human Chorionic Gonadotropin Concentrations," *Lancet*, Vol. 355:7125, 2000.

[6] S. P. Mohanty, E. Kougianos, "Biosensors: a Tutorial Review," *IEEE Potentials*, vol. 25, issue 2, pp. 35-40, 2006.

[7] Y. Wang, F. Makedon, J. Ford, and J. Pearlman, "HykGene: A Hybrid Approach for Selecting Marker Genes for Phenotype Classification Using Microarray Gene Expression Data," *Bioinformatics*, Vol. 21, pp. 1530-1537, 2005.

[8] J. P. Fitch, E. Raber, D. R. Imbro, "Technology Challenges in Responding to Biological or Chemical Attacks in the Civilian Sector," *Science*, Vol. 21, pp. 1350-1354, 2003.

[9] S. M. Huse, J. A. Huber, H. G. Morrison, M. L. Sogin, D. M. Welch, *Genome Biology*, Vol. 8, 2007.

[10] J. P. Noonan, G. Coop, S. Kudaravalli, D. Smith, J. Krause, J. Alessi, F. Chen, D. Platt, S. Paabo, J.K. Pritchard, E. M. Rubin, *Science*, Vol. 17, 2006.

[11] G. J. Zhang *et al*, "Production of Nanopatterns by a Combination of Electron Beam Lithography and a Self-assembled Monolayer for an Antibody Nanoarray," *J. Nanosci. Nanotech*, vol. 7, pp. 410C417, 2007.

[12] T. K. Moon, Error Correction Coding. New Jersey: John Wiley and Sons. 2005.

[13] C. Wingren ,and A. K. Borrebaeck, "Progress in Miniaturization of Protein Arraysa Step Closer to High-density Nanoarrays," *Drug Discov Today*, Vol. 12, Issue:19-20, pp. 813-819, 2007.

[14] A. Hassibi, "Integrated Microarrays," Ph.D. Thesis, Stanford University, 2006.

[15] D. Janasek, J. Franzke, and A. Manz, "Scaling and the Design of Miniaturized Chemical-Analysis Systems," *Nature*, Vol. 442, pp. 19-27, July 2006.

[16] L. L. Lv, B. C. Liu, C. X. Zhang, Z. M. Tang, L. Zhang, Z. H. Lu, " Construction of an Antibody Microarray based on Agarose-Coated Slides," *Electrophoresis*, Vol. 28, pp. 406-413, 2007.

[17] F. Vinet, P. Chaton, Y. Fouillet, "Microarrays and Microfluidic Devices: Miniaturized Systems for Biological Analysis," *Microelectronic Engineering*, Vol. 61-62, pp. 41-47, July 2002.

[18] R. L. Stears, T. Martinsky, and M. Schena , "Trends in microarray analysis," *Nature Medicine*, Vol. 9, pp. 140-145, 2003.

[19] A. Bulsara, L. Gammaitoni, "Tuning in to Noise". Physics Today, Vol. 49, pp. 39C45, 1996.

[20] P. Hanggi, "Stochastic Resonance in Biology. How Noise Can Enhance Detection of Weak Signals and Help Improve Biological Information Processing," *Chemphyschem*, Vol. 3, pp. 285C90, 2002.

[21] K. Wiesenfeld, F. Moss, "Stochastic Resonance and the Benefits of Noise: From Ice Ages to Crayfish and Squids," *Nature*, Vol. 373, pp. 33-36, 1995.

[22] W. R. Heineman, and W. B. Jensen, "Leland C. Clark Jr. (1918C2005)," *Biosensors and Bioelectronics*, vol. 21, issue 8, pp. 1403-1404, 2006.

[23] D. R. Thevenot, K. Toth, R. A. Durst, and G. S. Wilsond, "Electrochemical Biosensors: Recommended Definitions and Classification," *Biosensors and Bioelectronics*, vol. 16, no. 1, pp. 121-131, January 2001.

[24] J. Luong, P. Bouvrette, and K. B. Male, "Developments and Applications of Biosensors in Food Analysis," *Trends in Biotechnology*, Vol. 15, Issue. 9, pp. 369-277, 1997.

[25] R. Freitag, "Current Opinion in Biotechnology," *Applied biosensors*, Vol. 4, Issue. 1, pp. 75-79, 1993.

[26] C. M. Grisham, R. H. Garrett, Biochemistry, Philadelphia: Saunders College Pub, pp. 426-427, 1999.

[27] M. J. Madou, and M. Tierney, "Required Technology Breakthroughs to Assume Widely Accepted Biosensors," *Applied Biochemistry and Biotechnology*, vol. 41, 1993.

[28] A. Bairoch, "The Enzyme Database in 2000," *Nucleic Acids Res*, Vol. 28 (1), pp. 304C305, 2000.

[29] J. S. Schultz, Biosensors: Fundamentals and Applications ed A P F Turner, I Karube and G S Wilson (New York: Oxford University Press), pp 638C54, 1987.

[30] G. W. Litman, J. P. Rast, M. J. Shamblott, "Phylogenetic Diversification of Immunoglobulin Genes and the Antibody Repertoire," *Mol. Biol. Evol*, Vol. 10, pp. 60-72, 1993.

[31] E. Market, F. N. Papavasiliou, "V(D)J Recombination and the Evolution of the Adaptive Immune System," *PLoS Biology*, 1(1): e16, 2003.

[32] http://www.biology.arizona.edu/IMMUNOLOGY/tutorials/antibody/structure.html.

[33] C. R. Lowe, Y. Hin, D. C. Cullen, S. E. Evans, S. Stephens, and P. Maynard, *J. Chromatography*, Vol. 510, pp. 347, 1990.

[34] J. C. Andle, J. F. Vetelino, M. W. Lade and D. J. McAllister, "An acoustic plate mode biosensor," *Sensors and Actuators B*, Vol. 8, pp. 191-198, 1992.

[35] J. C. Andte and J. F. Vetelino, "Acoustic Wave Biosensors," *Sensors and Aetaators A*, Vol. 44, pp. 167-176, 1994.

[36] W. Saenger, Principles of Nucleic Acid Structure, New York: Springer-Verlag, ISBN 0387907629, 1984.

[37] B. Alberts, A. Johnson, J. Lewis, M. Raff, K. Roberts, and P. Walters, Molecular Biology of the Cell, Fourth Edition, New York and London: Garland Science, ISBN 0-8153-3218-1, 2002.

[38] R. Lacowicz, Principles of Fluorescence Spectroscopy, 2nd ed. Plenum, New York, 1999.

[39] A. D. Ellington, and J. K. Szostak, "In vitro Selection of RNA Molecules that Bind Specific Ligands," *Nature*, Vol. 346, pp. 818-822, 1990.

[40] D. V. Lim, J. M. Simpson, J.M, Kearns, E. A. and M. F. Kramer, "Current and Developing Technologies for Monitoring Agents of Bioterrorism and Biowarfare," *Clin. Microbiol. Rev.*, Vol. 18, pp. 583-607, 2005.

[41] E. Luzi, M. Minunni, S. Tombelli, and M. Mascini, "New Trends in Affinity Sensing-Aptamers for Ligand Binding," *Trends in Analytical Chem*, Vol. 22, pp. 810-818, 2003.

[42] T.M.A. Gronewold, S. Glass, E. Quandt, and M. Famulok, "Monitoring Complex Formation in the Blood Coagulation Cascade using Aptamer-coated SAW Sensors," *Biosens. Bioelectron*, Vol. 20, pp. 2044-2052, 2005.

[43] C. A. Savran, S. M. Knudsen, A. D. Ellington, and S. R. Manalis, "Micromechanical Detection of Proteins using Aptamer-based Receptor Molecules," *Anal. Chem*, Vo. 76, pp. 3194-3198, 2004.

[44] M. Liss, B. Petersen, H. Wolf, and E. Prohaska, "An Aptamer-based Quartz Crystal Protein Biosensor," *Anal. Chem.*, Vol. 74, pp. 4488-4495, 2002.

[45] M. Piliarik, H. Vaisocherov, J. Homola, "Surface Plasmon Resonance Biosensing," *Biosensors and Biodetection*, Methods in Molecular Biology, Vol. 503, editors A. Rasooly, K. E. Herold, Humana Press, pp. 65-88, 2009.

[46] M. P. Marco, D. Barcel, "Environmental Applications of Analytical Biosensors," *Measurement Science and Technology*, Vol. 7, No. 11, pp. 1547-1562, 1996.

[47] S. Jeon, R. Desikan, F. Tian, T. Thundat, "The Influence of Nanobubbles on the Bending of Microcantilevers," *Appl. Phys. Lett*, Vol. 88, 2006.

[48] J. Edwards, D. Ausserre, H. Hervet, and F. Rondelez, "Quantitative Studies of Evanescent Wave Intensity Profiles using Optical Fluorescence," *Applied Optics*, Vol. 28, Issue 10, pp. 1881-1884, 1989.

[49] A. F. Collings and F. Caruso, "Biosensors: Recent Advances," *Rep. Prog. Phys*, Vol. 60, pp. 1397C1445, 1997.

[50] T. Dubrovsky, S. Vakula, C. Nicolini, "Preparation and Immobilization of Langmuir Blodgett Films of Antibodies Conjugated to Enzyme for Potentiometric Sensor Application," *Sensors and Actuators*, Vol. 22, pp. 69-73, 1994.

[51] J. E. Zull, J. Reed-Mundell, Y. W. Lee, D. Vezenov D, N. P. Ziats, J. M. Anderson, and C. N. Sukenik, "Problems and Approaches in Covalent Attachment of Peptides and Proteins to Inorganic Surfaces for Biosensor Applications," *J Ind Microbiol*, Vol. 13(3), pp. 137-143, 1994.

[52] G. J. Leggett, C. J. Roberts, P. M. Williams, M. C. Davies, D. E. Jackson, and S. J. B. Tendler, "Approaches to the Immobilization of Proteins at Surfaces for Analysis by Scanning Tunneling Microscopy," *Langmuir* Vol. 9, pp. 2356-2362, 1993.

[53] N. J. Geddes, E. M. Paschinger, D. N. Furlong, F. Caruso, C. L. Hoffmann, and J. F. Rabolt, "Surface Chemical Activation of Quartz Crystal Microbalance Gold Electrodes - Analysis by Frequency Changes, Contact Angle Measurements and Grazing Angle FTIR," *Thin Solid Films*, Vol. 260, pp. 192-199, 1995.

[54] C. J. Brinker and G. W. Scherer, Sol-Gel Science, (New York: Academic), 1990.

[55] I. V. Turko, I. S. Yurkevich, and V. L. Chashchin, *Thin Solid Films*, Vol. 205, pp. 113, 1991.

[56] I. V. Turko, I. S. Yurkevich, and V. L. Chashchin, *Thin Solid Films*, Vol. 210, pp. 710, 1992.

[57] R. Lacowicz, Principles of Fluorescence Spectroscopy, 2nd ed. (Plenum, New York, 1999).

[58] R. Wiese, Y. Belosludtsev, T. Powdrill, P. Thompson, M. Hogan, "Simultaneous Multianalyte ELISA Performed on a Microarray Platform," *Clinical Chemistry*, vol. 47, pp. 1451-1457, 2001.

[59] C. R. Taitt, J. P. Golden, Y. S. Shubin, L. C. Shriver-Lake, K. E. Sapsford, A. Rasooly, F. S. Ligler, "A Portable Array Biosensor for Detecting Multiple Analytes in Complex Samples," *Microbial Ecology*, vol. 47, no. 2, pp. 175-185, 2004.

[60] M. Schena, Microarray Analysis (Wiley, New York, 2003).

[61] P. Fromherz, "Joining Ionics and Electronics: Semiconductor Chips with Ion Channels, Nerve Cells, and Brain Tissue," *IEEE Int. Solid-state Circuits Conf*, pp. 76-77, 2005.

[62] R. A. Kaul, N. I. Syed, and P. Fromherz, "Neuron-Semiconductor Chip with Chemical Synapse between Identified Neurons," *Phys. Rev. Lett.*, Vol. 92, pp. 38102-38104, 2004.

[63] B. Eversmann, C. Paulus, F. Hofamann, R. Brederlow, B. Holzapfl, et.al, " A 128 X 128 Biosensor Array for Extra-Cellular Recording of Neural Activity," *IEEE Int. Solid-state Circuits Conf.Dig.*, pp. 222-223, 2003.

[64] R. Harrison, P. Watkins, R. Kier, R. Kier, R. Lovejoy, D. Black, R. Normann, and F. Solzbacher, "A Low-Power Integrated Circuit for a Wireless 100-electrode Neural Recording System," *IEEE Int. Solid-state Circuits Conf.Dig.*, pp. 2258-2267, 2006.

[65] F. Heer, S. Hafizovic, W. Franks, A. Blau, C. Ziegler, and A. Hierlemann, "CMOS Microelectrode Array for Bidirectional Interaction with Neuronal Networks," *IEEE J. Solid-State Circuits*, Vol. 41, pp. 1620-1629, 2006.

[66] Y. Song, W. R. Patterson, C. W. Bull, J. Beals, N. Hwang, A. P. Deangelis, C. Lay, J. L. McKay, A. V. Nurmikko, M. R. Fellows, J. D. Simeral, J. P. Donoghue, and B. W. Connors, "Development of a Chipscale Integrated Microelectrode/Microelectronic Device for Brain Implantable Neuroengineering Applications," *IEEE Trans. Neural Rehabil.Eng.*, Vol. 13, pp. 220-226, 2005.

[67] M. Xue, J. Li, Z. Liu, C. Feng, Z. Zhang, P. Ko, and M. Chan, "A High Density Conduction Based Micro-DNA-Identification Array Fabricated in a CMOS Compatible Process," *IEEE Int. Solid-state Circuits Conf.Dig.*, pp. 198-199, 2003.

[68] R. Thewes, F. Hofmann, A. Frey, B. Holzapfl, M. Schienle, C. Paulus, P. Schindler, G. Eckstein, C. Kasse, M. Stanze, R. Hintsche, E. Nebling, J. Albers, J. Hassman, J. Schulen, W. Goemann, and W. Gumbrecht, "Sensors Arrays for Full-electronic DNA Detection on CMOS," *IEEE Int. Solid-state Circuits Conf.Dig.*, pp. 350-351, 2002.

[69] M. Schienle, A. Frey, F. Hofmann, B. Holzapfl, C. Paulus, P. Schindler, and R. Thewes, "A Fully Electronic DNA Sensor with 128 Positions and in-pixel A/D Conversion," *IEEE Int. Solid-state Circuits Conf.Dig.*, pp. 220-221, 2004.

[70] H. Lee, D. Ham, and R. Westervelt, *CMOS Biotechnology*. NY: Springer, 2007.

[71] M. Augustyniak, C. Paulus, R. Brederlow, N. Persike, G. Hartwich, D. SchmittLandsidel, and R. Thewes, "A 24 X 16 CMOS-based Chronocoulometric DNA Microarray," *IEEE Int. Solid-state Circuits Conf.Dig.*, pp. 46-47, 2006.

[72] N. Gemma, S. Ouchi, H. Funaki, J. Okada, and S. Hongo, "CMOS Integrated DNA Chip for Quantitative DNA analysis." *IEEE Int. Solid-state Circuits Conf.Dig.*, pp. 560-561, 2006.

[73] M. Barbaro, A. Bonfiglio, L. Raffo, A. Alessandrini, P. Facci, and I. Barak, "A CMOS Fully Integrated Sensor for Electronic Detection of DNA Hybridization," *IEEE Electron Letters*, Vol. 27, pp. 595-597, 2006.

[74] P. Swanson, R. Gelbart, E. Atlas, L. Yang, T. Grogan, W. Butler, D. Ackley, and E. Sheldon, "A Fully Multiplexed CMOS Biochip for DNA analysis," *Sensors and Actuators: B*, Vol. 64, No. 1, pp. 22-30, 2000.

[75] D. Ham and R. M. Westervelt, "The silicon that moves and feels small living things," *IEEE Solid-State Circuits Society Newsletter*, Vol. 12, pp. 4-9, 2007.

[76] G. Patoukanis, K. Shepard, and R. Levicky, "Active CMOS Biochip for Time-Resolved Fluorescene Detection," *Proc. Symp. VLSI Circuits*, pp. 68-71, 2005.

[77] H. Eltoukhy, K. Salama, and A. E. Gamal, "A 0.18 um CMOS Bioluminescence Detection Lab-on-Chip," *IEEE J. Solid-State Circuits*, Vol. 41, pp. 651-662, 2006.

[78] A. Romani, N. Manaresi, L. Marzocchi, G. Medoro, A. Leonardi, L. Altomare, M. Tartagni, and R. Guerrier, "Capacitive Sensor Array for Localization of Bioparticles in CMOS Lab-on-a-Chip," *IEEE Int. Solid-state Circuits Conf.Dig.*, pp. 224-225, 2004.

[79] P. Cailat, M. Belleville, F. Clerc, and C. Massit, Active CMOS Biochips: an Electro-addressed DNA probes," *IEEE Int. Solid-state Circuits Conf.Dig.*, pp. 272-272, 1998.

[80] Yong Liu, CMOS Magnetic Cell Manipulator and CMOS NMR Biomolecular Sensor, Ph.D. thesis, Harvard University, 2007.

[81] P. M. Levine, P. Gong, R. Levicky, and K. L. Shepard, "Active CMOS Sensor Array for Electrochemical Biomolecular Detection," *IEEE Journal OF Solid-State Circuits*, Vol. 43, No. 8, pp. 1859-1871, 2008.

[82] D. Malamud, H.Bau, S.Niedbala, and P.Corstjens, "Point Detection of Pathogens in Oral Samples," *Proceeding of a Symposium on Saliva-/Oral-fluid-based Diagnostic Markers of Disease*, March 12, 2004.

[83] Y. Gao, G. Hu, Y. H. Lin, P. M. Sherman, D. Li, "An Electrokinetically-controlled Immunoassay for Simultaneous Detection of Multiple Microbial Antigens," *Biomedical Microdevices*, vol 7, no. 4, pp. 301-312, 2005.

[84] F. Patolsky, G. Zheng, O. Hayden, M. Lakadamyali, X. Zhuang, C. M. Lieber, "Electrical Detection of Single Viruses," *Proceedings of the National Academy of Sciences*, vol. 101, no. 39, pp. 14017-14022, 2004.

[85] G. Zheng, F. Patolsky, Y. Cui, W. U. Wang, and C. M. Lieber, "Multiplexed Electrical Detection of Cancer Markers with Nanowire Sensor Arrays," *Nature Biotechnology*, vol. 23, pp. 1294 - 1301, 2005.

[86] E. Marshall, "Getting the Noise Out of Gene Arrays," *Science*, news, vol. 306, pp. 630-631, 2004.

[87] M. Bakay, Y. W. Chen, R. Borup, P. Zhao, K. Nagaraju, E. P. Hoffman, "Sources of Variability and Effect of Experimental Approach on Expression Profiling Data Interpretation," *BMC Bioinformatics*, Vol. 3(4), 2002.

[88] T. Bammler, et al, "Standardizing Global Gene Expression Analysis between Laboratories and Across Platforms," *Nat Methods*, Vol. 2, pp. 351-356, 2005.

[89] D. Gold, et.al, "A Comparative Analysis of Data Generated using Two Different Target Preparation Methods for Hybridization to Highdensity Oligonucleotide Microarrays," *BMC Genomics*, Vol. 5(2), 2004.

[90] T. Yuen, et.al, "Accuracy and Calibration of Commercial Oligonucleotide and Custom cDNA Microarrays," *Nucleic Acids Res*, Vol. 30, e48, 2002.

[91] J. H. Willisa, G. Isayab, O. Gakhb, R. A. Capaldia and M. F. Marusicha, "Lateral-flow Immunoassay for the Frataxin Protein in Friedreichs Ataxia Patients and Carriers," *Molecular Genetics and Metabolism*, Vol. 94, Issue 4, pp. 491-497, August 2008.

[92] A. Hassibi, H. Vikalo, A. Hajimiri, "On Noise Processes and Limits of Performance in Biosensors," *Journal of Applied Physics*, vol. 102, Issue 1, pp. 014909(12pp), 2007.

[93] A. Hassibi, S. Zahedi, R. Navid, R. W. Dutton, and T. H. Lee, "Biological Shot-noise and Quantum-limited Signal-to-Noise Ratio in Affinity-based Biosensors," *Journal of Applied Physics*, vol. 97, Issue 8, pp. 084701(10pp), 2005.

[94] Y. Tu, G. Stolovitzky, and U. Klein, "Quantitative Noise Analysis for Gene Expression Microarray Experiments," *Proc. Natl. Acad. Sci.*, pp. 14031-14036, 2002.

[95] S. Draghici, "Draghici S: Data Analysis Tools for DNA Microarrays," Chapman and Hall/CRC Press, 2003.

[96] M. L. Lee, F. C. Kuo, G. A. Whitmore, J. Sklar, "Importance of Replication in Microarray Gene Expression Studies: Statistical Methods and Evidence from Repetitive cDNA Hybridizations," *Proceedings of the National Academy of Sciences of the United States of America*, vol. 97, no. 18, pp. 9834-9839, August 2000.

[97] W. Zhang and I. Shmulevich (editors), Computational and Statistical Approaches to Genomics (Kluwer Academic Publishers, New York, 2002).

[98] S. Jones, B. Jumarhon, S. McKee, and J. A. Scott, "A Mathematical Model of a Biosensor," *Journal of Engineering Mathematics*, Vol. 30, No. 3, pp. 321-337, 1996.

[99] C. Heitzinger, R. Kennell, G. Klimeck, N. Mauser, M. McLennan, and C. Ringhofer1, "Modeling and Simulation of Field-effect Biosensors (BioFETs) and Their Deployment on the NanoHUB," *Journal of Physics: Conference Series*, Vol. 107 (012004), 2008.

[100] F. Ivanauskas and R. Baronas, "Modelling an Amperometric Biosensor Acting in a Flowing Liquid," *International Journal for Numerical Methods in Fluids*, Vol. 56, Issue 8, pp. 1313-1319, 2007.

[101] Y. Liu and Q. Wang, "Mathematical and Computational Modeling of Biosensors: Modeling for Enzyme-substrate Interaction and Biomolecular Interaction," *Recent Advances In Biology And Biomedicine, Proceedings of the 2nd WSEAS international conference on Computational chemistry table of contents*, pp. 38-42, 2008.

[102] N. D. Botkin, M. Schlensog, M. Tewes and V. L. Turova, "A Mathematical Model of a Biosensor," *Nanotech*, Vol. 1, pp. 231-234, 2001.

[103] B. M. Patre and V. G. Sangam, "Mathematical Model of an Amperometric Biosensor for the Design of an Appropriate Instrumentation System," *Journal of Medical Engineering and Technology*, Vol. 31, Issue. 5, pp. 351-360, 2007.

[104] V. Rossokhaty, and N. Rossokhataja, "A Mathematical Model of Silicon-based Thermobiosensors," *IMA Journal of Management Mathematics*, Vol. 10, No. 1, pp. 41-53, 1999.

[105] P. Rachela, N. Amir, and S. D. Yosi, "Mathematical Model of Whole Cell based Biochip: An Electrochemical biosensor for Water Toxicity Detection," *Journal of electroanalytical chemistry*, Vol. 602, No. 1, pp. 17-23, 2007.

[106] M. Schlosshauer and D. Baker, "Realistic Protein-Protein Association Rates from a Simple Diffusional Model Neglecting Long-Range Interactions, Free Energy Barriers, and Landscape Ruggedness," *Protein Sci.*, Vol. 13, pp. 1660-1669, 2004.

[107] J. F. Tait and S. A. S. Tait, "The effect of Plasma Protein Binding on the Metabolism of Steroid Hormones," *Journal of Endocrinology*, Vol. 131, pp. 339-357, 1991.

[108] C. E. Shannon, A Mathematical Theory of Communication, University of Illinois Press, 1949 (reprinted 1998).

[109] P. J. Kuekes, W. Robinett, G. Seroussi, and R. S. Williams, "Defect-tolerant Interconnect to Nanoelectronic Circuits: Internally Redundant Demultiplexers Based on Error-correcting Codes," *Nanotechnology*, vol. 16, No. 6, pp. 869-882, 2005.

[110] S. Gregori, A. Cabrini, O. Khouri, and G. Torelli, "On-chip Error Correcting Techniques for New-generation Flash Memories," *Proceedings of the IEEE*, vol. 91, no.4, pp.602-616, 2003.

[111] L. Fedichkin, E. Katz, and V. Privman, "Error Correction and Digitalization Concepts in Biochemical Computing," *Journal of Computational and Theoretical Nanoscience*, vol. 5, pp. 36-43, 2008.

[112] E. E. May, A. M. Johnston, W. E. Hart, J. Watson, R. J. Pryor, and M. D. Rintoul, "Detection and Reconstruction of Error Control Codes for Engineered and Biological Regulatory Systems," *Sandia National Laboratories, SAND Report*: 2003-3963, Oct. 2003.

[113] A. H. Khan, A. Ossadtchi, R. M. Leahy, D. J. Smith, "Error-correcting Microarray Design," *Genomics*, vol. 81, No. 2, pp. 157-165, 2003.

[114] O. Milenkovic, "Error and Quality Control Coding for DNA Microarrays," *in Inaugural Workshop of the Center for Information Theory and Application*, San Diego, February 2006.

[115] R. Gallager, "Low-Density Parity-Check Codes," *IRE Trans. Information Theory*, pp. 21-28, January 1962.

[116] T. K. Moon, Error Correction Coding. New Jersey: John Wiley and Sons. 2005.

[117] A. Hassibi, S. Zahedi, R. Navid, R. W. Dutton, and T. H. Lee, "Biological Shot-Noise and Quantum-Limited Signal-to-Noise Ratio in Affinitybased Biosensors," *J. Appl. Phys.*, Vol. 97, no. 8, pp. 084701(10pp), 2005.

[118] A. Hassibi, H. Vikalo, and A. Hajimiri, "On Noise Processes and Limits of Performance in Biosensors," *J. Appl. Phys.*, Vol. 102, no. 1, pp. 014909(12pp), 2007.

[119] R. Christensen, "Linear and Log-linear Models," *J. Amer. Statist. Assoc.*, Vol. 95, 2000.

[120] Z. Muhammad-Tahir, and E. C. Alocilja, "A Conductimetric Biosensor for Biosecurity," *Biosensors and Bioelectronics*, vol. 18, pp. 813-819, 2003.

[121] Z. Muhammad-Tahir, and E. C. Alocilja, "Fabrication of a Disposable Biosensor for Escherichia coli o157:H7 Detection, " *IEEE Sensors Journal*, vol. 3, pp. 345-351, 2003.

[122] Z. Muhammad-Tahir, and E. C. Alocilja, "Rapid Detection of Bovine Viral Diarrhea Virus as Surrogate of Bioterrorism Agents," *EEE Sensors Journal*, vol. 4, pp. 757-762, 2005.

[123] Y. Iribe, and M. Suzuki, "Integrated Enzyme Switch as a Novel Biosensing Device," *Biosensors and Bioelectronics, The 7th world congress of biosensors*, Japan, 2002.

[124] T. A. Sergeyeva, S. A. Piletskii, A. E. Rachkov, A. V. El'Skaya, N. V. Lavrik, "Polyaniline Label-based Conductometric Sensor for IgG Detection," *Sensors and Actuators B: Chemical*, vol. 34, No. 1, pp. 283-288, 1996.

[125] J. H. Kim, J. H. Cho, G. S. Cha, C. -W. Lee, H. -B. Kim, S. -H. Paek, "Conductimetric Membrane Strip Immunosensor with Polyaniline Bound Gold Colloids as Signal Generator," *Biosensors and Bioelectronics*, vol. 14, no. 12, pp. 907-915, 2000.

[126] A. J. Heeger, "Semiconducting and Metallic Polymers: the Fourth Generation of Polymeric Materials," *Synth. Met*, Vol. 125, pp. 23-42, 2002.

[127] A. G. MacDiarmid, "Synthetic Metals: A Novel Role for Organic Polymers (Nobel Lecture)," *Angew. Chem. Int. Ed. Engl.*, Vol. 40, pp. 2581-2590, 2001.

[128] A. Ray, G. E. Astrius, D. L. Kershiner, A. F. Richter, A. G. MacDiarmid, A. J. Epstein, "Polyaniline: Doping, Structure and Derivatives. Synthetic Metals," Vol. 29, pp. 141-150, 1989.

[129] A. G. MacDiarmid, A. J. Epstein, "Polyanilines: A Novel Class of Conducting Polymers," *Faraday Discussions*, Vol. 88, pp. 317-332, 1989.

[130] E. M. Genies, A. Boyle, M. Lapkowski, C. Tsintavis, "Polyaniline: A Historical Survey," *Synth. Met.*, pp. 139-182, 1990.

[131] A. J. Epstein, A. G. MacDiarmid, "Protonation of Emeraldine: Formation of a Granular Polaronic Polymeric Metal," *Mol. Cryst. Liq. Cryst.*, Vol. 160, pp. 165-173, 1988.

[132] F. Wudl, R. O. Angus, Jr., Lu, F.L., P. M. Allemand, D. J. Vachon, M. Nowak, Z. X. Liu, A. J. Heeger, "Poly(p-phenyleneamineimine): Synthesis and Comparison to Polyaniline," *J. Am. Chem. Soc.*, Vol. 109, pp. 3677-3684, 1987.

[133] C. Sivakumar, A. Gopalan, T. Vasudevan, T. C. Wen, "Kinetics of Polymerization of Nmethyl Aniline using UV-VIS Spectroscopy," *Synth. Met*, Vol. 126, pp. 123-135, 2002.

[134] M. Gerard, A. Chaubey, and B. D. Malhotra, "Application of Conducting Polymer to Biosensors," *Biosensors and Bioelectronics*, Vol. 17, pp. 345-359, 2002.

[135] J. J. Langer and K. Langer, "Polyaniline Nanobiodetector," *Rev. Adv. Mate. Sci*, pp. 434-436, 2005.

[136] K. S. Ryder, D. G. Morris, and J. M. Cooper, "Role of Conducting Polymeric Interfaces in Promoting Biological Electron Transfer," *Biosensors and Bioelectronics*, Vol. 12(8), pp. 721-727, 1997.

[137] B. D. Malhotra, A. Chaubey, and S. P. Singh, "Prospect of conducting polymers in biosensors," *Analytica Chimica Acta*, Vol. 578, pp. 59-74, 2006.

[138] Rapid Lateral Flow Test Strips—Considerations for Product Development, Millipore.

[139] M. A. Harvey, Optimization of Nitrocellulose Membrane Based Immunoassays, (Keene, NH: Schleicher and Schuell), 1991.

[140] Y. Liu, S. Chakrabartty, and E. C. Alcilja, "Fundamental Building Blocks for Molecular Bio-wire based Forward-error Correcting Biosensors," *Nanotechnology*, vol. 18, No. 42, pp. 424017(6pp), October 24, 2007.

[141] Y. Liu, E. C. Alocilja, and S. Chakrabartty, "Forward Error Correcting Biosensors: Modeling, Algorithm, and Fabrication," *IEEE Biomedical Circuits and Systems Conference*, pp. 249-252, 2008.

[142] Y. Liu, A. Gore, S. Chakrabartty, E. C. Alocilja, "A Molecular Bio-wire based Multi-array Biosensor with Integrated Potentiostats," *IEEE Biomedical Circuits and Systems Conference*, pp. 29-32, 2007.

[143] M. E. Cromwell, E. Hilario, F. Jacobson, "Protein Aggregation and Bioprocessing," *AAPS Journal*, Vol. 8(3), 2006.

[144] A. S. Rosenberg, "Effects of Protein Aggregates: an Immunologic Perspective," *AAPS J*, Vol. 8, 2006.

[145] E. Y. Chi, S. Krishnan, T. W. Randolph, J. F. Carpenter, "Physical Stability of Proteins in Aqueous Solution: Mechanism and Driving Forces in Non-native Protein Aggregation," *Pharm Res*, Vol. 20, pp. 1325-1336, 2003.

[146] Y. B. Zhang, J. Howitt, S. McCorkle, P. Lawrence, K. Springer, P. Freimuth, "Protein Aggregation during Overexpression Limited by Peptide Extensions with Large Net Negative Charge," *Protein Expr Purif*, Vol. 36, pp. 207-216, 2004.

[147] V. V. Robert, L. P. Donald, L. O. Hendersona, W. Whitfielda, and F. W. Spiertoa, "Quantitative Differences among Various Proteins as Blocking Agents for ELISA Microtiter Plates," *Journal of Immunological Methods*, Vol. 101, pp. 43-50, 1987.

[148] M. A. Harvey, "Optimization of Nitrocellulose Membrane Based Immunoassays," Keene, NH: Schleicher and Schuell, 1991.

[149] A. M. Campbell, "Monoclonal Antibody and Immunosensor Technology," Amsterdam, The Netherlands: Elsevier, 1992.

[150] K. D. Jones and A. K. Hopkins, "Evaluation of the Efficiency of a Range of Membrane Blocking Agents for Nitrocellulose Membrane Based In Vitro Diagnostic Disease," *Annual Meeting of the American Association for Clinical Chemistry*, Chicago, poster no.3, 1998.

[151] Tsividis,Y.P, Operation and Modeling of the MOS Transistor, New York: McGraw-Hill, 1988.

[152] A.Gore, S.Chakrabartty, S.Pal, E.C.Alocilja, "A Multichannel Femtoampere-Sensitivity Potentiostat Array for Biosensing Applications," *IEEE Transactions on Circuits and Systems I*, Vol. 53, Issue. 11, pp. 2357-2363, Nov. 2006.

[153] Y.Liu, A.Gore, S.Chakrabartty, and E.C.Alcilja, "Characterization of Sub-systems of a Molecular Bio-wire based Biosensor Device," *Microchimica Acta*, Vol. 163, No. 1-2, pp. 49-56, 2008.

[154] S. Gupta, S. Huda, P. K. Kilpatrick, and O. D. Velev, "Characterization and Optimization of Gold Nanoparticle-Based Silver-Enhanced Immunoassays," *Anal. Chem*, Vol. 79, No. 10, pp. 3810-3820, 2007.

[155] R. H. Shyu, H. F. Shyu, H. W. Liu, S. S. Tang, "Colloidal Gold-based Immunochromatographic Assay for Detection of Ricin," *Toxicon*, Vol. 40, No. 3, pp. 255-258, 2002.

[156] O. D. Velev and E. W. Kaler, "In Situ Assembly of Colloidal Particles into Miniaturized Biosensors, *Langmuir*, Vol. 15, No. 11, pp. 3693-3698, 1999.

[157] K. T. Liao and H. J. Huang, "Femtomolar Immunoassay based on Coupling Gold Nanoparticle Enlargement with Square Wave Stripping Voltammetry," *Analytica chimica acta*, Vol. 538, No. 1-2, pp. 159-164, 2005.

[158] Y. Liu, A. Gore, S. Chakrabartty, E. C. Alocilja, "A Molecular Bio-wire based Multi-array Biosensor with Integrated Potentiostat," *IEEE Biomedical Circuits and Systems Conference*, pp. 29-32, Montreal, Canada, 2007.

[159] R. H. Shyu, H. F. Shyu, H. W. Liu, S. S. Tang, "Colloidal Gold-based Immunochromatographic Assay for Detection of Ricin," *Toxicon*, Vol. 40, No. 3, pp. 255-258, 2002.

[160] S. J. Park, T. A. Taton, C. A. Mirkindagger, "Array-Based Electrical Detection of DNA with Nanoparticle Probes, *Science*, Vol. 295, No. 5559, pp. 1503-1506, 2002.

[161] R. Elghanian, J. J. Storhoff, R. C. Mucic, R. L. Letsinger, C. A. Mirkin, "Selective Colorimetric Detection of Polynucleotides Based on the Distance-Dependent Optical Properties of Gold Nanoparticles," *Science*, Vol. 277, pp. 1078-1081, 1997.

[162] J. D. Gibson, B. P. Khanal, and E. R. Zubarev, "Paclitaxel-Functionalized Gold Nanoparticles," *J. Am. Chem. Soc.*, Vol. 129, pp. 11653-11661, 2007.

[163] X. Qian, "In Vivo Tumor Targeting and Spectroscopic Detection with Surface-Enhanced Raman Nanoparticle Tags." *Nature Biotechnology*, Vol. 26, 2008.

[164] S.K.Bhatia, L.C.Shriver-Lake, K.J.Prior, J.H.Georger, J.M.Calvert, R.Bredehorst, and F.S.Ligler, "Use of Thiol-terminal Silanes and Heterobifunctional Crosslinkers for Immobilization of Antibodies on Silica Surfaces," *Analytical Biochemistry*, Vol. 178, Issue 2, pp. 408-413, 1989.

[165] Hans-Andrea Loeliger, "An Introduction to Factor Graphs," *IEEE Signal Processing Magazine*, Vol. 21, pp:28-41, Jan.2004.

[166] F. R. Kschischang, B. J. Frey, and H. A. Loeliger, "Factor Graphs and the Sum-Product Algorithm,", *IEEE Trans. Inform. Theory*, pp. 498-519, 2001.

[167] N. Wiberg. Codes and Decoding on General Graphs. Ph.D. thesis, Univ. Linkoping, Sweden, 1996.

[168] G. D. Forney, Jr., "Codes on Graphs: Normal Realizations," *IEEE Trans. Inform. Theory*, vol. 47, no. 2, pp. 520C548, 2001.

[169] R. G. Gallager, Low-Density Parity-Check Codes. Cambridge, MA: MIT Press, 1963.

[170] D. Divsalar, H. Jin, and R. J. McEliece, "Coding Theorems for "Turbo-Like" Codes," *Proceedings of 36th Allerton Conference on Communication, Control, and Computing*, pp. 201-210, 1998.

[171] F. R. Kschischang, and B. J. Frey, "Iterative Decoding of Compound Codes by Probability Propagation in Graphical Models," *IEEE Journal on Selected Areas in Communications*, Vol. 16, pp. 219-230, 1998.

[172] C. Berrou, A. Glavieux, and P. Thitimajshima, "Near Shannon Limit Error Correcting Coding and Decoding: Turbo Codes," *Proceedings of the International Conference on Communications*, pp. 1064-1070, 1993.

[173] D. J. C. Mackay, and R. M. Neal, "Good Codes based on Very Sparse Matrices," *Cryptography and Coding, Fifth IMA Conference*, pp. 100-111, 1995.

[174] S. Draghici, P. Khatri, A. C. Eklund, Z. Szallasi, "Reliability and Reproducibility Issues in DNA Microarray Measurements," *Trends in Genetics*, Vol. 22, Issue. 2, pp. 101-109, 2006.

[175] R. Almog, S. Zaitsev, O. Shtempluck, E. Buks, "Signal Amplification in a Nanomechanical Duffing Resonator via Stochastic Resonance," *Appl. Phys. Lett*, Vol. 90, pp. 013508, 2007.

[176] D. F. Russell, L. A. Wilkens, and F. Moss, "Use of Behavioural Stochastic Resonance by Paddlefish for Feeding," *Nature*, Vol. 402, pp. 291-294, 1999.

[177] F. Patolsky, G. Zheng, C. M. Lieber, "Nanowire-based Biosensors," *Anal Chem*, Vol. 78, pp. 4260-4269, 2006.

[178] R. M. Grant, S. Buchbinder, W. Cates, E. Clarke, T. Coates, M. S. Cohen, M. Delaney, G. Flores, P. Goicochea, G. Gonsalves, M. Harrington, J. R. Lama, K. M. MacQueen, J. P. Moore, L. Peterson, J. Sanchez, M. Thompson, M. A. Wainberg, "AIDS: Promote HIV Chemoprophylaxis Research, Don't Prevent It," *Science*, Vol. 309, pp. 2170-2171, 2005.